



PEOPLE'S DEMOCRATIC REPUBLIC OF ALGERIA

UNIVERSITY AKLI MOHAND OULHADJ BOUIRA

MINISTRY OF HIGHER EDUCATION

AND SCIENTIFIC RESEARCH

FACULTY OF SCIENCES
AND APPLIED SCIENCES



MECHANICAL ENGINEERING DEPARTMENT

Field: Mechanical Engineering

Specialty: Energetic

Presented By:

- ZIANE AYOUB
- MEKID MOHAMMED

Theme:

Numerical simulation of diesel engine internal

Combustion using OpenFoam software

Presented on 02/07/2024 before a jury consisting of:

President: Dr.Mahfoud.B

Examiner: Dr.Messai.T

Supervisor: Dr.bensalem.Ch

Academic year 2023-2024



نموذج التصريح الشرفي الخاص بالالتزام بقواعد النزاهة العلمية لإنجاز بحث.

انا الممضي اسفله،

السيد(ة)..... **محمد مريد**.....الصفة: طالب، استاذ، باحث..... **طالب**
الحامل(ة) لبطاقة التعريف الوطنية: **7522130316993760228** والصادرة بتاريخ: **2022/08/04**
المسجل(ة) بكلية / معهد **العلوم التطبيقية** قسم **الهندسة الميكانيكية**
والمكلف(ة) بإنجاز اعمال بحث(مذكرة، التخرج، مذكرة ماستر، مذكرة ماجستير، اطروحة دكتوراه).
عنوانها: **numerical simulation of diesel engine internal combustion using open foam substrate**
تحت إشراف الأستاذ(ة): **بن هاجم شفيق**
أصرح بشرفي اني ألتزم بمراعاة المعايير العلمية والمنهجية الاخلاقيات المهنية والنزاهة الاكاديمية المطلوبة
في انجاز البحث المذكور أعلاه.

التاريخ: **2024 07 17**

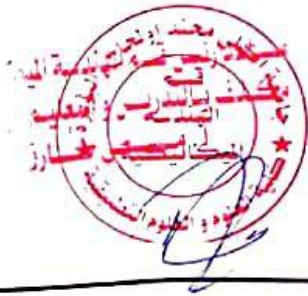
توقيع المعني(ة) **شفيق**

رأي هيئة مراقبة السرقة العلمية:

النسبة:

% **16**

الامضاء:





نموذج التصريح الشرفي الخاص بالالتزام بقواعد النزاهة العلمية لإنتاج بحث.

أنا الممضي أسفله،

السيد(ة) زييان أبووب الصفة: طالب، استاذ، باحث له
الحامل(ة) لبطاقة التعرف الوطنية: 10.29.9.9.3.5.2.07.02.1.0000 والصادرة بتاريخ: 2022.08.17.0.17.6
المسجل(ة) بكلية / معهد العلوم للتكنولوجيا قسم العلوم السيد
والمكلف(ة) بإنجاز اعمال بحث(مذكرة، التخرج، مذكرة ماستر، مذكرة ماجستير، اطروحة دكتوراه).
عنوانها:
numerical simulation of diesel engine internal
combustion using open FOAM soft ware
تحت إشراف الأستاذ(ة):
أصرح بشرفي اني ألتزم بمراعاة المعايير العلمية والمنهجية الاخلاقيات المهنية والنزاهة الاكاديمية المطلوبة
في انجاز البحث المذكور أعلاه.

التاريخ: 2022.08.17

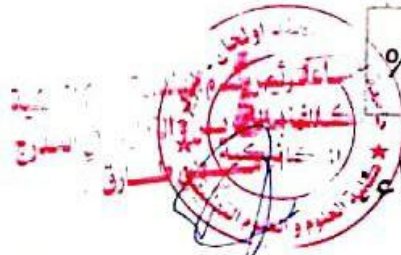
توقيع المعني(ة)

رأي هيئة مراقبة السرقة العلمية:

النسبة:

16 %

الامضاء



ACKOWLEGMENTS

First of all , we are grateful for the guidance and blessings of Allah throughout my academic journey.

We would like to express our deepest gratitude to President Dr. Messai T. for his unwavering support and encouragement throughout my master's degree in mechanical engineering. His guidance and mentorship have been invaluable in shaping our academic journey and research endeavours.

We are profoundly grateful to Examiner Dr. Aghbari for his insightful feedback and constructive criticism, which have significantly enriched the quality of our thesis. His expertise and rigorous examination have been instrumental in refining my work and broadening my understanding of mechanical engineering principles.

I am indebted to Supervisor Dr. Bensalem for his exceptional guidance, patience, and expertise. His mentorship has been pivotal in shaping my research, and his dedication to our academic and professional development has been truly inspiring.

Finally, we extend our sincere thanks to the Department of Mechanical Engineering at the University of Bouira for providing a nurturing academic environment and the resources necessary for the successful completion of my master's degree.

The department's commitment to excellence has been instrumental in shaping my academic and research pursuits.

Dedication

I dedicate this work, first and foremost, to ALLAH, who granted me the will, strength, health, and patience to complete this endeavour.

To my dear father, who has always encouraged and guided me on the right path.

To my loving mother, my source of tenderness, who sacrificed everything for me.

To my siblings, who have always been there to offer help and support.

To my esteemed supervisor, who generously provided me with invaluable guidance and advice.

To all my friends, who have always been a source of inspiration and support.

And to everyone who has shared their knowledge with me and contributed to my educational journey.

To all of you, I dedicate this work as a token of my deep gratitude and appreciation.

Dedication

With gratitude to ALLAH, my parents, my teachers, and my friends, I complete my journey in Master 2. To all of you, I express heartfelt thanks for your unwavering support and trust. Thank God for His guidance and benevolence that have illuminated my path.

To my parents, I convey my deep appreciation for their love, sacrifice, and constant support. I couldn't have achieved this milestone without them. To the teachers, I express my profound gratitude for their knowledge and inspiration. They have been a crucial pillar in my academic journey.

To my siblings and friends, who shared with me moments of difficulty and joy, I thank them for their sincere friendship and continuous encouragement. Together, we overcame challenges and celebrated successes.

This dedication is a testament to my gratitude to those who have helped shape my academic path."

Abstract:

This thesis investigates how spray injectors impact combustion engine flow dynamics through a combined approach of literature review and computer simulations with a focus on soot formation. The review explores internal combustion engine fundamentals, particularly diesel engines, focusing on thermodynamics and injector technology advancements. It then delves into the characteristics of the exiting spray under cold (non-combusting) and hot (combusting) conditions, along with the resulting flame structure. The simulation section details the use of OpenFOAM software's finite volume method to represent the injector geometry digitally and define inlet conditions. It also explains the models used to simulate combustion-turbulence interaction and includes a soot model for a more comprehensive understanding of particulate matter formation within the engine. Finally, the research presents results from baseline and variable fuel reactivity simulations in both cold and hot flow conditions. The concluding discussion compares these findings, highlighting the insights gained from the soot model on how spray injectors influence not only flow dynamics but also particulate matter formation within the engine. This knowledge can ultimately contribute to improved engine design and performance with potentially reduced soot emissions.

Résumé:

Cette mémoire étudie l'impact des injecteurs à spray sur la dynamique des flux dans les moteurs à combustion interne en combinant une revue de la littérature et des simulations informatiques, en mettant l'accent sur la formation de suie. L'examen explore les fondements des moteurs à combustion interne, en particulier les moteurs diesel, en se concentrant sur la thermodynamique et les progrès technologiques des injecteurs. Ensuite, il se penche sur les caractéristiques du spray sortant du moteur dans des conditions froides (sans combustion) et chaudes (avec combustion), ainsi que sur la structure de la flamme résultante. La section simulation détaille l'utilisation de la méthode des volumes finis du logiciel OpenFOAM pour représenter la géométrie de l'injecteur numériquement et définir les conditions d'entrée. Il explique également les modèles utilisés pour simuler l'interaction combustion-turbulence et intègre un modèle de suie pour une compréhension plus complète de la formation de particules à l'intérieur du moteur. Enfin, la recherche présente les résultats de simulations de réactivité de carburant de base et variable dans des conditions de flux froides et chaudes. La discussion finale compare ces résultats, en soulignant les connaissances acquises grâce au modèle de suie sur la façon dont les injecteurs à spray influencent non seulement la dynamique des flux, mais également la formation de particules à l'intérieur du moteur. Ces connaissances peuvent ultimement contribuer à l'amélioration de la conception et des performances du moteur avec une réduction potentielle des émissions de suie.

ملخص :

يبحث هذا البحث في كيفية تأثير حاقنات الرذاذ على ديناميكيات تدفق محركات الاحتراق الداخلي من خلال نهج يجمع بين مراجعة المراجع والمحاكاة الحاسوبية مع التركيز على تكوين السخام. يستكشف الاستعراض الأساسية النظرية لمحركات الاحتراق الداخلي ، خاصة محركات الديزل ، مع التركيز على التطورات في مجال الديناميكا الحرارية وتكنولوجيا الحاقنات. ثم يتعمق في خصائص الرذاذ الخارج من المحرك في ظروف البرودة (بدون احتراق) والحرارة (مع الاحتراق) ، إلى جانب بنية اللهب الناتجة. يوضح قسم المحاكاة استخدام طريقة الحجم النهائي لبرنامج OpenFOAM لتمثيل هندسة الحاقن رقمياً وتحديد ظروف المدخل. كما أنه يوضح النماذج المستخدمة لمحاكاة تفاعل الاشتعال والاضطراب. أخيراً ، يقدم البحث نتائج من محاكاة تفاعلية الوقود الأساسية والمتغيرة في كل من ظروف التدفق البارد والحرار. تقارن المناقشة الختامية هذه النتائج ، مع تسليط الضوء على الأفكار المستسقة من نموذج السخام حول كيفية تأثير حاقنات الرذاذ ليس فقط على ديناميكيات التدفق ولكن أيضاً على تكوين الجسيمات داخل المحرك. ويمكن أن تساهم هذه المعرفة في نهاية المطاف في تحسين تصميم المحرك وأدائه مع تقليل محتمل لانبعاثات السخام

General introduction	1
Chaptre 01 : Technological study and state of art	3
<u>I.1 Introduction</u>	4
<u>I.2. Internal combustion engine</u>	4
<u>I.2.1: Historic of internal combustion engine</u>	4
<u>I.2.2 definition</u>	6
<u>I.2.3 Architecture of an internal combustion engine</u>	6
<u>I.2.4 Classification Of Internal Combustion Engines</u>	15
<u>I.2.5. Spark ignition and compression ignition</u>	18
<u>I.2.6 Engine Configurations</u>	19
<u>I.3 Diesel engine combustion interne</u>	23
<u>I.4 Thermodynamics cycles</u>	25
<u>I.4.1 Definition</u>	25
<u>I.4.2: The Diesel cycle</u>	25
<u>I.5 The Current Studies in Internal Combustion Engine</u>	27
<u>I.6 characterstics of flow at the outlet of an injector</u>	32
<u>I.6.1 Cold Flow Analysis</u>	33
<u>I.6.2 Hot Flow Analysis</u>	34
<u>I.7 Conclusion</u>	35
Chapter 02 : Numerical modeling (finite volume method)	36
<u>II.1 Introduction</u>	37
<u>II.2 Equation Modeling</u>	37
<u>II.2.1 GOVERNING EQUATIONS</u> :.....	38
<u>II.2.2 Continuity Equation</u>	39
<u>II.2.3 Momentum equation</u>	39
<u>II.2.4 Turbulent Kinetic Energy and Dissipation Models</u>	39
<u>II.2.5 Internal energy</u>	40
<u>II.2.5 Internal energy</u>	40
<u>II.2.7 Chemical reaction</u>	42
<u>II.3 Equations of aerothermochemistry</u>	44
<u>II.3.1 Continuity Equation</u>	44
<u>II.3.2 Equation of Conservation of Momentum</u>	44
<u>II.3.3 Energy Conservation Equation</u>	45
<u>II.3.4 Chemical Species Conservation Equation</u>	46

Chapter 03 : Numerical modeling (finite volume method)	47
<u>III.1 OpenFOAM (Open Field Operation and Manipulation)</u> :.....	48
<u>III.1.1 Openfoam content:</u>	48
<u>III.1.2 The Aachen Bomb:</u>	49
<u>III.1.3 Execution:</u>	52
<u>III.2 GEOMETRY:</u>	53
<u>III.2.1 Purpose of Accurate Geometry Representation in Diesel Injector Simulation Importanc.</u>	53
<u>III.2.2 Influence of Geometric Details</u>	53
<u>III.2.3 Benefits of geometry in Diesel Engine Research</u>	55
<u>III.3 Computational set up</u>	55
<u>III.3.1 Geometric pattern mesh:</u>	56
<u>III.4 Boundary condition at the injector inlet</u> :.....	59
<u>III.4.1 Common Boundary Conditions at the Injector Inlet</u>	59
<u>III.4.2 Reasoning the Selection: AachenBomb Simulation with C7H16 as Diesel Substitute;</u>	60
<u>III.4.3 Implementation in Simulations</u> :	61
<u>III.5 Turbulence Model</u> :.....	66
<u>III.5.1 Combustion Model</u> :	66
<u>III.5.2 Turbulent Combustion Models</u>	67
<u>III.6 The use of cold flow:</u>	68
<u>III.6.1 Implimentation of coldflow</u> :	69
<u>III.6.2 Explanation of Soot in the AachenBomb Simulation</u> :	69
<u>III.6.3 Purpose of the Soot implementation:</u>	70
<u>III.7 Implimentation of SootModel</u> :.....	70
<u>III.7.1 Execution</u>	71
<u>III.7.2 Generate Mesh:</u>	76
<u>III.8 Conclusion</u>	77
Chapter 04: Results and discussion	78
<u>IV.1 Introduction</u>	79
<u>IV.2 aachenBomb Simulation results</u>	80
<u>IV.2.1 Cold Flow</u> :	80
<u>IV.2.2 Hot Flow:</u>	87
<u>IV.2.3 Soot Modeling</u> :	96
<u>IV.3 Comparison of results:</u>	107
<u>IV.3.1 Combustion Characteristics: Comparison of Soot and Hot Flow Cases</u>	107
<u>IV.4 Conclusion</u>	113
<u>General conclusion</u>	114

Figures list:

Chapter 01

Figure.I. 1 Brayton petroleum Engine5
Figure.I. 2 : Representation of the main elements constituting an engine.....7
Figure.I. 3 : Anatomy and Design of the Modern Engine Block.....8
Figure.I. 4: Aluminium cylinder head9
Figure.I.5: Carter-of-motor-Chevrolet-spark.....9
Figure.I.6: Rocker Cover.....10
Figure.I.7: Piston of sport car.....11
Figure.I.8: Car's connecting rod11
Figure.I.9: schematic diagram of a crankshaft.....12
Figure.I.10: A Camshaft13
Figure.I.11: A flywheel of a car13
Figure.I.12: A timing belt of a timing chain.....14
Figure.I. 13 : injector of Mohamed Mekid's car father14
Figure.I.14: Engine of 4 Stroke16
Figure.I.15: Spark engine motor (SI engine).....18
Figure.I. 16: a diesel engine 4 cylinder (CI engine).....19
Figure.I.17: Straight Engine (Inline Engine).....20
Figure.I. 18 : An engine with 'V' shape20
Figure.I.19: A Boxer Engine21
Figure.I. 20: A 'W' Engine.....22
Figure.I.21: a Radial/Star Engines.....22
Figure.I. 22 The 'U' engine type.....22
Figure.I. 23: The Diesel cycle26
Figure.I.24: Calculated and measured toluene ignition delay for different pressures.27
Figure.I. 25: Calculated and measured toluene ignition delay for different pressures.28
Figure.I. 26: Time sequences of experiment and simulation for EGR-1.....28
Figure.I. 27 : Calculated and mesured Cylinder pressure for small diesel case.....29
Figure.I.28: NOx emission for small diesel29
Figure.I.29:Schematic of the experimental setup for the study of the reactive spray31
Figure.I. 30:Evolution of inert (blue) and reactive (red) spray penetration for PRF0 at 900 K, 15% O2 and 150 MPa, time after SoI.31
Figure.I. 31 : Normalized flame length (FLnorm) versus fuel composition at ambient temperature and oxygen concentration variations32
Figure.I.32: Air nozzle.....33

Chapter 03

Figure III. 1: terminal location in linux.....	49
Figure III. 2: OpenFoam running command using terminal	50
Figure III. 3: aachenbomb solvers content.....	50
Figure III. 4: “aachenBomb/0” content.....	50
Figure III. 5: aachenBomb/constant content	51
Figure III. 6: aachenbomb/system content	51
Figure III. 7: blockMesh execution information	52
Figure III. 8: aachenBomb/chemkin content.....	52
Figure III. 9: aachenbomb simulation results	53
Figure III. 10: “aachenBomb” Geometry simulation	56
Figure III. 11: “aachenBomb” Mesh simulation	57
Figure III. 12: “aachenBomb” chemistry equation	68
Figure III. 13: “aachenBomb” chemistryType	69

Chapter 04

Figure.IV.1: temperature distribution at 1.4ms within the Cold Flow in the combustion chamber ...	80
Figure.IV.2: temperature graph within a Cold flow in the combustion chamber	80
Figure.IV.3 : velocity distribution at 1.4ms within the Cold Flow combustion	81
Figure.IV.4: velocity graph within a Cold flow in the combustion chamber	82
Figure.IV.5 : Density distribution at 1.4ms within the Cold Flow combustion.....	82
Figure.IV.6: Density graph within a Cold flow in the combustion chamber.....	83
Figure.IV.7: Volume distribution of C7H16 at 1.4ms within the Cold Flow combustion	84
Figure.IV.8: C7H16 Volume graph within a Cold flow in the combustion chamber.....	84
Figure.IV.9: Volume distribution of O2 at 1.4ms within the Hot Flow combustion	85
Figure.IV.10: O2 Volume graph within a cold flow in the combustion chamber	85
Figure.IV.11: Volume distribution of N2 at 1.4ms within the Cold Flow combustion	86
Figure.IV.12: Temperature distribution at 1.4ms within the Hot Flow in the combustion chamber .	87
Figure.IV.13: Temperature graph within a Hot Flow in the combustion chamber	87
Figure.IV.14: Velocity distribution at 1.4ms within the Hot Flow combustion.....	88
Figure.IV.15: Velocity graph within the Hot Flow in the combustion chamber	88
Figure.IV.16: Density distribution at 1.4 ms within the Hot Flow combustion.....	89
Figure.IV.17: Density graph within a Hot flow in the combustion chamber.....	90
Figure.IV.18: Volume distribution of C7H16 at 1.4ms within a Hot flow combustion	90
Figure.IV.19: C7H16 volume graph within a Hot flow in the combustion chamber.....	91
Figure.IV.20: Volume distribution of CO2 at 1.4ms within the Hot Flow combustion.....	92
Figure.IV.21: CO2 volume graph within a Hot flow in the combustion chamber.....	92
Figure.IV.22: Volume distribution of H2O at 1.4ms within the Hot Flow combustion.....	93
Figure.IV.23: H2O volume graph within a Hot flow in the combustion chamber.....	94
Figure.IV.24: Volume distribution of O2 at 1.4ms within the Hot Flow combustion.....	94
Figure.IV.25: O2 Volume graph within a Hot flow in the combustion chamber.....	95
Figure.IV.26: Volume distribution of N2 at 1.4ms within the Hot Flow combustion.....	96

Figure.IV.27: Temperature distribution at 1.4ms within the ‘SootModel’ combustion.	97
Figure.IV.28: Temperature graph within a ‘SootModel’ in the combustion chamber.	97
Figure.IV.29: velocity distribution at 1.4ms within the ‘SootModel’ combustion.	98
Figure.IV.30: Velocity graph within a ‘SootModel’ in the combustion chamber.	99
Figure.IV.31: Density distribution within a ‘SootModel’ in the combustion chamber.	99
Figure.IV.32: Density graph within a ‘SootModel’ in the combustion chamber.	100
Figure.IV.33 : Volume distribution of C7H16 within a ‘SootModel’ in the combustion chamber. ...	100
Figure.IV.34: C7H16 Volume graph within a ‘SootModel’ in the combustion chamber.	101
Figure.IV.35: Volume distribution of Co2 within a ‘SootModel’ in the combustion chamber.....	102
Figure.IV.36: Co2Volume graph within a ‘SootModel’ in the combustion chamber	102
Figure.IV.37: Volume distribution of H2O within a ‘SootModel’ in the combustion chamber.....	103
Figure.IV.38: H2O Volume graph within a ‘SootModel’ in the combustion chamber.	103
Figure.IV.39: Volume distribution of O2 within a ‘SootModel’ in the combustion chamber.....	104
Figure.IV.40: O2 Volume graph within a ‘SootModel’ in the combustion chamber.	105
Figure.IV.41: Volume distribution of N2 within a ‘SootModel’ in the combustion chamber.....	105
Figure.IV.42: Volume distribution of “Soot” within a ‘SootModel’ in the combustion chamber.....	106
Figure.IV.43: Soot Volume graph within a ‘SootModel’ in the combustion chamber.....	106
Figure.IV.44: Temperature distribution of Hotflow and ‘SootModel’ in the combustion chamber.	107
Figure.IV. 45: Temperature graph within a Hold flow and SootModel in the combustion chamber.	108
Figure.IV.46: Velocity distribution of Hotflow and ‘SootModel’ in the combustion chamber.....	109
Figure.IV.47: Velocity graph within a Hold flow and SootModel in the combustion chamber.....	110
Figure.IV.48: Density distribution of Hotflow and ‘SootModel’ in the combustion chamber.....	111
Figure.IV.49: Density distribution of Hotflow and ‘SootModel’ in the combustion chamber.....	112
Figure.IV.50: Volume graph of the combustion species within a Hold flow and SootModel in the combustion chamber	112

Tables list

Chapter 01

Table I. 1: List of internal engine components	7
Table I. 2: Table of comparison between petrol and dissel fuel	19
Table I. 3: Diesel cycle transfotmation	27
Table I. 4: Oxidation mechanism and rate coefficients	30

Chapter 03

Table III. 1: Geometric inlet injector dimensions	54
Table III. 2: aachenbomb tutorial initial dimensions case.....	56
Table III. 3: Initial condition for aachenbomb cases	60
Table III. 4: Initial soecies concentration before the combustion	60
Table III. 5: Characteristics of (C7H16) heptane in standards condition	61
Table III. 6: Advantages and limitation of combustion models	66
Table III. 7: Advantantages and limitations of TyTurbulent Combustion Models	67

Nomenclature

t	[s]	Time
P	[pa]	Static pressure
∇	[m^{-1}]	Gradient or Divergence operator
u	[m/s]	Velocity vector
D	[m/s^2]	Diffusion coefficient
$\dot{\rho}_m^c$	[$kg/(m^3 * s)$]	Source term
K	[J/kg]	Turbulent kinetic energy
\tilde{I}		Identity tensor
Pr_k		Turbulent Prandtl number for K
Pr_ϵ		Turbulent Prandtl number for ϵ
$C_{\epsilon 1}, C_{\epsilon 2}, C_{\epsilon 3}$		Empirical constant for the production
\dot{Q}_c	[w/m^3]	Volumetric heat source term
T	[K]	Temperature
h_m	[J/kg]	Specific enthalpy of component m
R_0	[$J/(kg * K)$]	Universal gas constant
W_m	[$kg/kmol$]	Molecular weight of component m
C_p	[$J/(kg * K)$]	Specific heat capacity at constant pressure
C_{pm}	[$J/(kg * K)$]	Specific heat capacity for component m
$a_{1m}, a_{2m}, a_{3m}, a_{4m}, a_{5m}$		Coefficients in the polynomial expression for $C_p(T)$
S	[J/K]	Entropy
r		Reaction rate
X_m		Mole Fraction

Greek letters

μ	[kg/s]	Dynamic viscosity
μ_{eff}	[pa * s]	Effective viscosity
\emptyset		Porosity
σ	[Pa]	Deviatoric stress tensor (viscous stress tensor)
g	[m/s ²]	Gravitational acceleration vector
λ	[pa * s]	Second viscosity coefficient (related to bulk viscosity)
ε	[m ² /s ³]	Turbulent dissipation rate
$\dot{\omega}$	[s ⁻¹]	Rate of change of reaction progress
ρ	[kg/m ³]	Total mass density
ρ_m	[kg/m ³]	Mass density of a component (species mass density)

Abbreviations:

ICE	Internal Combustion Engine
PCV	Positive Crankcase Ventilation
TDC	Top Dead Center
BDC	Bottom Dead Center
CNG	Compressed Natural Gas
LPG	Liquefied Petroleum Gas
PRF	Primary Reference Fuel
CFD	Computational Fluid Dynamics

General introduction

The combustion in a diesel engine is a complex process involving the injection of diesel fuel into the combustion chamber, followed by its vaporization, mixing with the surrounding air, auto-ignition, and combustion. This process is important for power generation in a diesel engine. The quality of combustion directly affects the engine's energy efficiency, pollutant emissions, and overall system performance. A deep understanding of combustion in a diesel engine is essential for optimizing engine design, improving energy efficiency, reducing emissions, and meeting stringent environmental standards.

The numerical simulation of diesel engine internal combustion using OpenFOAM software represents a cutting-edge approach to understanding the complex physical and chemical processes occurring within diesel engines. OpenFOAM, an open-source computational fluid dynamics (CFD) software, provides a comprehensive suite of tools for simulating the intricate phenomena associated with diesel engine operation. This includes the modeling of fuel injection, spray formation, air-fuel mixing, combustion, heat transfer, and pollutant formation, all of which are crucial for optimizing engine performance and emissions characteristics.

By leveraging the capabilities of OpenFOAM, researchers and engineers can gain deep insights into the fundamental mechanisms governing diesel engine combustion, enabling them to explore innovative strategies for enhancing fuel efficiency, reducing emissions, and improving overall engine performance. The use of numerical simulations with OpenFOAM allows for a detailed analysis of combustion processes under various operating conditions,

providing a cost-effective and environmentally sustainable means of evaluating design modifications and alternative fuel formulations.

Furthermore, the open-source nature of OpenFOAM fosters collaboration and knowledge sharing within the scientific and engineering communities, facilitating the development of advanced simulation methodologies and the validation of computational models against experimental data. As a result, the application of OpenFOAM for numerical simulations of diesel engine internal combustion holds great promise for advancing the state-of-the-art in engine design, emissions control, and sustainable transportation technologies.

The study of internal combustion engines is pivotal in advancing automotive and energy technologies. With growing environmental concerns and the quest for efficiency, understanding the intricate dynamics of these engines is more important than ever. This research aims to delve deep into the technological and numerical aspects of diesel engines, offering insights that could pave the way for significant improvements. The problem at hand is optimizing engine performance while minimizing emissions. Our objectives include investigating current technologies, developing robust numerical

models, and analysing various scenarios to propose effective solutions. The journey begins with a comprehensive review of existing technologies and progresses through detailed numerical modeling, culminating in an in-depth analysis of simulation results.

In Chapter 1, we embark on a detailed exploration of internal combustion engines, with a particular focus on diesel engines. The chapter starts with an introduction to the fundamental principles and components of internal combustion engines, delving into their thermodynamic processes. A thorough review of the state of the art follows, highlighting the latest advancements and studies in engine technology. Key characteristics of flow at the injector outlet, including cold and hot flow dynamics and flame structure, are examined. This chapter sets the foundation for understanding the complexities of engine operation and paves the way for the numerical modelling efforts in the subsequent chapter.

In Chapter 2 delves into the realm of numerical modelling, emphasizing the finite volume method as a critical tool for simulating fluid dynamics and combustion processes in internal combustion engines. The chapter begins with an overview of OpenFOAM software, detailing its capabilities and applications. The importance of accurate geometric representation and mesh generation is discussed, followed by an exploration of boundary conditions at the injector inlet. The chapter also covers combustion interaction models, focusing on the Combustion model/Turbulence (RANS) approach. This section equips readers with the knowledge and tools necessary to conduct detailed simulations, setting the stage for the analysis of results in the next chapter.

In Chapter 3, the focus shifts to the analysis of simulation results, providing a thorough examination of the parametric analysis and case studies conducted. Starting with the baseline case, the chapter investigates the results of temperature, velocity, and density for both hot flow and cold flow scenarios. Additionally, the chapter explores the soot models introduced in the final simulation case. The impact of these reactivity properties on atomization and flame structure is analysed in detail. The chapter culminates in a comprehensive discussion and comparison of results, highlighting key findings and their implications for engine performance and efficiency. This section not only solidifies the understanding gained from the previous chapters but also points towards future research and potential advancements in internal combustion engine technology. Through this iterative process, the study aims to contribute significantly to the ongoing evolution of engine design and optimization.

Chapter 01:

**Technological study and
state of the art**

1.1 Introduction:

The internal combustion engine (ICE) remains a cornerstone of modern automotive technology, converting fuel into mechanical energy through the combustion of fuel-air mixtures within its cylinders. Current studies in this field focus on enhancing efficiency, reducing emissions, and improving performance through advanced simulations and modeling techniques. Researchers utilize sophisticated software to simulate combustion processes, airflow dynamics, and thermal management within the engine, allowing for detailed analysis and optimization of engine components and operating parameters. These simulations enable the testing of various design modifications and fuel types under different conditions, providing valuable insights that drive innovation without the need for extensive physical prototyping. By leveraging these computational tools, engineers are developing next-generation ICEs that meet stringent environmental regulations while delivering superior performance and fuel economy.

1.2. Internal combustion engine:

1.2.1: Historic of internal combustion engine

Since the late 17th century, pioneers such as “haute feuille” and “Huygens” had formulated the concept of the internal combustion engine and put it into practice. Following them, in 1860, “the Frenchmen Lebon” and “Lenoir” constructed the first spark-ignition engines, powered by gas and operating on a 2-stroke cycle. The principle of the 4-stroke engine was first articulated in 1862 by “Beau de Rochas”, and in 1876, the German Otto built the first engine based on this principle. The emerging needs of automobiles and aeronautics, along with the availability of new petroleum-derived fuels, combined to hasten the development of alternative thermal engines, associated with names like Benz, Daimler, “DeDion, Bouton”, Wright, Levavasseur, Seguin, Renault, and others.

Originally sharing a common technology, aviation and automobile engines began to diverge in the early 20th century, with the latter subsequently benefiting from the advancements made in the remarkable pursuit of power and reliability that characterized the aeronautical field between the two world wars.

World War II marked the pinnacle of spark-ignition engine technology, with achievements tending towards gigantism to meet the ever-increasing power demands of aviation.

A swift decline began in the 1950s with the emergence of turbine engines, which have since relegated "piston engines" to the domain of low power (less than 400 kW).

Regarding diesel engines, the first heavy fuel engine was invented by a German engineer, Rudolph Diesel (1858 - 1913). This engine was notably cost-effective and highly efficient. In 1896, he constructed his initial 4-stroke engine with pre-compression. The key distinction from gasoline engines is that it does not require spark plugs to ignite the fuel as it self-ignites. The Diesel engine found in

today's automobiles is the result of continuous evolution, which has been influenced by events such as the first oil crisis and the introduction of anti-pollution standards.

In 1897, the first engine designed by a thermodynamic engineer, Rudolf Diesel, was put into operation in Germany. It resulted from theoretical work aimed at improving thermodynamic efficiency. This engine, which had an efficiency of 26.2% (compared to the 20% of the gasoline engine at the time), produced a power of 27 kW with a displacement of around 20 litres.

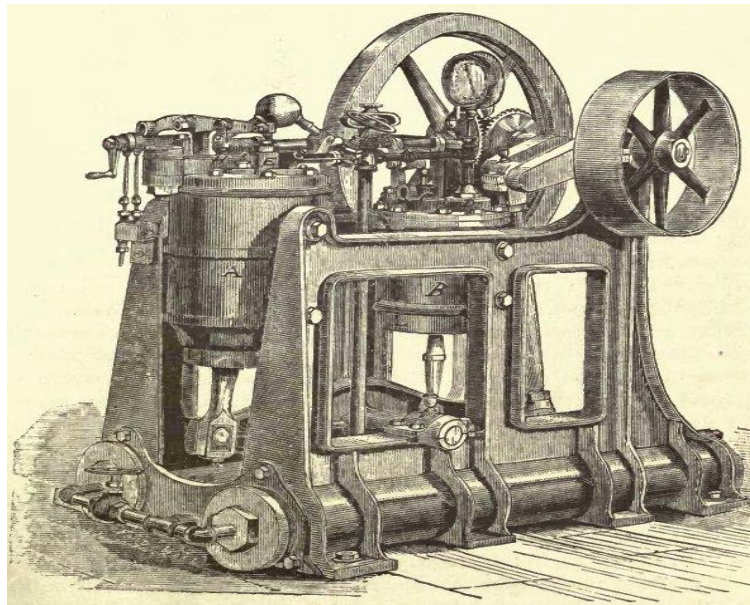


Figure.I.1: Brayton petroleum Engine

Figure.I.1: In 1936, Mercedes produced in small series the first car with a Diesel engine, the 260D.

- In 1938, Peugeot produced a series of a thousand 402 models after the Second World War, and this type of vehicle is still in production.
- In 1973, the oil crisis favored the widespread use of Diesel engine cars.
- In 1988, Fiat produced the first mass-produced car equipped with a direct injection engine.
- In 1989, Audi introduced the first car equipped with an electronically regulated direct injection engine.
- In 1998, Bosch carried out the first applications of common rail direct injection on production vehicles.
- In 2000, several European manufacturers produced a version of their luxury vehicle equipped with a V8 Diesel engine with common rail direct injection.[1]

1.2.2 definition

The internal combustion engine serves as a power machine, converting the stored energy in a fuel (calorific value) into thermal energy (heat, enthalpy, calorific energy), and subsequently into mechanical energy (mechanical work, torque). Within internal combustion engines, the generation of thermal energy occurs within a confined volume (combustion chamber, engine cylinder) delimited by the cylinder head, closed valves, piston head, and liner. The expansion of gases resulting from fuel combustion actuates active components (Piston-Connecting Rod-Crankshaft) to recover this energy and convert it into useful work (engine shaft)[2] The evolution of the internal combustion engine can be delineated into three significant phases:

- Phase 1: Enhancement of thermal efficiency, torque, and engine power: This phase witnessed the emergence of the spark-ignition engine and its widespread adoption in transportation and industry, followed by the introduction of the Diesel engine. The primary focus was on improving the performance of the internal combustion engine.
- Phase 2: Reduction in fuel consumption: Depletion of global energy resources, coupled with oil crises and high demands for hydrocarbons and fuel, prompted engine manufacturers to concentrate on reducing specific fuel consumption.
- Phase 3: Mitigation of engine emissions: With increasingly stringent pollution thresholds, engine manufacturers have been compelled to design cleaner engines. Specifications submitted to automotive and engine manufacturers worldwide now emphasize the production of powerful engines with acceptable fuel consumption while maintaining low emissions. In general, engine manufacturers are engaged in conducting thermal balances by measuring or calculating engine torque, power, efficiency, and specific fuelconsumption. [3]

1.2.3 Architecture of an internal combustion engine

the internal combustion engine is truly a marvel of engineering. Its intricate design and precise functionality are a testament to human ingenuity, by understanding the construction of this type of engines and their role in the internal combustion process. We gain a deeper appreciation for the harmony of different forces and mechanisms. It is like looking at a precise system of metals and energy, where each part works in harmony with the others to power the vehicles and machinery that drive our modern world forward.

Prior to elucidating the operation of an internal combustion engine, it is imperative to comprehend its principal constituents. These constituents

are categorized into fixed and mobile components. Let us delve into a detailed examination of the architecture of this engine type and its function within the internal combustion process. [4]

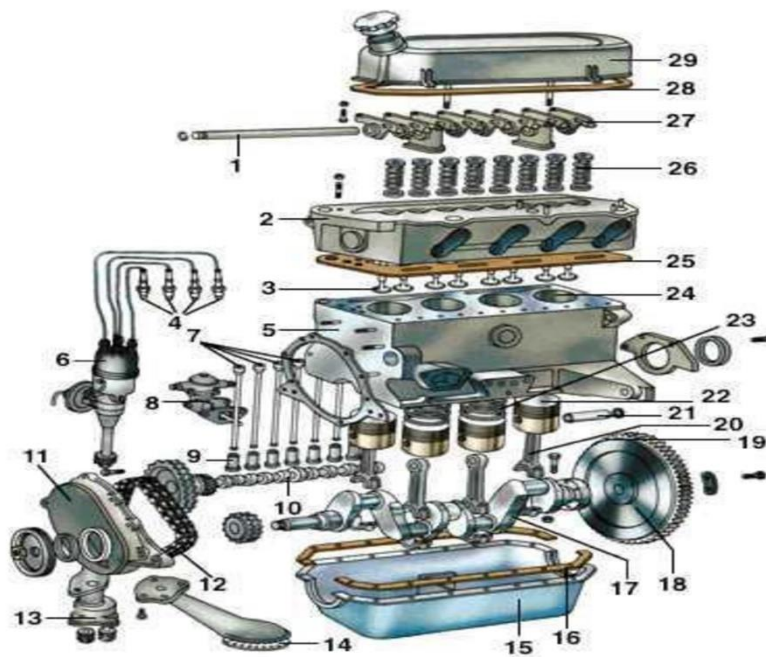


Figure.I. 2 : Representation of the main elements constituting an engine

Table.I.1 : List of internal engine components

1	Rocker arm axle	8	Fuel pump
2	Cylinder head	9	Pushers
3	Valves	10	Camshaft
4	Candles	11	Timing cover
5	Cylinder block	12	Timing belt (chain)
6	Igniter	13	Oil pump
7	Rocker arm control rods	14	Oil pump strainer
15	Engine oil sump	23	Segments
16	Crankcase gasket	24	Cylinder
17	Crankshaft	25	Head gasket
18	Flywheel	26	Valve springs
19	Crown gear driven by the starter	27	Rocker arms
20	Connecting rod	28	Rocker cover gasket
21	Piston shaft	29	Rocker cover
22	Piston		

1.2.3.a Fixed organs:

➤ Engine block:

The engine block, also referred to as the cylinder block, is the most massive part of the engine. It contains the cylinders and accommodates all the engine components: fuel injection equipment, crankshaft, timing system, electrical auxiliaries, and so on. The engine block must be both airtight and robust to withstand the high pressures present within the cylinders during combustion. [5]

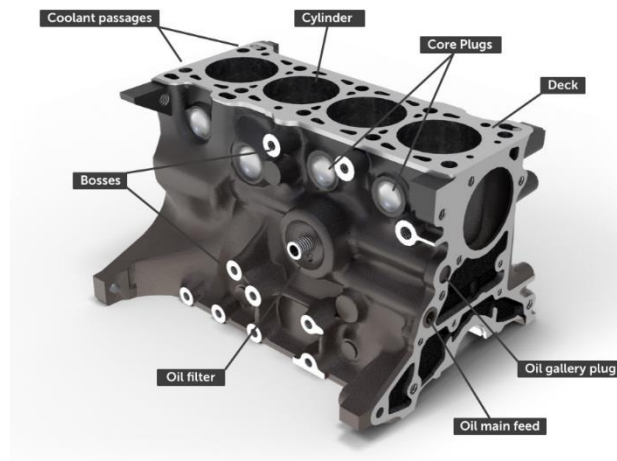


Figure.I. 3 : Anatomy and Design of the Modern Engine Block

➤ Cylinder head

The cylinder head is a critical component of an internal combustion engine, encapsulating the combustion chambers and housing the valve train mechanisms, including intake and exhaust valves, which regulate volumetric efficiency and gas exchange processes. It facilitates the ignition of the air-fuel mixture via spark plugs in gasoline engines or through compression ignition in diesel engines, requiring robust design to withstand high pressures and thermal stresses. The cylinder head's material composition, typically cast iron or aluminum alloys, is pivotal for thermal conductivity and structural integrity, incorporating cooling passages for effective heat dissipation to prevent thermal fatigue. Its intricate design, encompassing optimized port geometry and direct fuel injection pathways, significantly impacts combustion efficiency and engine performance. Additionally, the cylinder head gasket ensures a hermetic seal between the head and engine block, preventing coolant, oil, or combustion gas leaks, thereby maintaining engine integrity and operational efficiency.



Figure.I. 4: Aluminium cylinder head

➤ Oil sump

The oil sump, positioned beneath the engine block, serves as the reservoir for lubricating oil, ensuring a steady supply of oil to various engine components for effective lubrication and cooling. It typically houses a strainer to filter out large contaminants and may include an external or internal oil filter for finer filtration, maintaining oil cleanliness and protecting the engine from wear and damage. The design of the oil sump is crucial for proper oil circulation and heat dissipation, contributing to the engine's overall thermal management and operational efficiency. Additionally, it often features baffles to prevent oil sloshing during vehicle movement, ensuring consistent oil pickup and pressure, which is vital for maintaining optimal lubrication under various operating conditions.



Figure.I.5: Carter-of-motor-Chevrolet-spark

➤ Rocker cover (Valve cover):

The valve cover, also known as the rocker cover, is a protective component situated atop the cylinder head of an internal combustion engine. It encloses vital valve train components, such as rocker arms, camshafts, and lifters, shielding them from debris and contaminants. By preventing oil leaks, the valve cover maintains the engine's lubrication system, ensuring oil remains within to reduce friction and wear. Typically made from durable materials like aluminum or high-strength plastic, it withstands high temperatures and pressures. It usually includes a gasket for a secure seal and often features ventilation systems, such as PCV valves, to manage crankcase pressure and promote efficient oil vapor circulation. The design and integrity of the valve cover are crucial for the engine's longevity, as even minor leaks can lead to significant mechanical issues over time. Proper maintenance and timely replacement of the valve cover and its gasket are essential to ensure the engine operates smoothly and efficiently.



Figure.I.6: Rocker Cover.

1.2.3.b Moving Parts:

➤ piston:

Its primary function is to convert the energy generated by the combustion process into linear motion, transmitting it to the connecting rod, which then transfers it to the crankshaft. The piston rings that surround it ensure the piston's sealing. Typically, the piston head is forged from an aluminium and ceramic alloy to withstand the high temperatures present in the combustion chamber.

Many internal combustion engines incorporate a combustion chamber, often featuring a combustion bowl within the piston. This bowl is shaped according to the engine's injection system. The geometry of the combustion bowl is determined based on the injection system's characteristics to achieve an optimal air-fuel mixture for the engine's operation, with a focus on reducing fuel consumption and emissions.



Figure.I.7: Piston of sport car

➤ **Connecting rod**

The connecting rod in internal combustion engines comprises three main sections: the big end, small end (which houses the piston pin), and shank. Typically crafted from durable materials such as steel or aluminum alloys, it is designed to withstand high mechanical stresses and operating temperatures. The big end connects to the crankshaft via a crankpin bearing, enabling smooth rotation. Meanwhile, the small end attaches to the piston through a piston pin, allowing for controlled piston movement within the cylinder. Structurally, the shank of the connecting rod provides essential strength and rigidity to handle the engine's dynamic forces effectively. This design ensures efficient energy transfer from the piston to the crankshaft, supporting reliable engine performance in various automotive and industrial applications.

The connecting rod's design is often optimized to balance weight reduction with increased strength, employing techniques like forging and advanced alloy compositions. Modern engineering also focuses on minimizing friction and wear through precise bearing surface treatments and lubrication strategies. Additionally, advancements in manufacturing processes have enabled tighter tolerances and improved consistency in connecting rod production, enhancing overall engine efficiency and reliability.

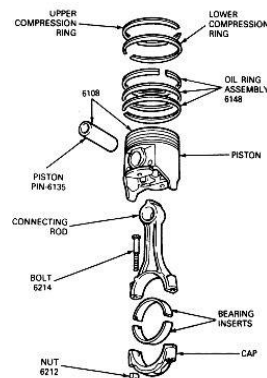


Figure.I.8: Car's connecting rod

➤ **Crankshaft**

The crankshaft, a fundamental component in internal combustion and Stirling engines, is the central element of the connecting rod-crank system. Its primary function is to convert the reciprocating linear motion generated by the pistons into a continuous rotary motion [6] This rotary motion is essential for driving various engine components, including the primary transmission, alternator, and counterbalance shafts, which are crucial for the overall operation and performance of the engine. The counterbalance shafts, for instance, are designed to offset the vibrations and forces produced by the engine, thereby enhancing its smooth operation and reducing noise. Additionally, the alternator is responsible for generating electrical power to charge the battery and power the electrical systems of the vehicle. The primary transmission, on the other hand, transfers the rotational motion from the crankshaft to the wheels, enabling the vehicle to move. Therefore, the crankshaft plays a pivotal role in the functionality and efficiency of the engine and the vehicle as a whole

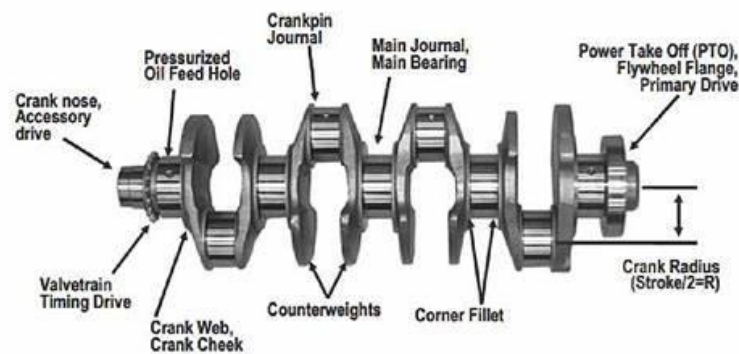


Figure.I.9: schematic diagram of a crankshaft

➤ Camshaft:

The camshaft, also referred to as the "distribution shaft," is integral to the operation of an internal combustion engine, serving to precisely time the opening and closing of intake and exhaust valves. It achieves this by translating the engine's rotational motion into linear motion through lobes or cams that interact with valve lifters or followers. This component is typically housed within the cylinder head or engine block and operates in synchronization with the crankshaft, often through a timing belt or chain connected to a toothed wheel. By regulating valve timing, the camshaft directly impacts the engine's efficiency in combustion, power output, and emissions performance. This meticulous control ensures optimal engine operation under varying loads and speeds, contributing significantly to overall engine durability and fuel efficiency.



Figure.I.10: A Camshaft

➤ Flywheel:

The flywheel is an integral part of an internal combustion engine, serving several essential functions. It acts as an inertial wheel connected to both the engine starter and clutch, primarily to dampen engine oscillations, vibrations, and noise. Additionally, it stores excess energy generated during the engine's combustion cycles, which helps in overcoming the compression dead centred during subsequent strokes. In a dual-mass flywheel configuration, it consists of two interconnected masses linked by a spring, lugs, and a ball bearing system. The primary mass synchronizes with the engine's crankshaft to maintain rotational balance, while the secondary mass interfaces with the transmission to mitigate vibrations and enhance drivetrain smoothness and durability.

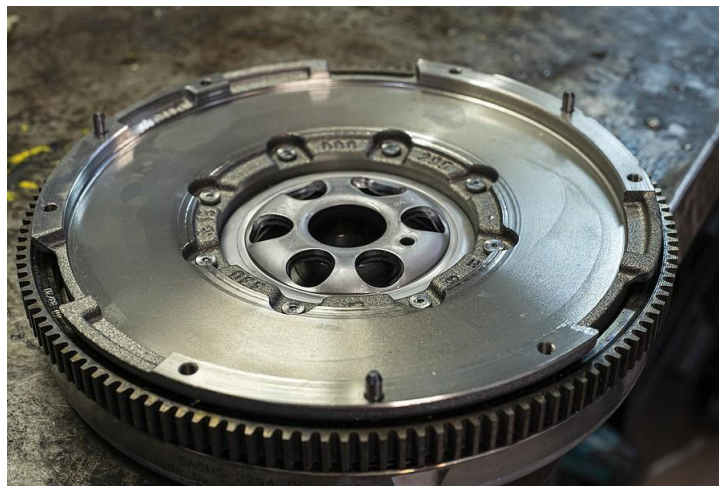


Figure.I.11: A flywheel of a car

➤ Timing belt (chain):

The timing belt is a pivotal component of an automobile's powertrain, responsible for synchronizing the rotational motion of the crankshaft and camshaft. This synchronization is crucial for the precise timing of the engine's valve opening and closing in relation to the position of the pistons. Furthermore, the timing belt may also actuate the water pump, which plays a critical role in maintaining the engine's optimal operating temperature



Figure.I.12: A timing belt of a timing chain

➤ Injectors

Injectors are electromechanical devices utilized in internal combustion engines to deliver precise amounts of fuel into the combustion chamber at the appropriate time. They are designed to atomize the fuel into a fine mist, ensuring efficient mixing with the incoming air for optimal combustion. This controlled delivery of fuel is essential for maintaining engine performance, fuel efficiency, and emission levels within specified limits. Modern injectors are often electronically controlled and can adjust fuel delivery based on various engine-operating parameters, contributing to improved engine efficiency and reduced emissions.



Figure.I.13 : injector of Mohamed Mekid's car father

I.2.4 Classification Of Internal Combustion Engines:

Internal combustion engines categorize into two groups based on their method of igniting the fuel-air mixture:

- Spark-ignition engines, which utilize gasoline.
- Compression-ignition engines, commonly known as Diesel engines, which use diesel fuel.

In spark-ignition engines, they introduce a suitable gasoline-air mixture into the cylinder's combustion chamber and ignite it by a spark.

In compression-ignition engines, they inject diesel fuel under pressure into a pre-compressed and heated air mixture in the combustion chamber, where it ignites spontaneously upon contact.

Both types of engines are considered internal combustion engines due to the combustion process occurring within the engine.

These engines are extensively employed across various industries, particularly in transportation, owing to their efficiency, compact design, and reliability. They serve as the primary source of mechanical power in numerous applications.

Internal combustion engines are commonly selected for land vehicle propulsion, with some exceptions such as electric vehicles, chosen for their favourable power density and relatively low manufacturing and servicing costs.

In an internal combustion engine, the movement of the piston within a cylinder, closed at the opposite end by the cylinder head, results in a cyclical variation of the cylinder's volume. The piston is connected to a connecting rod and a crankshaft, and its regular rotation causes a cyclical movement of the piston between two extreme positions: the top dead center (TDC, closest to the cylinder head) and the bottom dead center (BDC, farthest from the cylinder head). These two positions correspond to the minimum cylinder volume (dead volume, V_0) and the maximum cylinder volume (total volume, V_t), respectively. The difference between the maximum and minimum volumes is called the swept volume or displacement, denoted as V_c . Finally, the ratio between the maximum and minimum volumes is referred to as the compression ratio (τ).

Combustion engines can be classified into different categories. The two most important classifications are based on the combustion process (spark-ignition and compression-ignition) and the working cycle (2-stroke vs. 4-stroke). Additional classification can be based on air intake (naturally aspirated or supercharged), injection (indirect or direct injection), and the cooling system (air-cooled or water-cooled). Here, only the differences between the combustion processes will be presented.

1.2.4 a The different types of engines

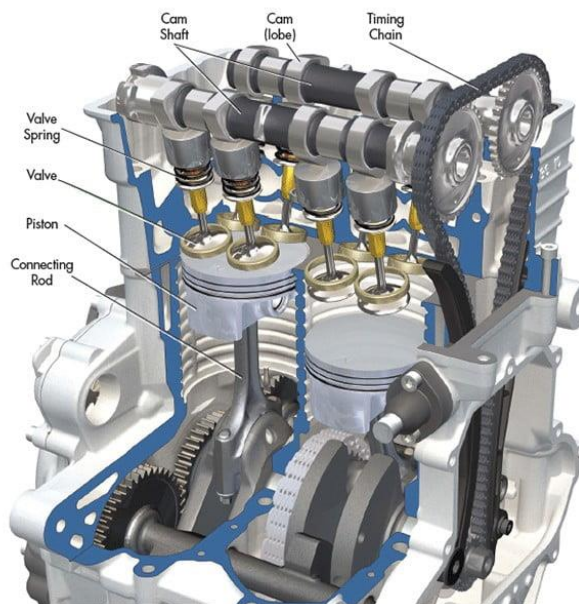
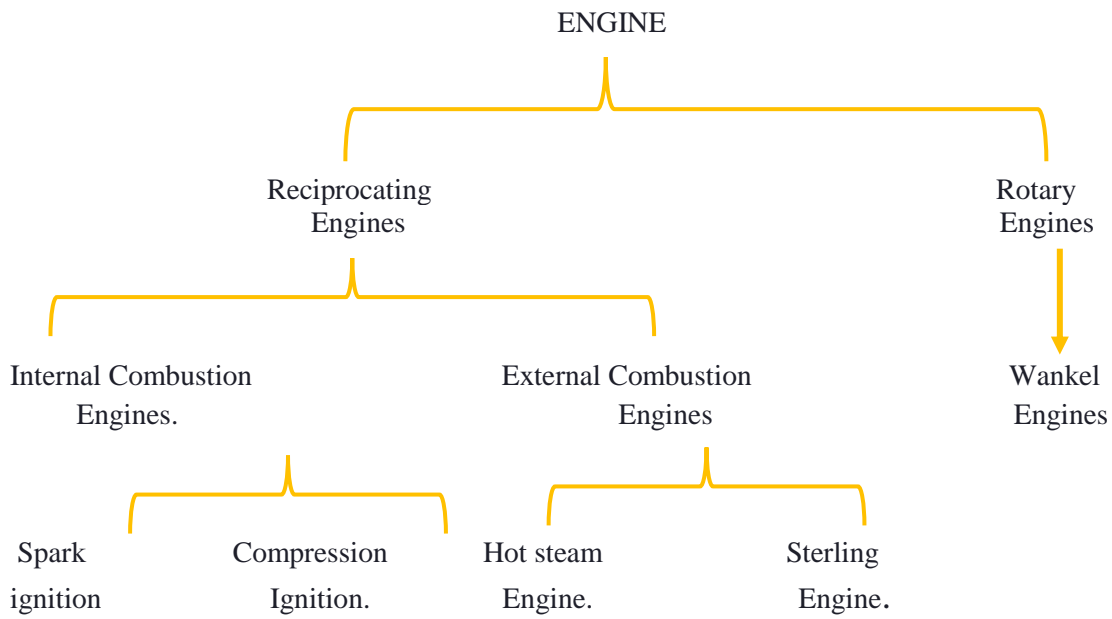
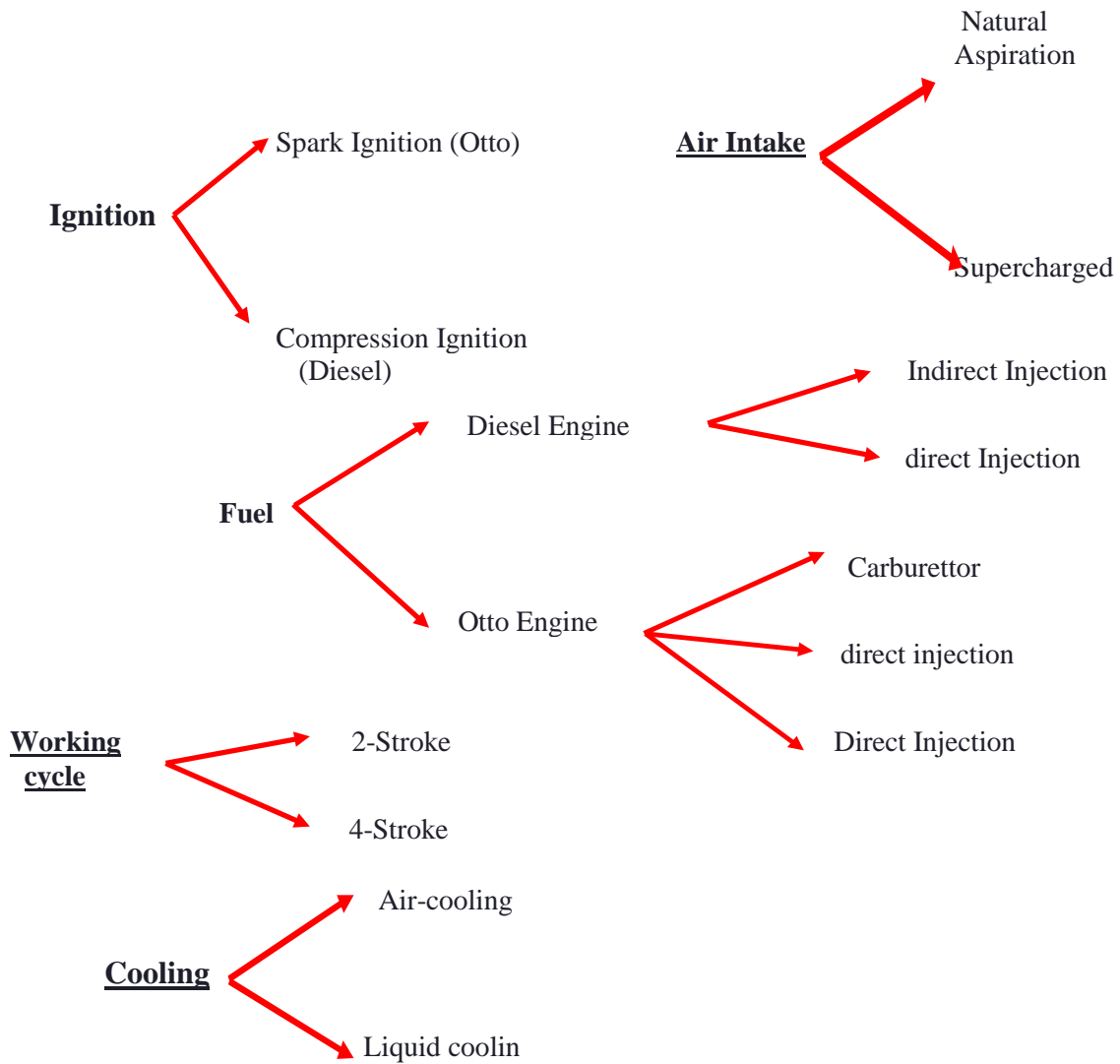


Figure.I.14: Engine of 4 Stroke

b) Comparing Diesel and Spark Ignition Engines



I.2.5. Spark ignition and compression ignition.

a) Spark Ignition: In spark-ignition engines, fuels with relatively low reactivity are used, such as gasoline, compressed natural gas (CNG), or liquefied petroleum gas (LPG). These fuels are mixed with air to form a homogeneous fuel-air mixture and compressed in the intake to reach air/fuel ratios, then compressed in the engine to reach temperatures of around 700 K (400 °C) and pressures of 20 bars, without any spontaneous ignition. This behavior can be explained by the molecular characteristics of the fuel: the fuels used in spark-ignition engines consist of short-chain molecules with a rigid and compact structure (such as CH₄ for CNG or iso-octane for gasoline C₈H₁₈), for which, even at high temperatures and pressures, the time required to initiate the combustion process is quite long. However, this concept should not be confused with the ability of a liquid fuel to evaporate at ambient temperature and form a combustible mixture in the surrounding air. Gasoline has a high capacity for this and poses an explosion risk if an ignition source is provided. In spark-ignition engines, combustion can only be initiated with an external energy source, such as an electric spark, as the energy supplied by the electrical discharge to the mixture is low but is sufficient for conventional combustion.



Figure.I.15: Spark engine motor (SI engine)

b) compression ignition: When fuels with higher reactivity are used, such as diesel, they cannot be mixed with air and then compressed in the cylinder because the combustion process would spontaneously ignite during the compression phase. Diesel is a mixture of hydrocarbons that can be represented by ‘Cetane’, C₁₆H₃₄, with a long straight chain molecule in which the preliminary reactions of the oxidation process proceed quite rapidly at high temperatures and pressures. Therefore, diesel is injected in the form of a liquid spray at high pressure into the already compressed air, immediately before the desired start of combustion (in the case of conventional diesel combustion). The small fuel droplets (approximately 10 μm in diameter), surrounded by the hot compressed air (approximately 900°K), evaporate rapidly, and the spontaneous combustion process begins with an extremely short auto-ignition delay.



Figure.I. 16: a diesel engine 4 cylinder (CI engine)

Table.I.2: table of comparison between Pertol and Diesel fuel

Petrol	Diesel
<p>In the context of a petrol engine, the efficacy of the fuel-air mixture is contingent upon the proximity of the petrol's vaporization temperature to the ambient air temperature. Conversely, the temperature at which petrol ignites within the compressed air must be maximized to prevent auto-ignition, given the compression of the mixture. The current compression ratio is constrained by this requirement.</p>	<p>In the Diesel engine, diesel fuel is non-volatile at ordinary temperatures, enhancing the impact force of the injected droplets. The temperature at which diesel ignites within the compressed air must be minimized. It should possess auto-ignition qualities, igniting rapidly within the combustion chamber at the moment of injection.</p>

1.2.6 Engine Configurations:

a)Straight Engine (Inline Engine): The cylinders are placed next to each other; in the automotive industry, small-displacement engines are often inline cylinder engines. For over 30 years, four-cylinder inline engines have become the standard in the automotive industry (Figure ...). These engines are known for their smooth operation. [7] Inline engines exist with 2, 3, 4, 5, and 6 cylinders. Inline engines can be mounted longitudinally or transversely. [8]

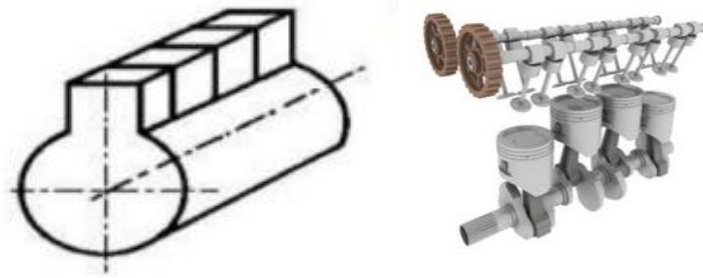


Figure.I.17: Straight Engine (Inline Engine)

b) V Engine: The cylinders are aligned in two offset rows at a certain angle (from 15° to 135°). This type of engine is more compact than an inline engine. It is also robust and wider, but smaller in height and length. V engines can also be mounted longitudinally or transversely. The name "V engine" comes from the fact that the rows of cylinders can be arranged in a V shape. [8]

A V engine can be more or less upright or inclined. When the angle is 90° and one of the two cylinders is horizontal, it is often referred to as "L-shaped cylinders."

Usage Example:

Generally, V engines are used in motorcycles.

- Engines with a 90° angle.
- Moto Guzzi engines with a 90° angle.
- Harley-Davidson and Buell engines with a 45° angle.



Figure.I. 18 : An engine with 'V' shape

C) Boxer Engine or "Flat" Engine:

The cylinders are opposed and horizontal (the cylinders face each other), called "Boxer." These engines help lower the center of gravity of cars. The pistons move in the same horizontal plane but in opposite directions, balancing the first and second-order inertia forces. However, in a twin-cylinder engine, the first and second-order inertia torques are not balanced because the opposing cylinders are not in the same transverse plane (Figure...).

In the case of a 4-cylinder engine, both the forces and the first-order inertia torques are balanced. [9]

Usage Examples:

- Citroën 2 CV engines for two-cylinder models.
- Volkswagen "Beetle" and Combi engines.
- Porsche 911 engines.
- Ferrari engines, including its 5-liter flat-twelve engine.



Figure.I.19: A Boxer Engine

d) W Engine: They can be Three-cylinder each cylinder is offset from the others by a certain angle, for example angle of the first cylinder relative to the second: 15° , angle of the third cylinder relative to the first: 30° . Also called a "fan" engine.

Usage Examples:

- W12 engines (12 cylinders).
- Bugatti Veyron 16.4 engines with W16 configuration (16 cylinders).



Figure.I.20: A 'W' Engine

e) **Radial / Star Engines:** Today, this type of engine is primarily used in propeller-driven aircraft. In aviation, it is crucial for the engine to be directly cooled (Figure I-21). These engines provide very high power, which is precisely what an aircraft requires.



Figure.I.21: a Radial/Star Engines

f) **U Engine:** The U engine is a type of combustion engine characterized by an arrangement of the cylinders in a U shape relative to each other and to the crankshafts. This type of engine is obtained when two inline engines are combined and connected to each other. [8]

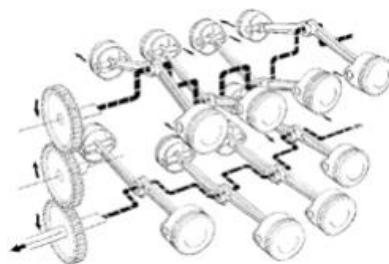


Figure.I.22 The 'U' engine type

I.3 Diesel engine combustion interne:

I.3.1principle:

A diesel engine operates distinctively from a gasoline engine. Despite their shared fundamental components and adherence to the same four-stroke cycle, diesel and spark-ignition engines exhibit notable differences, particularly in the ignition of the fuel-air mixture and the regulation of power output. In a gasoline engine, the fuel-air mixture ignites via an electric spark. Conversely, in a Diesel engine, ignition occurs through self-ignition of the fuel due to air compression-induced heating. A typical volumetric ratio for a diesel engine is around 20 to 1 (compared to 9 to 1 for a gasoline engine), which elevates the air temperature in the cylinder beyond 450°C. At this temperature, diesel fuel spontaneously ignites upon contact with air, obviating the need for spark ignition and ignition systems.

While a gasoline engine admits a variable mass of fuel-air mixture from cycle to cycle based on throttle opening, a Diesel engine consistently draws in the same air mass (at constant speed) through a conduit of constant section, with only the intake valve intervening (absent are carburetors or throttles). Following the intake phase, the intake valve closes, and the piston, driven by the inertia of the crankshaft-flywheel assembly, ascends towards the top of the cylinder, compressing the air to approximately 1/20 of its initial volume. At the end of this compression phase, a precisely metered quantity of diesel fuel is injected into the combustion chamber. Due to the high temperature of the compressed air, the fuel ignites immediately, and the expanding hot gases forcefully propel the piston. As the piston ascends during the exhaust phase, the exhaust valve opens to allow the burnt and expanded gases to evacuate into the exhaust system.

Upon completion of the exhaust phase, the cylinder is prepared to admit a fresh charge of air to initiate a new cycle.

I.3.2Advantages and disadvantages of the diesel engine :

a)The diesel engine provides better mechanical energy than the gasoline engine for the following reasons:

- Efficiency is high.
- The fuel used for diesel engines is relatively inexpensive.
- Exhaust gases are less toxic.
- Fire hazards are reduced. Indeed, diesel fuel only produces flammable vapors when heated to around 80°C, a temperature significantly higher than that of the ambient air. In contrast, gasoline produces flammable vapors at a much lower temperature.

combustion process contributes to improved thermodynamic performance and overall engine efficiency.

In the context of Diesel engine technology, the evolution towards common rail high-pressure injection systems with electronic management represents a thermodynamically favorable solution. These systems offer precise control over fuel delivery, ensuring optimal combustion conditions for enhanced efficiency and reduced emissions. The utilization of common rail technology, coupled with electronic control, allows for fine-tuning of injection parameters to maximize thermodynamic performance.

Overall, advancements in Diesel engine technology, driven by electronic control systems and high-pressure injection methods, are aimed at improving thermodynamic efficiency by optimizing combustion processes. By focusing on precise fuel delivery, combustion control, and emission reduction, manufacturers are striving to enhance the thermodynamic performance of Diesel engines while meeting stringent efficiency and environmental standards.

I.4 Thermodynamics cycles:

I.4.1 Definition: A thermodynamic cycle is a sequence of transformations where the thermodynamic system starts from a given state and returns to its initial state at the end of the cycle. This allows the same cycle to be repeated. Thermodynamic machines operate using such cycles.

During the cycle, the system undergoes changes in temperature, pressure, or other state parameters, while exchanging work and heat with the surroundings.

Cycles typically consist of four stages. The cycles presented here are theoretical thermodynamic cycles.

In real machines, these cycles are distorted

the best-known cycles are:

- The Carnot cycle (ideal cycle) which offers maximum yield.
- The Beau de Rochas (or Otto) cycle which is used by the gasoline engine
- The Diesel cycle
- The Stirling cycle
- The Brayton cycle (or Joule cycle) which is used by gas turbines.

I.4.2: The Diesel cycle: This is the operating cycle of compression ignition engines. The theoretical cycle consists of isobaric expansion, adiabatic expansion, and isochoric transformation. Initially, the operating cycle included a theoretical phase of combustion at constant pressure, as Rudolf Diesel had conceived. For a four-stroke engine operation, which occurs over two crankshaft revolutions and four piston strokes, the sequence of operations was as follows:

- Introducing air into the cylinder (either through natural aspiration or mechanically using a compressor).

- Compressing the air charge and spontaneously igniting the fuel.
- Combusting the mixture at nearly constant pressure, followed by the genuine expansion of the burnt gases, resulting in mechanical work production.
- Mechanically expelling combustion products through the piston's thrust action during its upward stroke. The thermal efficiency was characterized by two distinct ratios.

Future optimizations for diesel engines are likely to focus on advanced combustion technologies, including precision fuel injection systems such as higher-pressure direct injection and improved common rail designs, aimed at enhancing combustion efficiency and reducing fuel consumption. Additionally, advancements in lightweight yet durable materials for engine components, coupled with the integration of advanced sensors and electronic controls for optimized engine management, will contribute to improved performance and reduced emissions. Research into alternative fuels, hybridization, and enhanced exhaust after-treatment systems like advanced particulate filters and selective catalytic reduction (SCR) [11] will also play crucial roles in meeting future emission standards while maintaining engine reliability and efficiency.

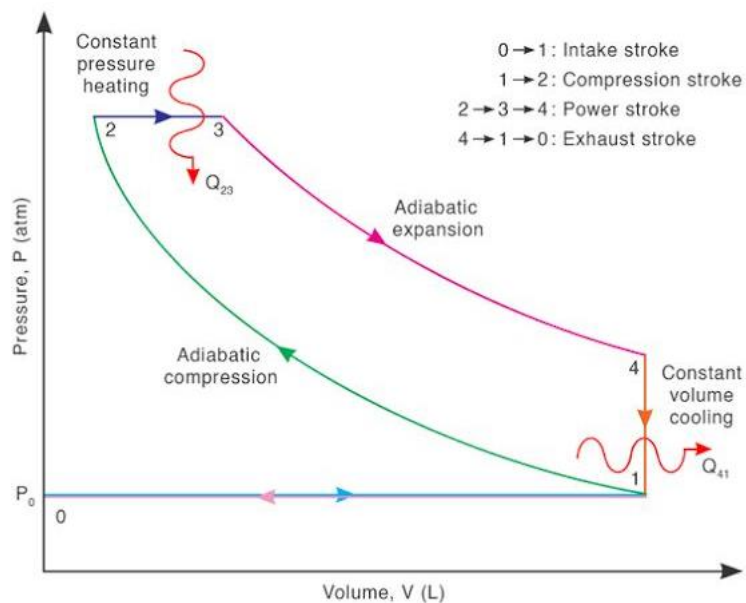


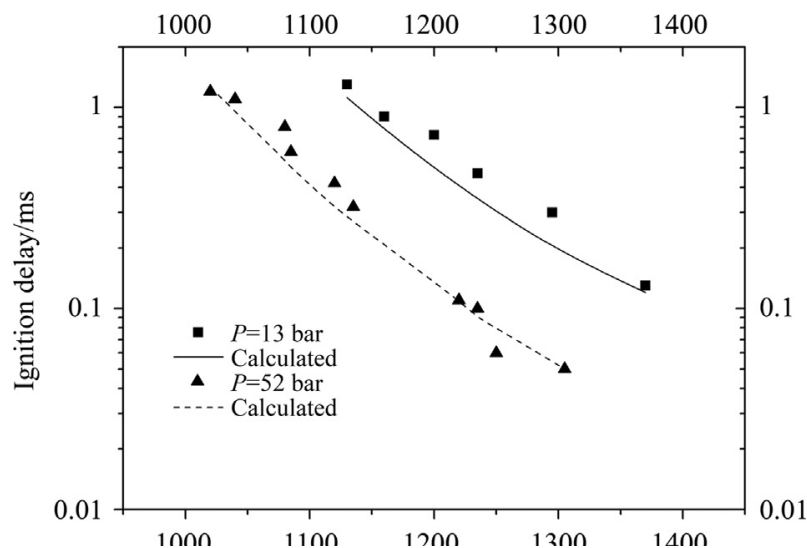
Figure.I.23: The Diesel cycle

Table.I.3 : Diesel cycle transformation

1	Isobaric transformation (pressure constant)	Air suction
2	Adiabatic transformation (without heat exchange with the external environment).	High air compression at a temperature of 600°C.
3	Isobaric transformation	Injection of diesel fuel which ignites spontaneously (combustion) thanks to the heat released during compression
4	Adiabatic transformation.	Relaxation providing motor work.
5	Isochoric transformation (volume constant)	Reduced pressure
6	Isobaric transformation	Exhaust of burnt gases

1.5 The Current Studies in Internal Combustion Engine

In the field of diesel combustion research, the development and validation of reduced oxidation mechanisms plays a crucial role in understanding and simulating the complex combustion processes. Researchers like Kesong Zhang, Qiangzhi Xin, Zhenqian Mu, Zhijian Niu, and Zhiming Wang have been actively involved in exploring the numerical simulation of diesel combustion using n-heptane and toluene as surrogate fuels [12].

**Figure.I.24:** Calculated and measured toluene ignition delay for different pressures.

These researchers have focused on developing reduced oxidation mechanisms that are essential for accurately predicting ignition delay, oxidation pathways, and combustion characteristics in diesel engines. Through combustion experiments in constant volume vessels and real diesel engines, they have highlighted the importance of selecting representative species for mechanism development and understanding the impact of additives on oxidation pathways [12].

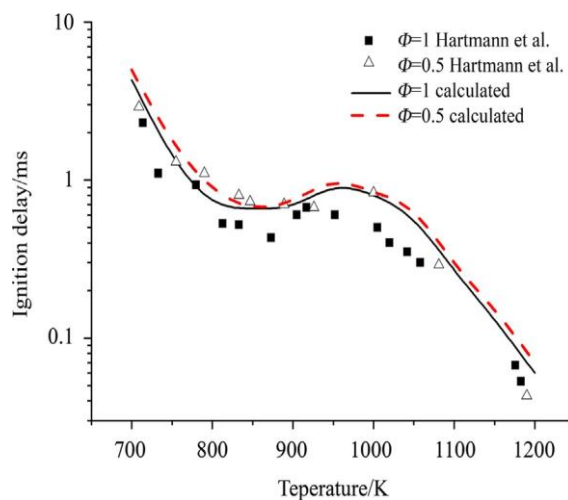


Figure.I. 25: Calculated and measured toluene ignition delay for different pressures.

By integrating experimental data and numerical simulations, the researchers have aimed to explore the applicability of reduced mechanisms for simulating diesel combustion under various conditions and in different engines. The study emphasizes the need for detailed reaction progress analysis, especially in diffusion combustion, to optimize combustion efficiency and reduce NO_x emissions [12].

The development of a systematic spray model for 3D CFD evaluation and the validation of reduced oxidation mechanisms for n-heptane and toluene further demonstrate the researchers' commitment to advancing the understanding of diesel combustion processes [12].

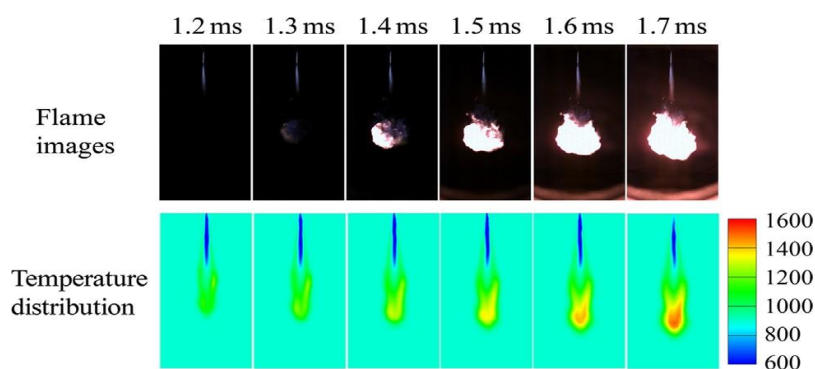


Figure.I. 26: Time sequences of experiment and simulation for EGR-1.

Moreover, the use of diesel surrogate fuels like n-heptane and toluene has provided valuable insights into the chemical properties of these fuels and their impact on combustion flame behaviour [12].

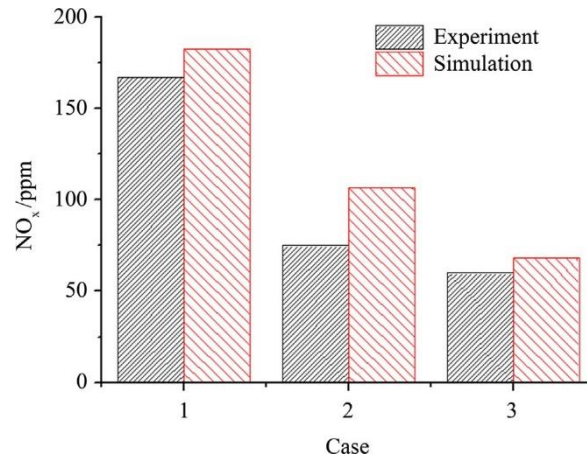


Figure.I. 27 : Calculated and mesured Cylinder pressure for small diesel case

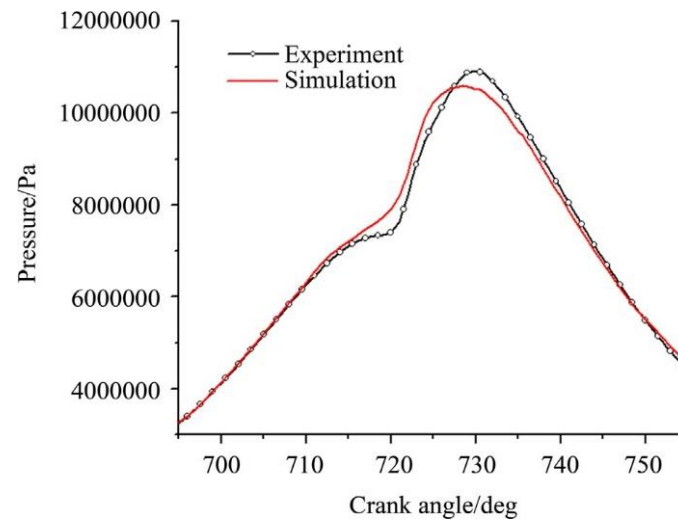


Figure.I.28: NO_x emission for small diesel

By carefully selecting these representative species and developing reduced oxidation mechanisms, researchers have been able to effectively simulate diesel combustion in various engines and conditions, contributing to the optimization of engine performance and emissions control [12].

Table I.4: Oxidation mechanism and rate coefficients.

No.	Reactions	$A/(\text{mol} \cdot \text{cm} \cdot \text{s} \cdot \text{K})$	b	$E/(\text{cal/mol})$
1	$\text{C}_7\text{H}_{16} + \text{O}_2 = \text{C}_7\text{H}_{15} + \text{HO}_2$	1.00E+16	0	46,000
	Reverse Arrhenius coefficients:	1.00E+12	0	0
2 ^a	$\text{C}_7\text{H}_{16} + \text{OH} = \text{C}_7\text{H}_{15} + \text{H}_2\text{O}$	6.00E+14	0	3000
3	$\text{C}_7\text{H}_{15} + \text{O}_2 = \text{C}_7\text{H}_{15}\text{O}_2$	1.00E+12	0	0
	Reverse Arrhenius coefficients:	2.51E+13	0	27,400
4	$\text{C}_7\text{H}_{15}\text{O}_2 = \text{C}_7\text{H}_{14}\text{OOH}$	1.51E+11	0	19,000
	Reverse Arrhenius coefficients:	1.00E+11	0	11,000
5	$\text{C}_7\text{H}_{14}\text{OOH} + \text{O}_2 = \text{O}_2\text{C}_7\text{H}_{14}\text{OOH}$	3.16E+11	0	0
	Reverse Arrhenius coefficients:	2.51E+13	0	27,400
6	$\text{O}_2\text{C}_7\text{H}_{14}\text{OOH} = \text{C}_7\text{KET} + \text{OH}$	8.91E+10	0	17,000
7	$\text{C}_7\text{KET} = \text{C}_3\text{H}_{11} + \text{CO} + \text{CH}_2\text{O} + \text{OH}$	2.40E+17	-2	30,000
8	$\text{C}_3\text{H}_{11} = 2\text{C}_2\text{H}_4 + \text{CH}_3$	1.00E+12	0	40,000
9 ^a	$\text{C}_7\text{H}_{15} = 3\text{C}_2\text{H}_4 + \text{CH}_3$	1.00E+15	0	42,000
10	$\text{C}_2\text{H}_4 + \text{O}_2 = 2\text{CH}_2\text{O}$	3.00E+13	0	30,000
11	$\text{C}_2\text{H}_2 + \text{OH} = \text{CH}_3 + \text{CO}$	5.00E+04	4	-2000
12	$\text{CH}_3 + \text{O}_2 = \text{CH}_2\text{O} + \text{OH}$	7.47E+11	0	14,250
13	$\text{CH}_2\text{O} + \text{OH} = \text{HCO} + \text{H}_2\text{O}$	3.43E+09	1.2	-447
14	$\text{CH}_2\text{O} = \text{HCO} + \text{H}$	3.31E+16	0	81,000
15	$\text{HCO} + \text{OH} = \text{H}_2\text{O} + \text{CO}$	1.00E+14	0	0
16	$\text{HCO} + \text{M} = \text{H} + \text{CO} + \text{M}$	1.50E+16	-1.3	18,000
	Reverse Arrhenius coefficients:	6.47E+13	0	-442
17	$\text{CO} + \text{OH} = \text{CO}_2 + \text{H}$	1.40E+05	2	-1347
18	$\text{CO} + \text{O} = \text{CO}_2$	1.80E+10	0	2384
19	$\text{CO} + \text{O}_2 = \text{CO}_2 + \text{O}$	1.62E+13	0	47,700
	Reverse Arrhenius coefficients:	1.43E+14	0	53,920
20	$\text{H} + \text{O}_2 = \text{O} + \text{OH}$	1.97E+14	0	16,540
	Reverse Arrhenius coefficients:	1.56E+13	0	425
21	$\text{H} + \text{OH} = \text{H}_2\text{O}$	2.21E+22	-2	0
22	$\text{HO}_2 + \text{OH} = \text{H}_2\text{O} + \text{O}_2$	2.89E+13	0	-500
23 ^a	$\text{A}_1\text{CH}_3 + \text{O}_2 = \text{A}_1\text{CH}_2 + \text{HO}_2$	2.18E+07	2.5	47,300
24	$\text{A}_1\text{CH}_3 + \text{OH} = \text{A}_1\text{CH}_2 + \text{H}_2\text{O}$	1.77E+05	2.4	-602
25	$\text{A}_1\text{CH}_2 + \text{O}_2 = \text{A}_1\text{CHO} + \text{OH}$	3.76E+15	-1.6	47
26	$\text{A}_1\text{CHO} + \text{OH} = \text{A}_1 + \text{CO} + \text{H}_2\text{O}$	2.89E+08	1.3	-1573
27	$\text{A}_1 + \text{O}_2 = \text{OC}_2\text{H}_4\text{O} + \text{H}$	3.00E+13	0	8981.8
28 ^a	$\text{OC}_2\text{H}_4\text{O} = 2\text{C}_2\text{H}_2 + 2\text{CO}$	1.00E+12	2.4	90,000
29	$\text{O} + \text{N}_2 = \text{NO} + \text{N}$	2.56E+12	0	75,502
30	$\text{N} + \text{O}_2 = \text{NO} + \text{O}$	6.40E+09	1	6286
31	$\text{N} + \text{OH} = \text{NO} + \text{H}$	3.28E+13	0	0

Note: ^a the reaction parameters have been refined by AGA.

In summary, the work of researchers like Kesong Zhang and team highlights the significance of reduced oxidation mechanism development in advancing the understanding of diesel combustion processes. Through their studies, they have demonstrated the importance of accurate numerical simulations for optimizing combustion efficiency and reducing emissions in diesel engines.

In the study by Pastor et al. , an experimental investigation was conducted to analyse the impact of fuel properties on reactive spray evolution using Primary Reference Fuels (PRFs). Six different binary blends of PRFs were tested under various conditions to understand the ignition and combustion behavior of fuel sprays. The focus was on transitioning from a conventional diesel fuel (n-heptane) to a gasoline-like one (iso-octane) by blending these two fuels [13]

The experiments were carried out in a high-temperature and high-pressure test chamber capable of replicating conditions similar to those in a diesel engine, with maximum ambient temperature reaching

1000 K and pressure up to 15 MPa Optical techniques such as schlieren imaging, broadband luminosity imaging, and OH chemiluminescence imaging were employed to study spray penetration, autoignition delay, sooting intensity, and flame lift-off length The optical setup included a CMOS camera, a Xenon lamp, parabolic mirrors, lenses, and filters to capture and analyse the spray behavior [13].

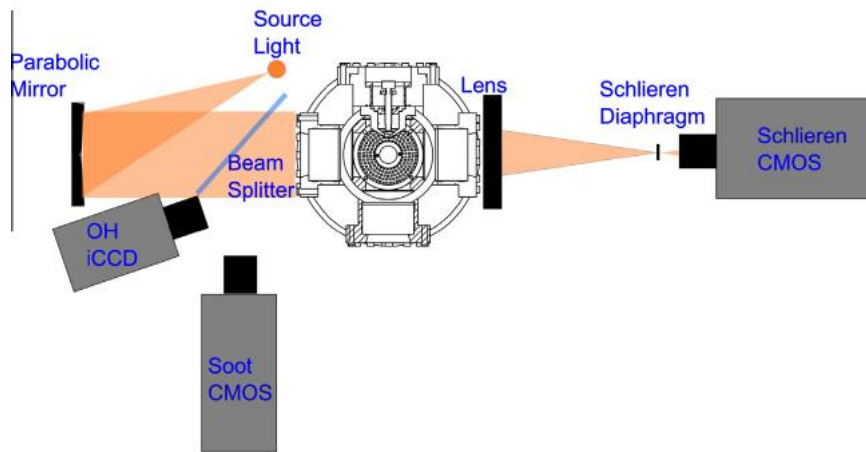


Figure.I.29: Schematic of the experimental setup for the study of the reactive spray

The results of the study revealed significant findings regarding the effects of fuel properties on spray penetration, ignition delay, and soot radiation. The evolution of the reactive spray showed distinct characteristics compared to the inert spray, especially during the ignition phase. The analysis of spray tip penetration, flame length, and soot onset length provided insights into the differences between inert and reactive conditions, highlighting the impact of fuel reactivity on spray behavior [13].

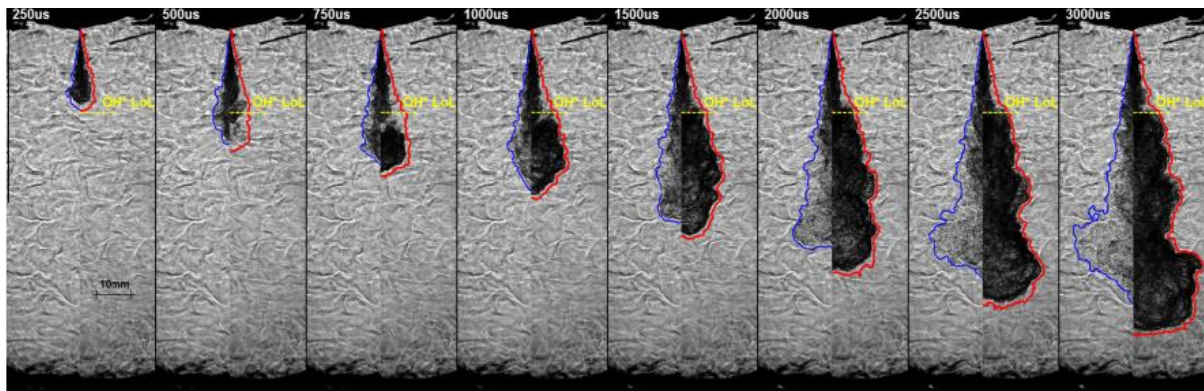


Figure.I. 30: Evolution of inert (blue) and reactive (red) spray penetration for PRF0 at 900 K, 15% O₂ and 150 MPa, time after SoI.

Furthermore, the study validated the momentum-controlled scaling law for stabilized flame length, confirming that the stabilization of the diffusion flame is primarily controlled by mixing arguments

rather than fuel reactivity. The normalized flame length (FL_{norm}) was found to be influenced by ambient temperature and oxygen concentration variations, indicating the importance of these parameters in spray ignition and combustion processes. Overall, the research contributed to a better understanding of fuel spray mixing, ignition, and sooting processes under varying conditions, shedding light on the complex interactions between fuel properties and combustion behaviour[13].

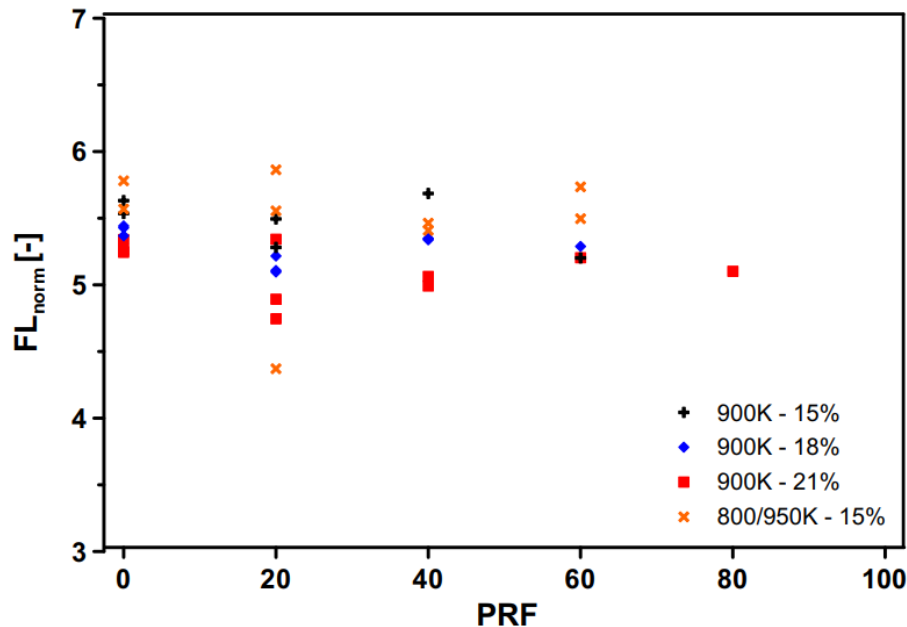


Figure.I. 31 : Normalized flame length (FL_{norm}) versus fuel composition at ambient temperature and oxygen concentration variations

1.6 characteristics of flow at the outlet of an injector

a) Spray Cone Angle: The spray cone angle refers to the divergence of the spray plume as it exits the injector nozzle. It is an important parameter that influences the spray pattern and distribution of fuel droplets in the combustion chamber.

b) Spray Penetration: Spray penetration is the distance travelled by the fuel spray from the injector nozzle to the point where the spray breaks up or vaporizes. It is a critical factor in determining the fuel-air mixing and combustion efficiency.

c) Droplet Size Distribution: The size distribution of fuel droplets in the spray affects the combustion process, as smaller droplets tend to evaporate more quickly and combust efficiently compared to larger droplets.

d) Spray Breakup and Atomization: The breakup and atomization of the liquid fuel spray into smaller droplets play a significant role in enhancing fuel-air mixing and combustion efficiency in the engine.

e) **Spray Plume Velocity:** The velocity of the spray plume at the outlet of the injector influences the momentum and penetration of the spray into the combustion chamber, impacting the overall combustion process.

f) **Spray Shape and Symmetry:** The shape and symmetry of the spray pattern at the outlet of the injector can affect the distribution of fuel droplets and the combustion stability within the engine.

These characteristics are crucial in optimizing the design and performance of injectors for efficient fuel atomization, mixing, and combustion in internal combustion engines



Figure.I.32: Air nozzle

I.6.1 Cold Flow Analysis: Cold flow analysis plays a crucial role in understanding the behaviour of fluids, such as air and fuel, before the combustion process in internal combustion engines. It involves studying the fluid dynamics, spray characteristics, and mixing processes that occur within the engine's intake system, fuel injectors, and combustion chamber. By simulating cold flow conditions, engineers can optimize the design of intake systems and fuel injectors to enhance fuel atomization, air-fuel mixing, and overall combustion efficiency.

One of the key aspects of cold flow analysis is the study of spray characteristics. This includes analysing the spray cone angle, spray penetration, droplet size distribution, and spray shape as the fuel is injected into the combustion chamber. Understanding these characteristics is essential for achieving proper fuel-air mixing, which directly impacts combustion efficiency and emissions performance. Cold flow simulations also help in identifying potential issues such as fuel impingement on the cylinder walls or incomplete vaporization of fuel droplets.

Moreover, cold flow analysis provides valuable insights into the fluid dynamics within the engine, including airflow patterns, turbulence levels, and pressure distribution. By optimizing these flow characteristics, engineers can improve engine performance, fuel efficiency, and emissions control. Cold

flow simulations are often used in the design and development of new engine components, such as intake manifolds, valves, and injectors, to ensure optimal performance under various operating conditions.

1.6.2 Hot Flow Analysis: Hot flow analysis focuses on the behavior of fluids at elevated temperatures during the combustion process in internal combustion engines. It involves studying combustion reactions, heat release mechanisms, flame propagation, and energy transfer within the combustion chamber. By simulating hot flow conditions, engineers can gain insights into the combustion efficiency, emissions formation, and overall performance of the engine.

One of the primary objectives of hot flow analysis is to optimize the combustion process for maximum efficiency and minimal emissions. This includes studying the ignition timing, fuel-air ratio, flame speed, and heat release rate to achieve complete combustion of the fuel mixture. Understanding the complex interactions between turbulence, chemical reactions, and heat transfer is essential for improving engine efficiency and reducing harmful emissions.

Hot flow simulations also help in predicting the temperature distribution within the combustion chamber, which is critical for preventing engine knock, thermal stress, and exhaust gas overheating. By accurately modeling the combustion process, engineers can optimize the design of combustion chambers, piston shapes, and fuel injection strategies to enhance performance and durability.

Comparison and Conclusion: In comparison, cold flow analysis focuses on fluid behavior and spray characteristics before combustion, while hot flow analysis delves into combustion processes and heat release during combustion. Cold flow simulations are essential for optimizing fuel atomization, air-fuel mixing, and intake system design, while hot flow simulations aid in understanding combustion efficiency, emissions formation, and combustion chamber performance.

Both cold flow and hot flow analyses are integral parts of the engine development process, providing valuable insights into fluid dynamics, combustion processes, and performance optimization. By combining cold flow and hot flow simulations, engineers can design more efficient and environmentally friendly internal combustion engines that meet stringent performance and emissions requirements.

In conclusion, cold flow analysis helps optimize fuel-air mixing and spray characteristics, while hot flow analysis is essential for enhancing combustion efficiency and emissions control in internal combustion engines. By leveraging the neologies that deliver superior performance, fuel efficiency, and environmental sustainability, insights gained from both cold and hot flow simulations, engineers can develop advanced engine tech

Conclusion

In summary, this chapter's exploration has provided a comprehensive understanding of internal combustion engines, particularly diesel engines, by delving into their composition, thermodynamic principles, and unique characteristics. The analysis of recent advancements, including fuel injection methods and combustion control techniques, has underscored the ongoing innovation in engine technology. Moreover, the examination of flow dynamics and combustion processes has deepened insights into engine performance and emissions. Looking ahead, the future of internal combustion engines hinges on further technological advancements aimed at enhancing performance, reducing emissions, and adapting to evolving regulatory standards. This will likely involve continued research into fuel injection systems, combustion optimization strategies, and the integration of hybrid or alternative power sources, while also addressing environmental concerns and promoting the development of sustainable fuel options for long-term viability in a changing automotive landscape

Chapitre2 :

Numerical modeling

II.1 Introduction

Numerical modeling stands as a cornerstone in engineering, particularly in the realm of internal combustion engines, where it plays a pivotal role in simulating complex fluid dynamics and combustion processes. Leveraging sophisticated methods like the finite volume approach, engineers utilize powerful software tools such as OpenFOAM to construct intricate computational models. These models are designed to meticulously predict and analyze a wide array of phenomena including flow patterns, temperature distributions, and combustion behaviors across diverse operational scenarios.

Central to the accuracy of these simulations is the creation of highly refined mesh structures that effectively discretize the computational domain. These meshes are crucial for capturing intricate details within the engine, ensuring simulations yield precise insights into performance metrics such as power output, fuel efficiency, and emissions characteristics. Moreover, the application of realistic boundary conditions—simulating factors like intake and exhaust dynamics, injector behavior, and thermal interactions—further enhances the fidelity of these virtual experiments to real-world conditions.

In the domain of combustion modeling, the integration of advanced combustion models with turbulence modeling techniques, such as Reynolds-averaged Navier-Stokes (RANS), enables engineers to delve deep into turbulent combustion processes. This integration provides comprehensive understanding and optimization of combustion efficiency, pollutant formation, and thermal management strategies within the engine.

Overall, numerical modeling empowers engineers and researchers to explore and refine designs, improve operational strategies, and optimize performance without the constraints of physical prototypes. By harnessing the capabilities of numerical simulations, advancements in internal combustion engine technology continue to drive innovation towards enhanced efficiency, reduced emissions, and sustainable energy solutions for the future.

II.2 Equation Modeling

The Navier-Stokes equations are fundamental in fluid mechanics, governing the behavior of viscous fluids by accounting for momentum, mass, energy conservation, viscosity, and pressure gradients. In computational fluid dynamics (CFD), these equations are essential for simulating diverse flow phenomena, including aerodynamics and combustion processes in internal combustion engines. Engineers and researchers utilize numerical methods such as the finite volume approach to discretize and solve these equations computationally.

Numerous software tools are employed for Navier-Stokes simulations, including OpenFOAM, a versatile open-source CFD toolbox renowned for its flexibility and robust solver library. Developed by the OpenFOAM Foundation, it supports various applications, from turbulent and multiphase flows to heat transfer processes. Other notable CFD software packages, like Fluent, STAR-CCM+, and

COMSOL Multiphysics, also provide comprehensive capabilities for simulating complex fluid dynamics across different industries.

By utilizing software such as OpenFOAM, engineers can conduct detailed simulations to analyze fluid behaviors, optimize designs, predict performance metrics, and explore complex flow phenomena under diverse operating conditions. These simulations are pivotal in advancing engineering solutions across aerospace, automotive, energy, and environmental sectors, driving innovation and efficiency in fluid mechanics applications.

OpenFOAM prioritizes a direct link between the governing equations and solver code. This is achieved by leveraging its object-oriented framework and built-in classes. For instance, the material derivative, expressed as $d\phi/dt$, which describes the time rate of change of an intensive property (ϕ), can be directly implemented within OpenFOAM code. This approach enhances code readability and maintainability, as the solver code closely resembles the mathematical notation of the governing equations.

$$\frac{\partial}{\partial t}(\rho\phi) + \nabla(\rho\phi\vec{u}) = \nabla(\Gamma\nabla\phi) + S_\phi \quad (1)$$

This equation, although more general, simplifies to the incompressible Navier-Stokes equation for fluids with constant density. It describes the balance of forces acting on a fluid element:

Left side: Represents the rate of change of density (which is typically zero for incompressible fluids) and the contributions of momentum transport (convection and viscous diffusion).

Right side: Represents the pressure gradient force acting on the fluid.

II.2.1 GOVERNING EQUATIONS :

This section focuses on governing equations for **continuum mechanics**. The characteristic scales (length and time) of these problems are much larger (orders of magnitude) compared to the microscopic structure of the matter involved (e.g., combustion chamber in an engine). Therefore, macroscopic properties like temperature (T), pressure (p), and mass fraction (Y) can be treated as continuous functions of space (r) and time (t). For conciseness, these equations are written in vector notation with unit vectors (i, j, k) for x, y , and z directions, and the position vector defined as \vec{r} :

$$\vec{r} = x\vec{i} + y\vec{j} + z\vec{k} \quad (2)$$

the vector operator ∇ is given by:

$$\nabla = \vec{i} \frac{\partial}{\partial x} + \vec{j} \frac{\partial}{\partial y} + \vec{k} \frac{\partial}{\partial z} \quad (3)$$

and the fluid velocity vector \vec{u} is given by:

$$\vec{u} = u(x, y, z, t)\vec{i} + v(x, y, z, t)\vec{j} + w(x, y, z, t)\vec{k} \quad (4)$$

In order to simulate the dynamics within a diesel engine's combustion chamber, we need to solve the conservative/transport equations for continuity, momentum, and energy. Additionally, other relevant physical models like combustion, heat transfer, equation of state, and turbulence must be incorporated. This study utilizes these equations and sub-models, specifically those applicable to Newtonian fluids, for simulating the behavior of the fuel-air mixture injected by the injectors.

II.2.2 Continuity Equation

The continuity equation for species m can be written as:

$$\frac{\partial \rho_m}{\partial t} + \nabla \cdot (\rho_m \vec{u}) = \nabla \cdot \left[\rho D \nabla \left(\frac{\rho_m}{\rho} \right) \right] + \dot{\rho}_m^c \quad (5)$$

This describes a model for reacting flows with multiple components. It tracks individual densities (ρ_m) and total density (ρ), incorporates fluid motion (\vec{u}), and uses Fick's Law for diffusion (D). Chemical reactions are included via a source term. Summing the governing equation across all components yields the total density equation and becomes:

$$\frac{\partial \rho}{\partial t} + \nabla \cdot (\rho \vec{u}) = 0 \quad (6)$$

As long as mass is conserved in chemical reactions.

II.2.3 Momentum equation:

$$\frac{\partial (\rho \vec{u})}{\partial t} + \nabla \cdot (\rho \vec{u} \vec{v}) = -\nabla p - \nabla \left(\frac{2}{3} \rho k \right) + \nabla \cdot \tilde{\sigma} + \rho \vec{g} \quad (7)$$

Where p is fluid pressure

The viscous stress tensor $\tilde{\sigma}$ is Newtonian in form, consequently:

$$\tilde{\sigma} = \mu_{eff} [\nabla \vec{u} + (\nabla \vec{u})^\tau] + \lambda \nabla \cdot \vec{u} \tilde{I} \quad (8)$$

The first and second coefficients of viscosity μ_{eff} and λ are defined below. The superscript τ denotes the transpose operator and \tilde{I} is the unit dyadic. The specific body force \vec{g} is assumed constant.

II.2.4 Turbulent Kinetic Energy and Dissipation Models :

Kinematic eddy viscosity (μ_{eff}), which reflects the turbulent mixing in a fluid, can be determined through various methods. Simple approaches use algebraic relations or local equilibrium assumptions. However, the most common method involves solving transport equations for two key turbulence properties: turbulent kinetic energy (k) and its dissipation rate (ϵ). This approach leads to the

development of two-equation turbulence models. In essence, these models predict μ_{eff} based on the interplay between the energy of turbulence (k) and how quickly that energy is dissipated (ε).

$$\frac{\partial(\rho k)}{\partial t} + \nabla \cdot (\rho \vec{u} k) = - \left(\frac{2}{3} \rho k \right) \nabla \cdot \vec{u} + \tilde{\sigma} : \nabla \vec{u} + \nabla \cdot \left[\frac{\mu_{eff}}{Pr_k} \nabla k \right] - \rho \varepsilon \quad (9)$$

And :

$$\begin{aligned} \frac{\partial(\rho \varepsilon)}{\partial t} + \nabla \cdot (\rho \vec{u} \varepsilon) = & - \left(\frac{2}{3} c_{\varepsilon 1} - c_{\varepsilon 3} \right) \rho \varepsilon \nabla \cdot \vec{u} + \nabla \cdot \left[\left(\frac{\mu_{eff}}{Pr_{\varepsilon}} \right) \nabla \varepsilon \right] \\ & + \frac{\varepsilon}{k} [c_{\varepsilon 1} \tilde{\sigma} : \nabla \vec{u} - c_{\varepsilon 2} \rho \varepsilon] \end{aligned} \quad (10)$$

Equations (9) and (10) extend the k - ε turbulence model with terms accounting for velocity dilation effects. Constants are derived empirically and theoretically. In Equation (9), terms represent changes in turbulent kinetic energy, convection, compressibility, turbulence generation by shear, self-diffusion, and dissipation. Equation (10) similarly defines terms for turbulence dissipation rate.

II.2.5 Internal energy

The internal energy equation is given by:

$$\frac{\partial(\rho I)}{\partial t} + \nabla \cdot (\rho \vec{u} I) = -p \nabla \cdot \vec{u} - \nabla \cdot \vec{J} + \rho \varepsilon + \dot{Q}^c \quad (11)$$

Here, I represents the specific internal energy, excluding chemical energy. The heat flux vector, \vec{J} encompasses contributions from both heat conduction and enthalpy diffusion, and is expressed as:

$$\vec{J} = -K \nabla T - \rho D \sum_m h_m \nabla (\rho_m / \rho) \quad (12)$$

Here, T denotes the fluid temperature and h_m the specific enthalpy of species m . The source term from chemical heat release, \dot{Q}_c , is defined below:

II.2.6 Equations of state

The state constitutive equations are assumed to follow those of an ideal gas mixture.

Therefore:

$$p = R_0 T \sum_m (\rho_m / W_m) \quad (13)$$

$$I(T) = \sum_m (\rho_m / \rho) I_m(T) \quad (14)$$

$$c_p(T) = \sum_m (\rho_m / \rho) c_{pm}(T) \cdot \frac{c_{pm}^0}{R_0} = \quad (15)$$

$$= a_{1m} + a_{2m} T_m + a_{3m} T_m^2 + a_{4m} T_m^3 + a_{5m} T_m^4$$

$$h_m(T) = I_m(T) + R_0 T / W_m \quad (16)$$

$$\Rightarrow \frac{h_{pm}^0}{R_0 T_m} = a_{1m} + \frac{a_{2m}}{2} T_m + \frac{a_{3m}}{3} T_m^2 + \frac{a_{4m}}{4} T_m^3 + \frac{a_{5m}}{5} T_m^4 + \frac{a_{6m}}{6}$$

$$\frac{s_m^0}{R_0} = a_{1m} \ln T_m + a_{2m} T_m + \frac{a_{3m}}{2} T_m^2 + \frac{a_{4m}}{3} T_m^3 + \frac{a_{5m}}{4} T_m^4 + a_{6m} \quad (17)$$

In this analysis, the notation "o" refers to the standard state defined at a pressure of 1 atmosphere. The universal gas constant is symbolized by R_0 , and W_m denotes the molecular weight of species m . The specific internal energy of species m is represented by $I_m(T)$, while C_{pm} indicates the specific heat capacity at constant pressure for species m . The specific entropy at standard state is denoted by s_m^0 . The parameters for $h_m(T)$, $C_{pm}(T)$, and s_m^0 are derived from the [14]

II.2.7 Chemical reaction:

The chemical reactions occurring within the combustion chamber are described by the following model:



where X_m represents one mole of species m , and a_{mr} and b_{mr} are integral stoichiometric coefficients for reaction r . The stoichiometric reaction coefficients must satisfy:

$$\sum_m (a_{mr} - b_{mr}) W_m = 0 \quad (19)$$

so that mass is conserved in the chemical reactions. The chemical reactions are divided into two categories: those that proceed kinetically and those that are assumed to be in equilibrium. The rate of a kinetic reaction r , denoted by $\dot{\omega}_r$, is given by:

$$\dot{\omega}_r = k_{fr} \prod_m (\rho_m / W_m)^{a'_{mr}} - k_{br} \prod_m (\rho_m / W_m)^{b'_{mr}} \quad (20)$$

The reaction orders are a'_{mr} and b'_{mr} , and they are not necessarily equal to a_{mr} and b_{mr} . Thus, empirical reaction orders can be utilized. The coefficients k_{fr} and k_{br} are assumed to follow a generalized “Arrhenius equation” form:

$$k_{fr} = A_{fr} T^{\xi_{fr}} \exp(-E_{fr}/T) \quad (21)$$

And

$$k_{br} = A_{br} T^{\xi_{br}} \exp(-E_{br}/T) \quad (22)$$

Where E_{fr} and E_{br} are the activation temperatures for the forward and backward reactions, respectively. The rates of equilibrium reactions are implicitly determined by the constraint conditions:

$$K_c^r(T) = \prod_m (\rho_m / W_m)^{(b_{mr} - a_{mr})} \quad (23)$$

where K_c^r , the concentration equilibrium constant, is assumed to have the form:

$$K_c^r(T) = \exp(A_r \ln T_A + B_r / T_A) + C_r + D_r \cdot T_A + E_r \cdot T_A^2 \quad (24)$$

Notice that : $T_A = T/1000 K$

From the previously mentioned equations, the reaction rates $\dot{\omega}_r$ are determined by Equation (19) or (20). Therefore, the chemical source term in the species continuity equation is given by:

$$\dot{\rho}_m^c = W_m \sum_m (a_{mr} - b_{mr}) \dot{\omega}_r \quad (25)$$

The chemical heat release term in the energy equation is defined as:

$$\dot{Q}^c = \sum_r Q_r \dot{\omega}_r \quad (26)$$

Where Q_r represents the negative of the heat of reaction at absolute zero temperature.

$$Q_r = \sum_m (a_{mr} - b_{mr}) (\Delta h_f^0)_m \quad (27)$$

and $(\Delta h_f^0)_m$ represents the heat of formation of species m at absolute temperature zero. The transport coefficients specified in the aforementioned equations are:

$$\mu = \mu_{air} + c_\mu k^2 / \epsilon \quad (28)$$

$$\lambda = A_3 \mu \quad (29)$$

$$K = \frac{\mu c_p}{Pr} \quad (30)$$

And,

$$D = \frac{\mu}{\rho S_c} \quad (31)$$

c_μ is an empirical constant with a standard value of 0.09. The Sutherland formula employed for μ_{air} is expressed as follows:

$$\mu_{air} = \frac{A_1 T^{3/2}}{T + A_2} \quad (32)$$

Where A_1 and A_2 represent constants. The constant A_3 is assumed to be $-\frac{2}{3}$ in the turbulent flow calculation. Pr and Sc denote the ‘‘Prandtl’’ and Schmidt numbers, respectively, and they are input constants.

II.3 Equations of aerothermochemistry :

Aerothermochemistry integrates the principles of thermodynamics, chemical kinetics, and fluid dynamics to analyze reacting flows, especially at high temperatures. This field uses the equations for species conservation, energy conservation, and momentum to model combustion processes, allowing us to optimize engine designs, understand hypersonic vehicle behavior, and develop advanced propulsion systems.

II.3.1 Continuity Equation

Since mass is conserved during chemical reactions, the equation expressing mass retention is given as follows:

$$\frac{\partial \rho}{\partial t} + \frac{\partial(\rho u_i)}{\partial x_i} = 0 \quad (33)$$

The conservation equation for species k is written as:

$$\frac{\partial \rho Y_k}{\partial t} + \frac{\partial(\rho(u_i + V_{k,i})Y_k)}{\partial x_i} = \omega_k \quad (34)$$

With $V_{k,i}$ the component of the diffusion velocity of species k, Y_k its mass fraction, and ω_k the rate of production of species k.

II.3.2 Equation of Conservation of Momentum:

$$\frac{\partial(\rho u_i)}{\partial t} + \frac{\partial}{\partial(x_i)}(\rho u_i u_j) = -\frac{\partial \rho}{\partial x_i} + \frac{\partial \tau_{ij}}{\partial x_i} + \rho F_i \quad (35)$$

Where

τ_{ij} : is the viscous stress tensor

F_i : represents the components of external body forces (such as gravity)

With

$$\tau_{ij} = \mu \left(\frac{\partial u_i}{\partial x_j} + \frac{\partial u_j}{\partial x_i} - \frac{2}{3} \delta_{ij} \frac{\partial u_k}{\partial x_k} \right) \quad (36)$$

II.3.3 Energy Conservation Equation:

The energy conservation equation for a reactive flow can be written using the enthalpy formulation as follows:

$$\frac{\partial(\rho h_t)}{\partial t} + \frac{\partial}{\partial x_i}(\rho h_i u_i) = \frac{\partial P}{\partial t} + \frac{\partial J_j^h}{\partial x_i} + \frac{\partial(u_i \tau_{ij})}{\partial x_i} \quad (37)$$

With

$$J_j^h = -\frac{\mu_l}{P_r} \left[\frac{\partial h}{\partial x_j} + \Sigma \left(\frac{P_r}{s_{ck}} - 1 \right) h_k \frac{\partial Y_k}{\partial X_j} \right] \quad (38)$$

- Conservation Equation:

$\frac{\partial(\rho h_t)}{\partial t}$: Change in total enthalpy over time.

$\frac{\partial}{\partial x_i}(\rho h_i u_i)$: Convective transport of total enthalpy.

$\frac{\partial P}{\partial t}$: Change in pressure over time.

$\frac{\partial J_j^h}{\partial x_i}$: Flux of enthalpy.

$\frac{\partial(u_i \tau_{ij})}{\partial x_i}$: Work done by viscous forces.

- Enthalpy Flux (J_j^h)

$-\frac{\mu_l}{P_r}$: Represents the diffusion coefficient.

$\frac{\partial h}{\partial x_j}$: Gradient of enthalpy.

$\Sigma \left(\frac{P_r}{s_{ck}} - 1 \right) h_k \frac{\partial Y_k}{\partial X_j}$: Correction term for the flux of species kkk, considering the Prandtl and Schmidt numbers.

This formulation considers the enthalpy as a primary variable for energy conservation, incorporating contributions from convective transport, pressure changes, and viscous work, along with the diffusive flux of enthalpy adjusted by species-specific corrections.

II.3.4 Chemical Species Conservation Equation:

The determination of the mass fraction for each species Y_i is done by solving the transport equation for the i -th species, which has the following form

$$\frac{\partial(\rho Y_i)}{\partial t} + \frac{\partial(\rho u_j Y_i)}{\partial x_j} = -\frac{\partial}{\partial x_j} \left[\left(\rho D_{i,m} + \frac{\mu_t}{Sc_t} \right) \frac{\partial Y_i}{\partial x_j} \right] + R_i \quad (39)$$

y_i : Mass fraction of species i .

C_{s_t} : Turbulent Schmidt number, defined as the ratio of turbulent viscosity to the product of density and mass diffusivity .

$\frac{\mu_t}{Sc_t}$: Turbulent diffusivity, which accounts for the effect of turbulence on species diffusion.

a) Utilizing Navier-Stokes Equations in Combustion Modeling

Combustion models leverage the Navier-Stokes equations to simulate the complex interactions involved in combustion processes within internal combustion engines. These equations, which describe fluid flow dynamics and energy conservation, are essential for modeling the movement of air and fuel mixture, heat transfer, and chemical reactions during combustion. By integrating combustion models with turbulence models like Reynolds-averaged Navier-Stokes (RANS), engineers can simulate turbulent combustion phenomena with high accuracy. This approach allows for the analysis and optimization of combustion efficiency, pollutant formation, and thermal management strategies within engines, contributing to advancements in combustion technology and emissions reduction efforts.

Chapter 03:
Numerical simulation
under OpenFOAM

III.1 OpenFOAM (Open Field Operation and Manipulation) :

OpenFOAM (Open Field Operation and Manipulation) is a free and open-source software package for computational fluid dynamics (CFD). It is used for a variety of applications involving fluid flow, heat transfer, and other related processes. Developed by the OpenFOAM Foundation, it is widely recognized for its flexibility, robustness, and extensibility, making it a popular choice for both academic research and industrial applications, here are some key features of OpenFOAM:

a) Flexibility: OpenFOAM allows users to customize solvers, utilities, and libraries to fit specific application needs. It is modular in design, making it easy to extend and adapt.

b) Wide Range of Applications: OpenFOAM can handle a variety of fluid flow and associated processes, including incompressible and compressible flows, multiphase flows, heat transfer, chemical reactions, and more.

c) Mesh Handling: The software supports a variety of mesh types (e.g., structured, unstructured, and hybrid) and can handle complex geometries. It also includes tools for mesh generation and manipulation.

d) Parallel Processing: OpenFOAM supports parallel computing, allowing users to run simulations on multiple processors to improve computation speed and efficiency.

e) Post-Processing Tools: OpenFOAM comes with built-in tools for post-processing, allowing users to visualize and analyze simulation results directly from the software.

f) Community and Support: OpenFOAM has a large and active user community that contributes to its development and provides support through forums and mailing lists.

g) Documentation: The software includes comprehensive documentation and tutorials to help users get started and deepen their understanding of the software.

h) Interfacing and Integration: OpenFOAM supports integration with other software tools and libraries, such as MATLAB and ParaView for visualization.

III.1.1 Openfoam content:

Linux is an open-source operating system renowned for its flexibility and command-line interface, known as the terminal. The terminal allows users to interact with the system directly through text commands, providing powerful control over system operations and software management. Within this environment, OpenFOAM, an open-source computational fluid dynamics (CFD) toolbox, is extensively utilized for simulating fluid flows and other complex physical phenomena.

While OpenFOAM is commonly associated with Linux due to its origins and robust command-line capabilities, it is also available for Windows users. Users on Windows can install OpenFOAM using virtualization technologies like Docker or by setting up a Linux virtual machine. This allows Windows users to access and utilize OpenFOAM's powerful computational fluid dynamics capabilities, albeit

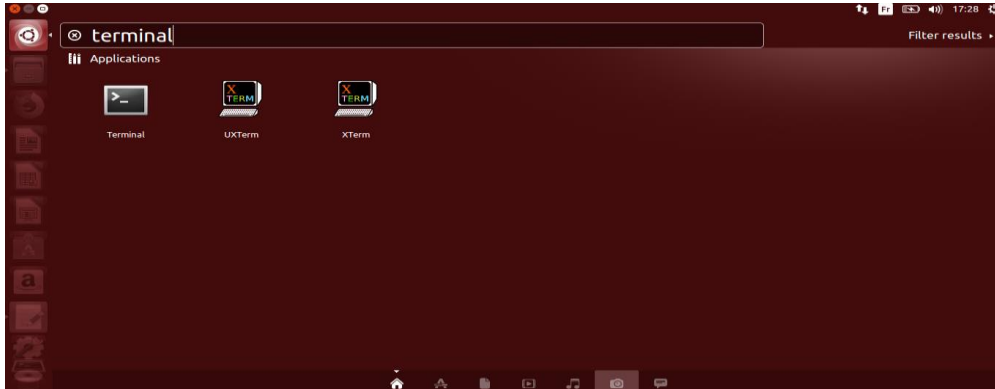


Figure III.1 : terminal location in linux

with some additional setup compared to Linux-native environments. Thus, OpenFOAM remains accessible across different operating systems, catering to a diverse range of engineering and research needs.

Users can access OpenFOAM through the terminal in Linux, where they execute commands to set up simulations, manipulate data, and run solvers. Linux's robust command-line interface complements OpenFOAM's capabilities by offering efficient workflow management and script automation, crucial for handling large-scale simulations and data processing tasks. This integration fosters a seamless workflow for engineers and researchers, enabling them to leverage OpenFOAM's advanced features while harnessing Linux's command-line power for optimal simulation performance and scalability.

III.1.2 The Aachen Bomb: The Aachen Bomb is an experimental setup used to study fuel spray behavior under high-pressure and high-temperature conditions, similar to those in diesel engines. It features a high-pressure chamber with optical access, allowing detailed observation and measurement of spray and combustion processes.

simulation Processes : To enter OpenFOAM from the terminal, you typically type the command ``source <installation_directory>/OpenFOAM-X.YY/etc/bashrc``, replacing ``<installation_directory>`` with the path where OpenFOAM is installed and ``X.YY`` with your specific version number.(exemple `openfFOAM-2.0.1`)

then use the command : `cd $FOAM_RUN`
as it shown in the **figure III.2** down bellow

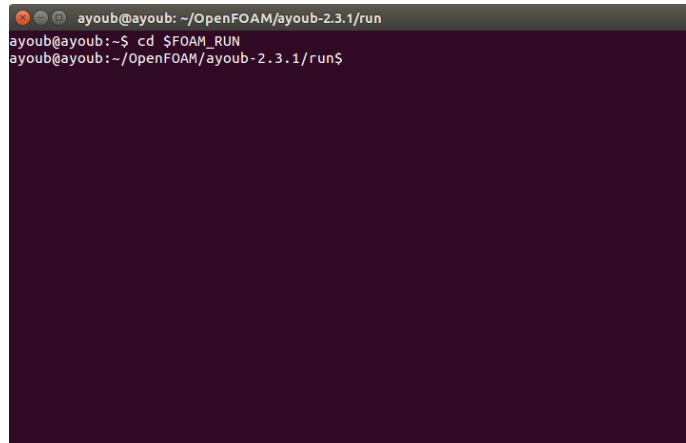


Figure III.2 : openFoam running command using terminal

To set up the "aachenBomb" tutorial in OpenFOAM, you need to follow a specific script provided in the tutorial documentation or setup files. This script initializes the necessary configurations and prepares the simulation environment according to the tutorial's instructions. To copy the "aachenBomb" tutorial in (OpenFOAM), use the command:

```
cp -r /opt/openfoam231/tutorials/lagrangian/sprayFoam/aachenBomb .`
```

Executing the command will copy the tutorial to your current directory



Figure III.3: aachenbomb solvers contant

containing:

- 0 Initial conditions for the simulation

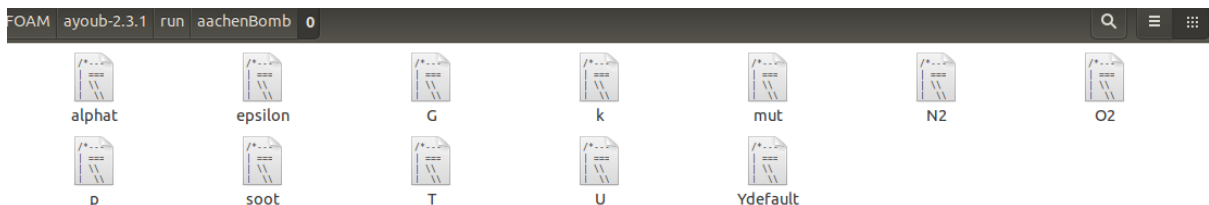


Figure III.4: "aachenBomb/0" content



Figure III.5: aachenBomb/constant content

- constant: Properties such as thermophysicalproperties and chemistryproperties and others.
- system: Includes iteration controls and mesh cell specifications, which can be found after running `blockMesh`. In OpenFOAM simulations, the system directory is essential for configuring and controlling various aspects of the simulation setup. It includes crucial files such as `controlDict`, which defines time steps, start and end times, and other runtime controls. The `blockMeshDict` file within `system` specifies mesh topology, cell sizes, and boundary conditions after mesh generation using `blockMesh`. Physical properties like density and viscosity are detailed in `thermophysicalProperties` in the `constant` directory. Solver settings, found in `system/<solver_name>.<solver_type>`, determine numerical schemes and turbulence models used in the simulation. Boundary conditions, defined in `system/boundaryConditions`, set conditions at domain boundaries for velocities, pressures, temperatures, and species concentrations. Together, these components in the `system` directory ensure accurate and comprehensive setup of computational fluid dynamics simulations, enabling detailed analysis and prediction of fluid flow phenomena in OpenFOAM.



Figure III.6 : aahcenbomb/system content

And here's some of information where it's taken from the terminal after applying the command “blockMesh”

however the blockMesh can identify the number of the cells of the mesh which is : 168100

```

Mesh Information
-----
boundingBox: (-0.01 0 -0.01) (0.01 0.1 0.01)
nPoints: 178164
nCells: 168100
nFaces: 514181
nInternalFaces: 494419
-----
Patches
-----
patch 0 (start: 494419 size: 19762) name: walls

```

Figure III.7 : blockMesh execution information

-Chemkin : Chemkin refers to a suite of software tools commonly used for modeling and simulating gas-phase chemical kinetics, particularly in combustion processes. It includes databases and libraries containing detailed chemical reaction mechanisms and thermodynamic data necessary for simulating combustion reactions accurately. These reaction mechanism files are essential for predicting and analyzing combustion phenomena within computational fluid dynamics (CFD) simulations and other combustion modeling applications.



Figure III.8 : aachenBomb/chemkin content

III.1.3 Execution:

Executing the commands bellow:

```

cd aachenbomb
blockMesh
sprayFoam

```

in sequence initiates the simulation process in OpenFOAM. First, changing directory (`cd`) into "aachenbomb" sets the working environment for the simulation. Next, `blockMesh` generates the computational mesh based on predefined settings, ensuring accurate representation of the simulation domain. Finally, `sprayFoam` launches the solver, starting calculations to simulate fluid flow and other physical phenomena as defined by the case setup.

The duration of the simulation depends significantly on the computational power of the processor. For instance, on an Intel Core i5-1035G1 CPU @1.00GHz 1.19 GHz processor, the simulation might

take approximately 15 hours to complete. This estimation varies based on factors such as the complexity of the simulation case, mesh resolution, solver settings, and the efficiency of the numerical algorithms employed. High-performance processors can significantly reduce computation time, whereas less powerful systems may require more time to achieve accurate simulation results.

Upon completion of the simulation in OpenFOAM, you will typically achieve exactly 200 iterations..

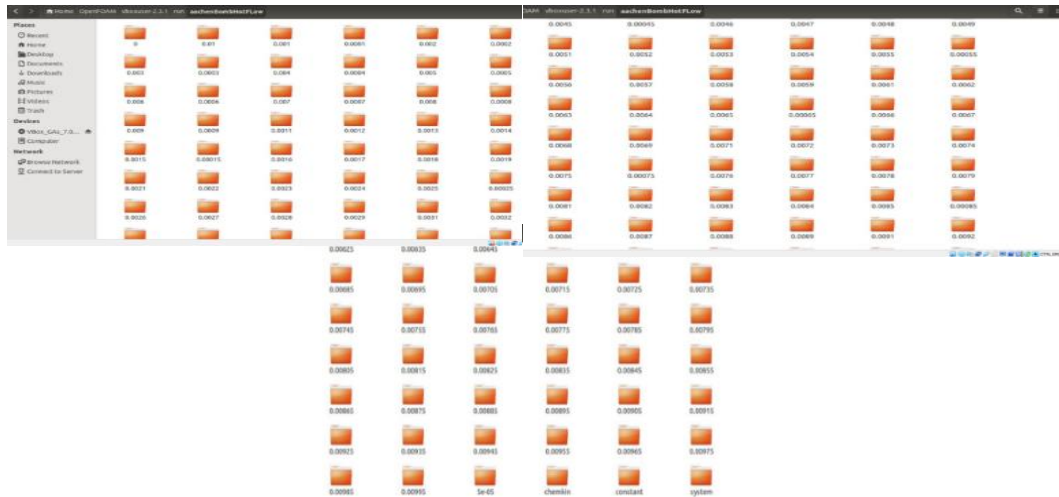


Figure III.9 : Aachenbomb simulation results

II.2 Geometry:

II.2.1 Purpose of Accurate Geometry Representation in Diesel Injector Simulation Importance

a)**Critical Component:** Diesel injector directly impacts engine performance, efficiency, and emissions.

b)**Simulation Accuracy:** Precise geometric representation ensures realistic simulation results.

II.5.2 Influence of Geometric Details

➤ Fuel Atomization

- Nozzle Design: Number, size, and shape of orifices affect fuel droplet size distribution.
- Impact: Accurate geometry enables correct prediction of atomization quality, essential for efficient combustion and reduction of unburned hydrocarbons.

➤ Spray Pattern

- Orifice Arrangement: Orientation and arrangement of nozzle holes dictate spray pattern.
- Impact: Ensures simulated spray pattern matches real-world behavior, optimizing air-fuel mixture and combustion completeness.

➤ **Flow Dynamics**

- Internal Geometry: Fuel passages and needle valve design influence fuel flow rate and pressure distribution.

- Impact: Accurate geometry captures complex flow dynamics, allowing precise prediction of fuel delivery rates and injection timing.

➤ **Combustion Efficiency**

- Fuel-Air Interaction: Injector geometry affects interaction with in-cylinder air motion (swirl, tumble).

- Impact: Enables correct modeling of fuel-air mixing, leading to better predictions of combustion efficiency and engine performance.

➤ **Emission Characteristics**

- Pollutant Formation: Combustion process and pollutant formation (NO_x, soot) are geometry-dependent.

- Impact: Accurate model predicts emission characteristics, aiding in emission reduction strategies.

➤ **Heat Transfer**

- **Thermal Interaction:** Injector geometry influences thermal characteristics of fuel spray.

- Impact: Ensures accurate prediction of heat transfer between fuel and air, critical for ignition and combustion kinetics.

The injector geometry used in this study is based on a common rail diesel injector typically employed in high-performance diesel engines

Table III.1: geometric inlet injector dimensions

Component	Dimension/Parameter	Value
Nozzle hole	Number of holes	6
	Hole diameter	0.2 mm
	Hole length	1.2 mm
Needle hole	Diameter at seat	1.0 mm
	Maximum lift	0.3 mm
Fuel passages	Inlet passage diameter	0.5 mm

III.2.3 Benefits of geometry in Diesel Engine Research

- a) **Accurate Spray Characterization:** Provides precise data on fuel atomization, spray penetration, and vaporization, which are critical for understanding fuel-air mixing in diesel engines.
- b) **Combustion Analysis:** Enables detailed examination of combustion characteristics, including flame development and pollutant formation, aiding in the design of cleaner and more efficient engines.
- c) **Model Validation:** Supplies benchmark data to validate and refine computational models, ensuring simulations accurately represent real-world engine behavior.
- d) **Injector Optimization:** Assists in optimizing fuel injector designs for better performance, enhanced fuel efficiency, and reduced emissions in diesel engines.

III.3 Computational set up

Different cases were considered in order to achieve the given goals. However, the simulation setup is the same for all the cases and hence the procedure is the same for all cases. The first step required to begin a new simulation is to input the actual mesh into the file structure of OpenFOAM. The computational domain for simulating a diesel engine injector is chosen based on the injector geometry. The geometry consists of the injector nozzle, needle, and the surrounding fluid domain. In our project, we created the geometry of the injector nozzle mesh using the meshing feature provided by blockMesh in OpenFOAM. Mesh Utility blockMesh is used to create high-quality hex dominant meshes based on arbitrary geometry. The boundary conditions are applied according to the physical conditions. The generated grid is fed to the solver for solving the governing equations. The details of the geometry are as shown in the following Figures.

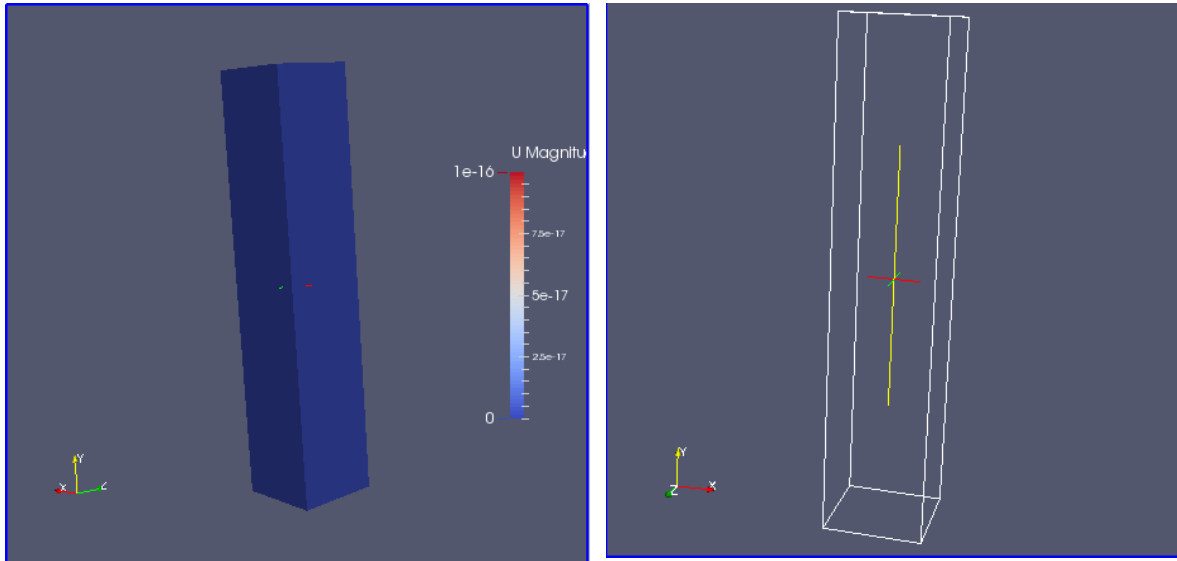


Figure III.10 : “aachenBomb” Geometry simulation

Table III.2:aachenbomb tutorial initial dimensions case

dimension	value
Height	0.1 meters
Length	0.02 meters
Width	0.02 meters
Injector Placement (below top)	5 mm
Injector Placement (from bottom)	0.995 meters

III.3.1 Geometric pattern mesh:

The aachenBomb tutorial in OpenFOAM utilizes a structured mesh for the constant volume chamber. This mesh consists of hexahedral cells, essentially 3D cubes, arranged in a uniform, grid-like pattern throughout the domain. The mesh resolution, defined by the number of cells, determines the level of detail captured. A finer mesh with more cells offers higher accuracy but demands greater computational resources. ParaView serves as a tool to inspect the mesh pattern, allowing visualization of the individual cells or their boundaries. This structured mesh approach is advantageous due to its simplicity and efficiency for the regular geometry of the chamber. However, it's important to acknowledge that structured meshes are less suitable for intricate geometries, where OpenFOAM can leverage unstructured meshes with irregular cells for improved adaptation.

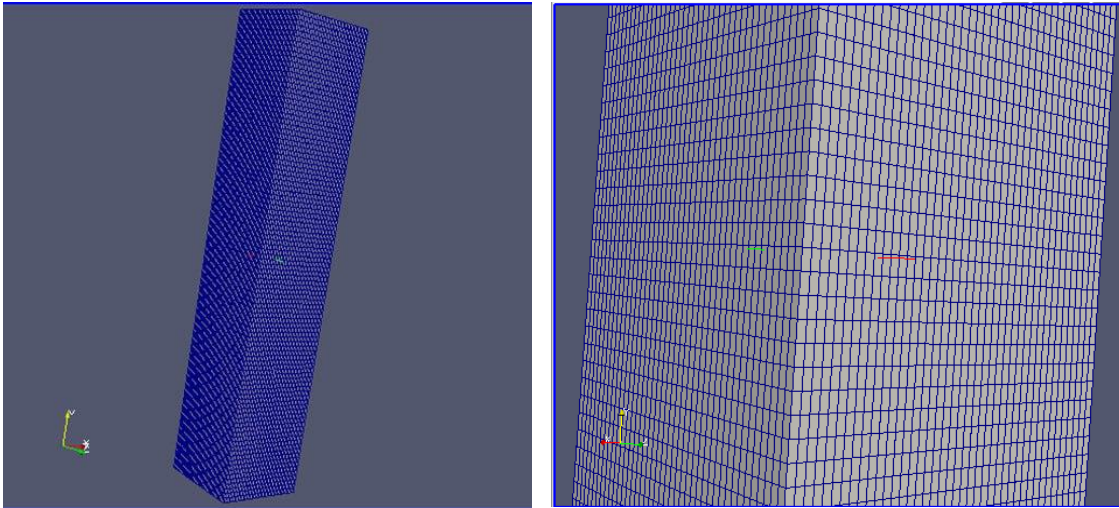


Figure III.11 : “aachenBomb” Mesh simulation

The following file is a blockMeshDict file used in OpenFOAM. This file serves as input for the blockMesh utility, a core component responsible for mesh generation. The blockMeshDict file defines the specifications for the mesh pattern, including cell types, sizes, and distribution within the computational domain

```

/*-----*- C++ -*-----*\
|=====|
|\ \ / Field | OpenFOAM: The Open Source CFD Toolbo |
| \ \ / Operation | Version: 2.3.1 |
| \ \ / A nd | Web: www.OpenFOAM.org |
| \ \ M anipulation |
\*-----*/

FoamFile
{
  version 2.0;
  format ascii;
  class dictionary;
  object blockMeshDict;
}

(-10 0 -10)
(-10 0 10)
(10 0 10)
(10 0 -10)
(-10 100 -10)
(-10 100 10)
(10 100 10)
(10 100 -10)
);
blocks
(
  hex (0 1 2 3 4 5 6 7) (41 41 100) simpleGrading (1 1 1)
);

edges
(
);

Patches
(
  wall walls
  (
    0 (2 6 5 1)
    (0 4 7 3)
    (0 1 5 4)
    (4 5 6 7)
    (7 6 2 3)
    (3 2 1 0)
  )
)

```

```

)
);
mergePatchPairs
(
);
// ***** //

```

III.4 Boundary condition at the injector inlet :

In fluid dynamics and combustion modelling, specifying the boundary conditions at the injector inlet is crucial for accurately predicting the flow characteristics and behaviour within the injector and downstream in the system. These boundary conditions define the state of the fluid entering the injector and significantly impact the simulation results. Here are the common types of boundary conditions used

III.4.1 Common Boundary Conditions at the Injector Inlet

a) Pressure Boundary Condition: Inlet Pressure: Specifies the pressure of the fluid at the injector inlet. This is commonly used in high-pressure injection systems, such as fuel injectors in internal combustion engines or gas turbines.

b) Velocity Boundary Condition: Inlet Velocity: Specifies the velocity of the fluid entering the injector. This can be a uniform velocity or a velocity profile depending on the injector design and the flow characteristics.

c) Mass Flow Rate Boundary Condition: Mass Flow Rate: Specifies the mass flow rate of the fluid entering the injector. This is useful when the exact pressure or velocity is not known, but the flow rate is controlled.

d) Temperature Boundary Condition: Inlet Temperature: Specifies the temperature of the fluid at the injector inlet. This is important for thermal analysis and combustion modeling.

e) Species Concentration Boundary Condition: Species Concentration: Specifies the concentration of different species (e.g., fuel, oxidizer) in the fluid at the injector inlet. This is crucial for combustion simulations

f) Turbulence Boundary Condition: Turbulence Intensity and Length Scale: Specifies the turbulence characteristics at the inlet, such as turbulence intensity, turbulent kinetic energy (k), and dissipation rate (ϵ).

Table III.3:Initial conditions for aachenBomb cases :

Initial boundary condition	Value
Gas temperature in the constant volume chamber	800K
Gas pressure in the constant volume chamber	50bar
Gas velocity in the constant volume chamber	0 m/s
Fuel	n-Heptane
Injection temperature	320K

Table III.4: initial species concentration before the combustion :

species	ratio
N_2 concentration in the constant volume chamber	76.6%
O_2 concentration in the constant volume chamber	23.4%
C_7H_{16} concentraion in the constant volume chamber	//
k	90 (uniform internal field, walls:epsilonWallFunction)
ε	1 (uniform internal field, walls:kqRWallFunction)

III.4.2 Reasoning the Selection: AachenBomb Simulation with C7H16 as Diesel Substitute;

In simulating the AachenBomb scenario using OpenFOAM, the choice of C7H16 (heptane) as a surrogate for diesel fuel is based on the close similarity of their boundary conditions. Specifically, the temperature, injection parameters, and velocity in the AachenBomb setup are carefully calibrated to be very close to or almost the same as those experienced during diesel injection in internal combustion engines. This meticulous calibration ensures that the simulation accurately replicates the high-pressure and high-temperature environment typical of diesel combustion. As a result, the use of C7H16 allows the simulation to provide realistic insights into the fuel spray dynamics, ignition delay, and combustion efficiency. These insights are directly applicable to the development and optimization of diesel injectors, making the choice of C7H16 a practical and effective surrogate for diesel in this context. By ensuring that the simulation conditions are nearly identical to actual diesel injection conditions, the results obtained are highly relevant and beneficial for enhancing the performance and efficiency of diesel engines.

N-heptane (C₇H₁₆) spray is often utilized as a surrogate for diesel fuel in combustion research, providing valuable insights into combustion behavior and spray characteristics relevant to diesel engines. Here is a table summarizing the characteristics of this spray:

Table III.5: characteristics of (C₇H₁₆)heptane in standards condition

Property	Value	Units
Molecular Weight	100.2	<i>g/mol</i>
Density (at 25°C)	0.684	<i>g/cm³</i>
Boiling Point	98.4	°C
Melting point	-90.6	°C
Flash point	-4	°C
Auto ignition Temperature	209	°C
Vapor Pressure (at 25°C)	5.2	<i>kPa</i>
Solubility in Water (at 25°C)	0.0094	<i>g/l</i>
Viscosity (at 25°C)	0.39	<i>cP</i>
Heat of Combustion	-47.920	<i>kJ/mol</i>
Heat of Vaporization	30.06	<i>kJ/mol</i>
Heat of Capacity (at constant pressure 25°C)	2.1	<i>J/g°C</i>
Heat Capacity (at constant volume, 25°C)	2.1	<i>J/g°C</i>
Lower Flammability Limit (LFL)	1	% volume
Upper Flammability Limit (UFL)	6.1	% volume
Chemical Formula	C ₇ H ₁₆	

II.4.3 Implementation in Simulations :

In computational fluid dynamics (CFD) simulations, these boundary conditions are implemented in the software to set the initial state of the fluid entering the injector. Proper specification of these conditions is essential for accurate simulation results.

Pressure Inlet Boundary: Used when the pressure is known but the flow rate or velocity is not. **Velocity Inlet Boundary:** Used when the velocity is known but the pressure is not.

Mass Flow Inlet Boundary: Used when the mass flow rate is known, commonly in controlled injection systems. **Temperature and Species Inlet:** Essential for thermal and combustion simulations to define the state of the fluid entering the system.

Turbulence Boundary: Provides the necessary details for modelling turbulent flows, impacting the mixing and combustion processes. Accurately defining these boundary conditions helps in predicting

the flow characteristics, mixing, combustion efficiency, and performance of the injection system, thereby allowing engineers to optimize the design and operation of such systems.

```

/*-----*- C++ -*-----*\
|=====|
|\      / Field | OpenFOAM: The Open Source CFD Toolbox |
| \    / Operation | Version: 2.3.1 |
|  \  /  A nd | Web: www.OpenFOAM.org |
|   \//   M anipulation | |
\*-----*/
FoamFile
{
  version 2.0;
  format binary;
  class dictionary;
  location "constant";
  object SprayCloudProperties;
}
// *****

solution
{
  active true;
  coupled true;
  transient yes;
  cellValueSourceCorrection on;
  maxCo 0.3;
  sourceTerms
  {
    schemes
    {
      rho explicit 1;
      U explicit 1;
      Yi explicit 1;
      h explicit 1;
      radiation explicit 1;
    }
  }
  interpolationSchemes
  {
    rho cell;
    U cellPoint;
    thermo:mu cell;
    T cell;
    Cp cell;
    kappa cell;
    p cell;
  }
}

```

```
}
integrationSchemes
{
U Euler;
T analytical;
}
}
constantProperties
{
T0 320;
// place holders for rho0 and Cp0
// - reset from liquid properties using T0
rho0 1000;
Cp0 4187;
constantVolume false;
}
subModels
{
particleForces
{
sphereDrag;
}
injectionModels
{
model1
{
type coneNozzleInjection;
SOI 0;
massTotal 6.0e-6;
parcelBasisType mass;
injectionMethod disc;
flowType flowRateAndDischarge;
outerDiameter 1.9e-4;
innerDiameter 0;
duration 1.25e-3;
position ( 0 0.0995 0 )
direction ( 0 -1 0 );
parcelsPerSecond 20000000;
flowRateProfile table
(
(0 0.1272)
(4.16667e-05 6.1634)
(8.33333e-05 9.4778)
(0.000125 9.5806)
(0.000166667 9.4184)
(0.000208333 9.0926)

```

```

(0.00025 8.7011)
(0.000291667 8.2239)
(0.000333333 8.0401)
(0.000375 8.8450)
(0.000416667 8.9174)
(0.000458333 8.8688)
(0.0005 8.8882)
(0.000541667 8.6923)
(0.000583333 8.0014)
(0.000625 7.2582)
(0.000666667 7.2757)
(0.000708333 6.9680)
(0.00075 6.7608)
(0.000791667 6.6502)
(0.000833333 6.7695)
(0.000875 5.5774)
(0.000916667 4.8649)
(0.000958333 5.0805)
(0.001 4.9547)
(0.00104167 4.5613)
(0.00108333 4.4536)
(0.001125 5.2651)
(0.00116667 5.2560)
(0.00120833 5.1737)
(0.00125 3.9213)
(0.001251 0.0000)
(1000 0.0000)
);
Cd constant 0.9;
thetaInner constant 0.0;
thetaOuter constant 10.0;
sizeDistribution
{
  type RosinRammler;
  RosinRammlerDistribution
  {
    minValue 1e-06;
    maxValue 0.00015;
    d 0.00015;
    n 3;
  }
}
dispersionModel none;
patchInteractionModel standardWallInteraction;

```

```
heatTransferModel RanzMarshall;
compositionModel singlePhaseMixture;
phaseChangeModel liquidEvaporationBoil;
surfaceFilmModel none;
atomizationModel none;
breakupModel ReitzDiwakar; // ReitzKHRT;
stochasticCollisionModel none;
radiation off;
standardWallInteractionCoeffs
{
type rebound;
}
RanzMarshallCoeffs
{
BirdCorrection true;
}
singlePhaseMixtureCoeffs
{
Phases
(
liquid
{
C7H16 1;
}
);
}
liquidEvaporationBoilCoeffs
{
enthalpyTransfer enthalpyDifference;
activeLiquids ( C7H16 );
}
ReitzDiwakarCoeffs
{
solveOscillationEq yes;
Cbag 6;
Cb 0.785;
Cstrip 0.5;
Cs 10;
}
/*
ReitzKHRTCoeffs
{
solveOscillationEq yes;
B0 0.61;
B1 40;
Ctau 1;
```

```

CRT 0.1;
msLimit 0.2;
WeberLimit 6;
}
*/

TABCoeffs
{
y0 0;
yDot0 0;
Cmu 10;
Comega 8;
WeCrit 12;
}
}
cloudFunctions
{}
// ***** //
    
```

III.5 Turbulence Model :

Combustion interaction models are essential for understanding and predicting the behavior of flames in turbulent flow fields. Two common approaches to modeling these interactions in the context of Reynolds-Averaged Navier-Stokes (RANS) simulations are the Turbulent Combustion Model.

II.5.1 Combustion Model

The turbulence model in combustion assumes that a turbulent flame consists of multiple thin, laminar flame structures embedded within the turbulent flow. These structures, known as "combustion models," retain laminar flame properties but are influenced by surrounding turbulence. Key features include the assumption of thin reaction zones compared to turbulence scales, pre-tabulated chemistry where complex reactions are computed as functions of parameters like mixture fraction and scalar dissipation rate, and combustion equations governed by conservation laws (e.g., species, energy) aligned with the flame front. The model also considers how turbulent mixing impacts the distribution of mixture fraction and scalar dissipation rate, thereby coupling turbulence with combustion chemistry.[14]

Table III.6 : advantages and limitations of combustions models

Advantages	Limitations
- Efficiency: Reduces the computational cost by using pre-tabulated chemistry. - Accuracy: Capable of capturing detailed	- Assumptions: Relies on assumptions that may not hold in all combustion regimes, particularly where flame thickness is not

chemical kinetics. - Simplicity: Easier to implement in RANS simulations.	small. - Limited Applicability: Best suited for premixed or partially premixed flames with thin reaction zones.
--	--

II.5.2 Turbulent Combustion Models

Turbulent combustion models aim to describe the interaction between turbulence and combustion by incorporating the effects of turbulence on the flame structure and vice versa.

a) Types of Turbulent Combustion Models :

- Eddy Dissipation Concept (EDC): Assumes that reaction rates are controlled by the turbulent mixing rates of eddies. Chemical reactions occur in the fine structures of the turbulent flow, and reaction rates are proportional to the rate at which these structures mix.
- Probability Density Function (PDF) Methods: Use statistical approaches to model the distribution of reacting scalars within the turbulent flow. The PDF approach directly solves for the statistical distribution of quantities like temperature and species concentrations.
- Level Set Methods: Represent the flame front as a level set of a scalar field, often the G-equation. The propagation of this front is governed by a combination of advection by the flow and flame speed relative to the unburned mixture.

b) Key Features:

- Turbulence-Chemistry Interaction: Explicitly model how turbulence affects the reaction rates and flame propagation.
- Detailed Reaction Mechanisms: Can incorporate complex chemical kinetics directly or through simplified models.
- Versatility: Applicable to a wide range of combustion regimes, including premixed, non-premixed, and partially premixed flames[15].

Table III.7: Advantages and limitations of Turbulent Combustion Models

Advantages	Limitations
- Flexibility: Can handle a variety of combustion scenarios and turbulence intensities. - Accuracy: Capable of capturing the	- Complexity: More computationally intensive than combustion models. - Implementation: Requires detailed

interplay between turbulence and combustion more accurately than simpler models.	turbulence modeling and often more sophisticated numerical methods.
--	---

III.6 Cold flow:

If you use “cold flow” in OpenFOAM, you will focus on the dynamic of the environment without any complications associated with the heat or other chemical reactions. This allows an analysis of the hydraulic parameters, such as the pressure and pressure, with a solid base for more complex simulations. If there are limited hydrodynamic aspects, this application will simplify the validation of the models and the use in place of more advanced scans. Outside, it is possible to explore diverse operating conditions without the combination of thermal interactions. This method is particular used to value the performance of the fluid systems at the first temps, before the use of new complex supplements. In the calculation, the use of “cold flow” in OpenFOAM allows an analysis to apply to the devices used, to simplify the simulation process for a better comparison of fluid systems.

```

ELEMENTS
  H  O  C  N  AR
END
SPECIE
C7H16 O2 N2 CO2 H2O
END
REACTIONS
  C7H16 + 11O2          => 7CO2 + 8H2O          5.00E+8  0.0  15780.0!  1
      FORD      / C7H16 0.25 /
      FORD      / O2 1.5 /
END

```

Figure III.12 : “aachenBomb” chemistry equation

III.6.1 Implementation of coldflow :

```
chemistryType
{
    chemistrySolver    ode;
    chemistryThermo    psi;
}

chemistry            off;

initialChemicalTimeStep 1e-07;

odeCoeffs
{
    solver            seulex;
    eps                0.05;
}
```

Figure III.13 : “aachenBomb” chemistryType

When chemistry is disabled in OpenFOAM, chemical reactions are ignored in the simulation, meaning that chemical reactions such as combustion or gas reactions are not considered. As a result, any chemical changes in the simulated domain will not be accounted for. Additionally, no heat production associated with those reactions will be calculated. This simplifies the model, making it easier to use and speeding up the simulation. However, it also means that you won't be able to analyse chemical or heat effects in the system, and the model will primarily be determined by the hydrodynamic aspects of the flow, potentially limiting your ability to study some complex phenomena involving chemical reactions.[16]

III.6.2 Explanation of Soot in the AachenBomb Simulation :

In the OpenFOAM simulation of the AachenBomb case, "soot" refers to the particulate matter composed primarily of carbon, formed as a by-product of incomplete combustion. Soot particles are generated during the combustion of hydrocarbon fuels and consist of a complex mixture of amorphous carbon and organic compounds. In the context of the AachenBomb simulation, the inclusion of soot models allows for a detailed examination of the formation and oxidation of these particles within a combustion process. By simulating soot, researchers can analyse the spatial and temporal distribution of particulate matter, its impact on combustion efficiency, and its interaction with other species in the flow. The accurate modelling of soot is crucial for understanding its effects on engine performance, emissions, and the environment .[17]

II.6.3 Purpose of the Soot implementation:

The primary purpose of this study is to investigate the formation, growth, and oxidation of soot particles in a combustion environment, specifically within the AachenBomb case. By modifying the base Hotflow case to include soot modelling, the research aims to gain deeper insights into the mechanisms of soot production and its impacts on combustion processes. This study is essential for several reasons: reducing harmful emissions, improving fuel efficiency, and enhancing overall engine performance. Understanding soot formation is critical for developing cleaner combustion technologies and meeting stringent environmental regulations. Additionally, this research contributes to the broader field of combustion science by providing valuable data and validation for soot models, which can be applied to various combustion systems and enhance the design of future engines and fuel formulations [18].

II.7 Implimentation of SootModel :

a) Copy AachenBomb Case: This involves duplicating the base AachenBomb tutorial case into your working directory. It ensures you have a working copy that can be modified without affecting the original and this text should be followed:

```
OF23x
cd mkdir $WM_PROJECT_USER_DIR/
mkdir $FOAM_RUN
cd $WM_PROJECT_DIR/ cp -r tutorials/lagrangian/sprayFoam/aachenBomb/ $FOAM_RUN
```

b) Copy Radiation Library: This step requires transferring the necessary radiation model files into your user directory. This library is crucial for accurately simulating the thermal radiation aspects of combustion. So this is done as follows

```
OF23x
cd $WM_PROJECT_DIR
cp -r --parents src/thermophysicalModels/radiation/ $WM_PROJECT_USER_DIR/
cd $WM_PROJECT_USER_DIR/src/thermophysicalModels/radiation/submodels/sootModel/
```

c) Rename and Modify Soot Library: The soot library needs to be appropriately renamed and its configuration adjusted to fit the specific requirements of your simulation. This customization allows the soot model to work correctly within your case setup by entering this following text in terminal :

```

mv mixtureFractionSoot mymixtureFractionSoot
cd mymixtureFractionSoot/
mv mixtureFractionSoot.C mymixtureFractionSoot.C
mv mixtureFractionSoot.H mymixtureFractionSoot.H
sed -i s/mixtureFractionSoot/mymixtureFractionSoot/g mymixtureFractionSoot.H
sed -i s/mixtureFractionSoot/mymixtureFractionSoot/g mymixtureFractionSoot.C
sed -i s/mixtureFractionSoot/mymixtureFractionSoot/g mixtureFractionSoots.C

```

```

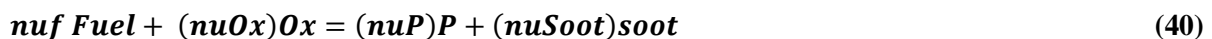
cd $WM_PROJECT_USER_DIR
cd src/thermophysicalModels/radiation/
sed -i s/FOAM_LIBBIN/FOAM_USER_LIBBIN/g Make/files
sed -i s/libradiationModels/libmyradiationModels/g Make/files
sed -i s/mixtureFractionSoot/mymixtureFractionSoot/ Make/files

```

III.7.1 Execution

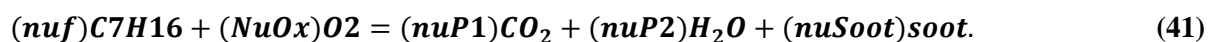
As we discussed earlier, the soot model describes this process in stages, highlighting the formation of Polycyclic Aromatic Hydrocarbons (PAHs) as precursors to soot particles.

To account for soot formation, the model employs a generalized single step reaction



Modifying soot properties relies on influencing these stages. The following steps outline the fundamental approaches to manipulating soot characteristics during combustion.

We define nuf , $nuOx$, nuP , and $nuSoot$ to represent the number of moles of fuel, oxidizer, products, and soot, respectively. The single-step reaction for this tutorial will be based on these quantities:



Following the definition of $nuSoot$ as the number of moles of soot, we can calculate the mass fraction of soot using the formula...

$$\mathbf{soot[cell I]} = \mathbf{sootMax} * (\mathbf{YCO2[cell I]}/\mathbf{YCO2stoch}) \quad (42)$$

To modify soot formation in your simulation:

a) Prepare Input Files: Copy the soot and G (incident radiation) files to the 0/ folder within your case directory.

```
run
cd aachenBomb
cp -r $FOAM_TUTORIALS/combustion/fireFoam/les/smallPoolFire2D/0/soot 0/
```

And :

```
run
cd aachenBomb
cp -r $FOAM_TUTORIALS/combustion/fireFoam/les/smallPoolFire2D/0/G 0/
```

b) Update Solver Settings: In the fvSolution file, add the entry for Gfinal (needed by the radiation model).

```
GFinal
{
  solver PCG;
  preconditioner DIC;
  tolerance 1e-05;
  relTol 0.1;
}
```

c) Modify Material Properties:

Edit the thermophysicalProperties file (located in the constant folder) to include inputs for your single-step reaction.

```

/*-----*- C++ -*-----*\
|===== ||
|\\ / F ield | OpenFOAM: The Open Source CFD Toolbox |
|\\ / O peration | Version: 3.0.x |
|\\ / A nd | Web: www.OpenFOAM.org |
|\\ / M anipulation | |
\*-----*/FoamFile
{
  version 2.0;
  format ascii;
  class dictionary;
  location "constant";
  object thermophysicalProperties;
}
// ***** //

thermoType
{
  type h ePsiThermo;
  //mixture reactingMixture;
  mixture singleStepReactingMixture;
  transport sutherland;
  thermo janaf;
  energy sensibleEnthalpy;
  equationOfState perfectGas;
  specie specie;
}
CHEMKINFile "$FOAM_CASE/chemkin/chem.inp";
CHEMKINThermoFile "$FOAM_CASE/chemkin/therm.dat";
newFormat yes;
inertSpecie N2;
fuel C7H16;
liquids

```

```

{
  C7H16
  {
    defaultCoeffs yes;
  }
}
Solid
{
  // none
  // ***** //

```

d) Set Breakup Model:

Configuring Breakup Model:

The `sprayCloudProperties` file controls the secondary breakup of droplets within the spray. This process is governed by submodels, of which there are seven available in the `$FOAM_SRC/lagrangian/spray/submodels/BreakupModel/` directory. This tutorial focuses on the PilchErdman breakup model. However, the default setting in the `sprayCloudProperties` file is the ReitzDiwakar model. To switch models, simply modify the file[19] as follows:

Change the `breakupModel` line to:

```
breakupModel PilchErdman;
```

Following the `liquidEvaporationBoilCoeffs` section, add the following section dedicated to PilchErdman model coefficients:

```

PilchErdmanCoeffs
{
  solveOscillationEq yes;
  B1 0.375;
  B2 0.2274;
}

```

These changes ensure the simulation utilizes the desired PilchErdman model for secondary breakup calculations.

e) **Configure Radiation Model:**

Edit the radiationProperties file (located in **constant**) according to the instructions provided in the "Input files" section (refer to the paragraph named "radiationProperties and changes needed to be made to include soot model")

Enabling Soot Model in radiationProperties: The radiationProperties file, located in the constant folder of your case directory, defines the type of radiation model and its submodels. These submodels include absorptionEmissionModel, scatterModel, and, importantly for our purposes, sootModel.

By default, radiation is disabled within this file. To activate the sootModel and include soot calculations, you'll need to replace the entire contents of radiationProperties with the information provided in the following section.

```

/*-----*- C++ -*/
| ===== | |
| \\ / F i e l d | OpenFOAM: The Open Source CFD Toolbox |
| \\ / O p e r a t i o n | Version: 3.0.x |
| \\ / A n d | Web: www.OpenFOAM.org |
| \\ \ M a n i p u l a t i o n | |
\*-----*/

FoamFile
{
  version 3.0;
  format ascii;
  class dictionary;
  location "constant";
  object radiationProperties;
}

// ***** //

radiation on;

radiationModel P1;

//Number of flow iterations per radiation iteration
solverFreq 10;

absorptionEmissionModel none;

```

```
scatterModel none;

sootModel mymixtureFractionSoot;

mymixtureFractionSootCoeffs { nuSoot 0.055; Wsoot 12;
}

// ***** //

scatterModel none;

sootModel mymixtureFractionSoot;
```

II.7.5 Post possessing :

To observe Lagrangian droplets using glyphs in ParaView, first, create the necessary VTK files for both the continuous and Lagrangian phases and place them in the appropriate directories within your

f) Generate Mesh:

Run the `blockMesh` command as explained in the "Geometry and initial conditions" section (refer to previous instructions if needed).

Run Simulation:

Execute **the** `sprayFoam` command to launch **the** `aachenBomb` case simulation.

This revised version simplifies the instructions, clarifies user actions, and references previous sections for more detailed explanations (if available).

```
cp -r $FOAM_TUTORIALS/lagrangian/sprayFoam/aachenBomb
aachenBomb
cd aachenBomb
blockMesh
sprayFoam
paraFoam
```

II.8 Conclusion

In conclusion, the thorough exploration of numerical modelling techniques provided in this chapter equips readers with a solid foundation for understanding the complexities of internal combustion engine simulations. Through discussions on geometry representation, boundary conditions, and combustion interaction models, valuable insights into engine processes have been gained. Looking ahead to Chapter 3, we anticipate a more profound analysis of the results obtained from these simulations. By correlating these results with the theoretical framework established in this chapter, we aim to uncover key insights into flow dynamics, combustion behavior, and performance characteristics of internal combustion engines. Through this iterative process of simulation, analysis, and discussion, we aim to contribute significantly to the ongoing advancements in internal combustion engine technology.

Chapter 04:

Results and discussion

IV.1 Introduction

Here's the revised paragraph focusing on parametric analysis, case studies, and soot formation, removing the oxygen reference:

Delving into the results and discussion, this study emphasizes parametric analysis and case studies within the context of internal combustion engine simulations. A baseline case serves as a reference point, allowing for the exploration of distinct behaviors in cold and hot flow conditions within the engine. The investigation progresses by analyzing the impact of varying fuel reactivity levels on these flow regimes. This analysis explores how different reactivity properties influence the atomization processes during cold flow and the resulting flame structure during hot flow. Through a meticulous comparison of results, the study highlights key findings and their implications for engine performance and efficiency. By correlating these observations with theoretical frameworks and numerical models, the research aims to achieve a deeper understanding of the complex dynamics governing internal combustion engines, particularly focusing on soot formation. This knowledge can ultimately pave the way for engine design optimization and technological advancements that contribute to cleaner and more efficient engines.

IV.2 aachenBomb Simulation results :

IV.2.2 Cold Flow:

a) For Temperature :

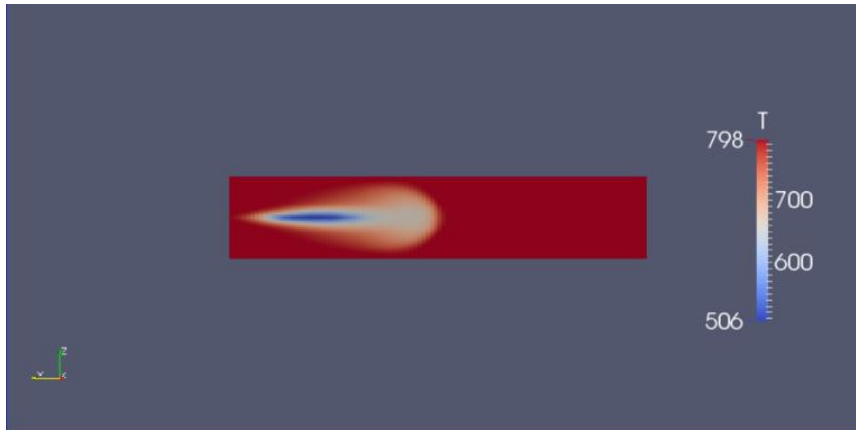


Figure.IV.1: Temperature distribution at 1.4ms within the Cold Flow combustion.

This ParaView *Figure IV.1*, captured at 1.4 milliseconds, reveals the temperature distribution within the spray. The color variation, with red representing warmer and blue cooler regions, clearly shows a decrease in temperature compared to potential hot flow scenarios. This observation aligns with the use of a cold flow injection, where the overall temperature of the spray is demonstrably lower.

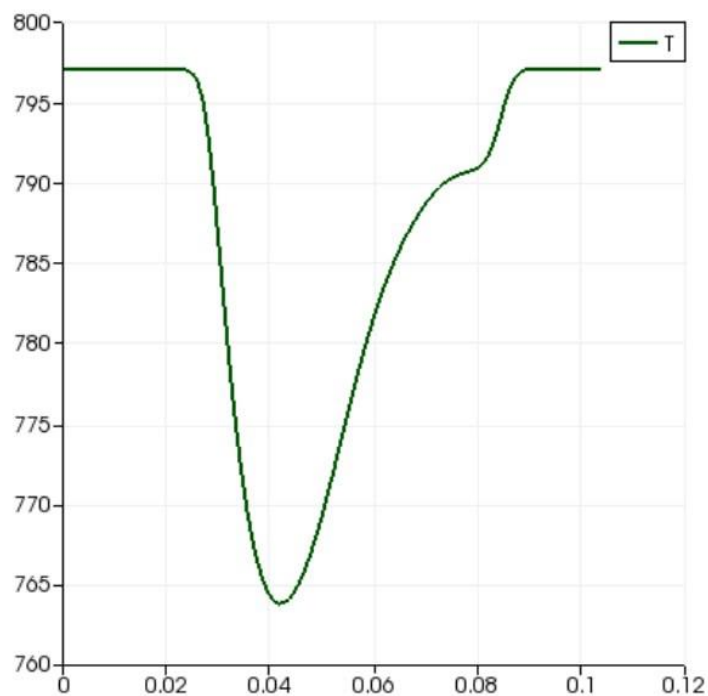


Figure.IV.2: Temperature graph within a cold flow in the combustion chamber

The curve initially shows a decreasing behavior, with the temperature decreasing linearly. The temperature reaches its peak at 797.089 degrees at a distance of 0.0228 units. It then continues to decrease until it reaches its lowest value of 773.842 degrees at a distance of 0.041569 units. After this turning point, the curve changes direction to become upward at 796.929 degrees at a distance of 0.0883346

b) For Velocity :

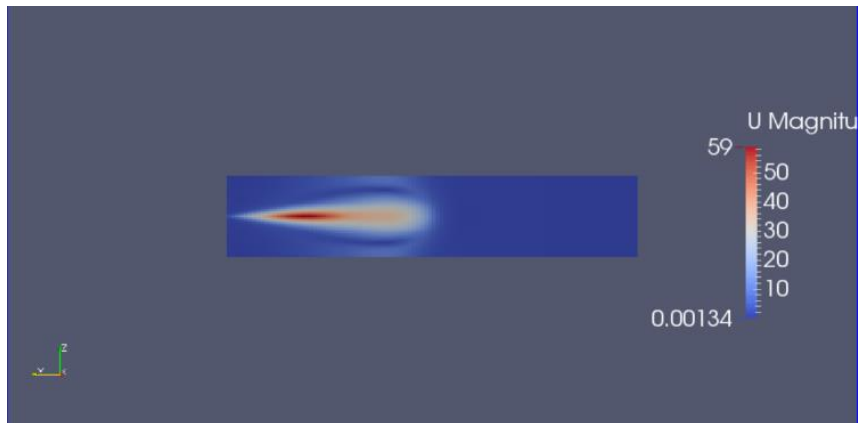


Figure.IV.3: velocity distribution at 1.4 within a cold flow in the combustion chamber

This cold flow spray image shows its speed at 1.4 milliseconds. Colors represent speed, with blue being slower and, interestingly, some white areas on the edges that might be moving a bit faster. These white bits are likely just a touch warmer than the rest, but not hot enough to ignite anything. Overall, the spray is nice and cool, just like you would expect with cold flow.

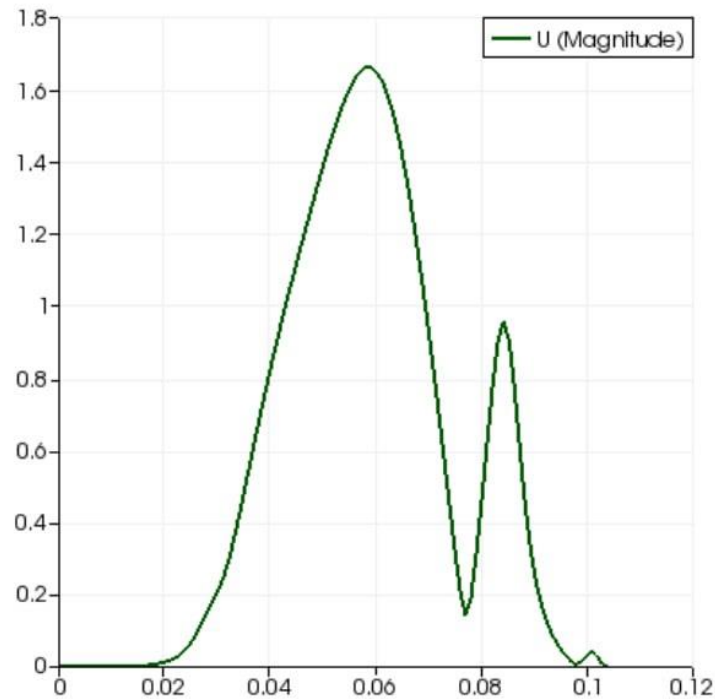


Figure.IV.4: velocity graph within a cold flow in the combustion chamber

The curve represents changes in speed as a function of distance, showing an increase in speed from a distance of 0.019 to 1.65272 at the point (0.0571577, 1.65272), then a decrease to 0.143014 at the point (0.0769031, 0.143014). After that, the speed rises again to 0.957846 at the point (0.0841777, 0.957846), and finally, the speed decreases gradually until it reaches zero. This behavior indicates different influences on speed across the distance, starting with acceleration due to a driving force, followed by the effect of resisting forces reducing speed, then another increase in speed due to a different force, and finally a gradual decrease in speed to zero due to opposing or resisting forces.

c) For Density :

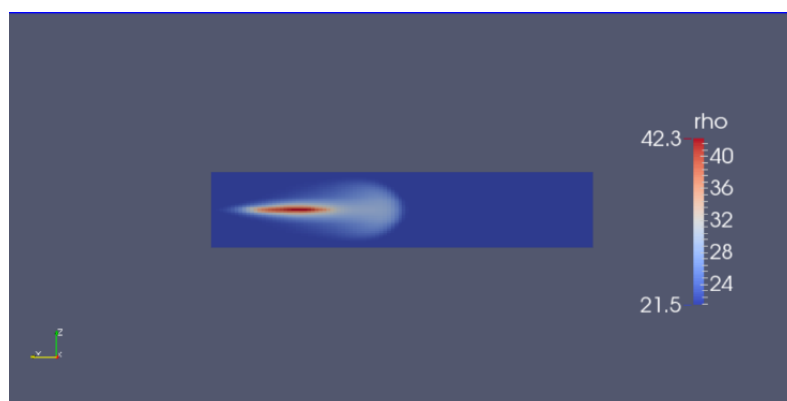


Figure.IV.5: Density distribution at 1.4ms within the Cold Flow combustion.

This image shows the density of the cold flow spray at 1.4ms. Blue shades indicate density. Darker blue is denser, lighter blue is looser. The spray is mostly even blue means consistent density, while slight variations at the edges could be due to flow or the injector.

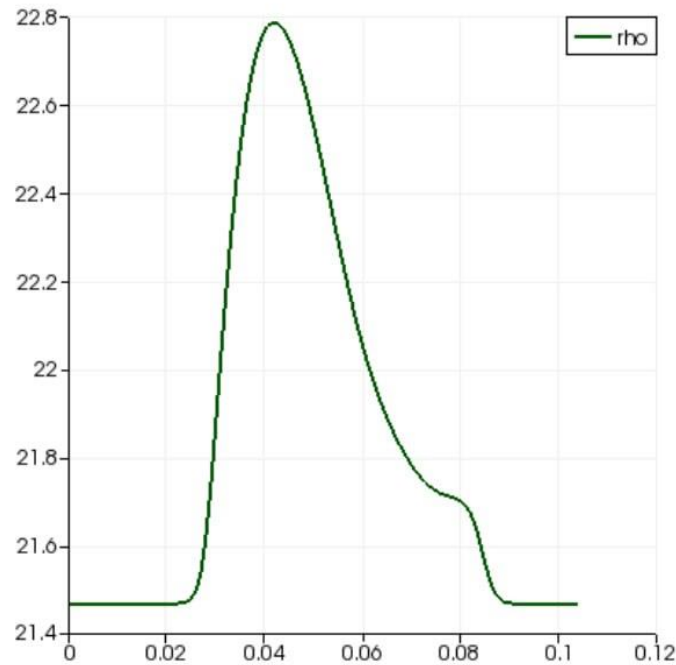


Figure.IV.6: Density graph within a cold flow in the combustion chamber

The curve represents density as a function of distance, showing stability at 21.4686 until the point (0.00227846, 21.4686), then rising to a maximum value of 22.7793 at the point (0.04053, 22.7793), and finally decreasing back to 21.4686. This behavior indicates specific effects on density across the distance: initially, the system is stable, then an effect increases density, and afterward, this effect ceases or conditions change, leading to a return to the original density level

d) For C7H16 Volume :

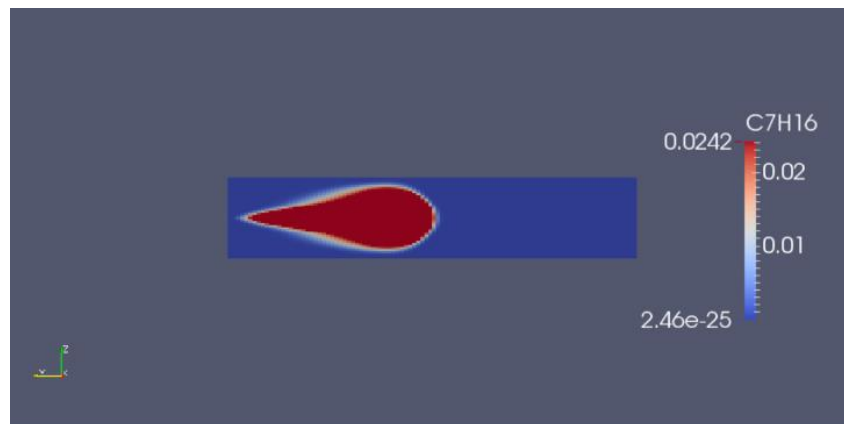


Figure.IV.7: Volume distribution of C7H16 at 1.4ms within the Cold Flow combustion.

This cold flow spray image shows the amount of C7H16 fuel at 1.4 milliseconds. Colors represent the amount, with red likely having more fuel and blue having less. Since there's no CO₂ or water vapor (shown in other pictures), the spray is cool and the C7H16 isn't burning.

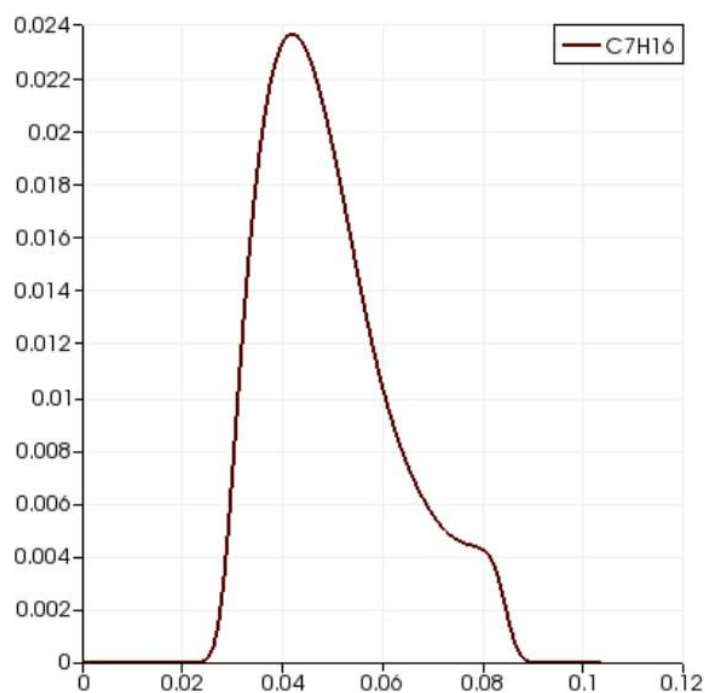


Figure.IV.8: C7H16 graph within a cold flow in the combustion chamber.

The curve represents the concentration of C7H16 as a function of distance, where it remains at 0.0 from the start to a distance of 0.0225, indicating no presence of C7H16 in this region. Then, the concentration rises to 0.0235433 at the point (0.04053, 0.0235433), indicating the emission or release of C7H16 from

a certain source. Finally, the concentration decreases to zero after this point, suggesting the consumption or dispersion of C_7H_{16} or the end of its emitting source

e) For O_2 Volume :

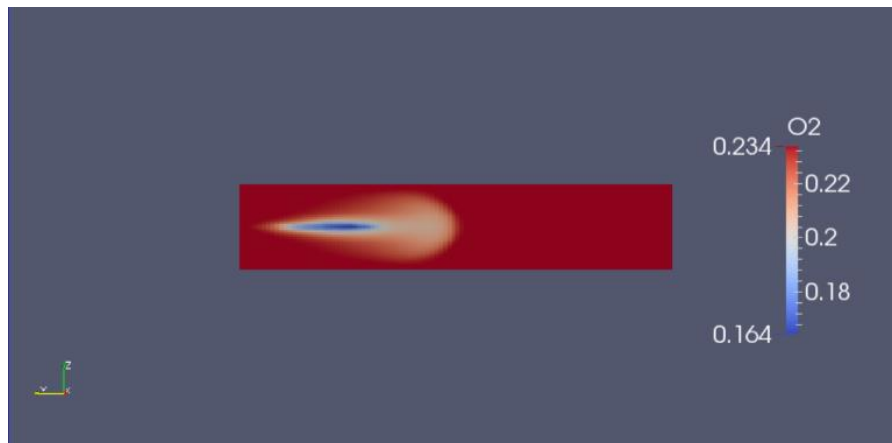


Figure.IV.9: Volume distribution of O_2 at 1.4ms within the Cold Flow combustion.

This ParaView visualization depicts a cold flow spray at 1.4 milliseconds. The red color distribution clearly represents the distribution of oxygen (O_2) within the spray. Since this is a cold flow scenario with no combustion, the O_2 isn't being consumed in a reaction. Therefore, the red color highlights the relatively uniform presence of O_2 throughout the spray.

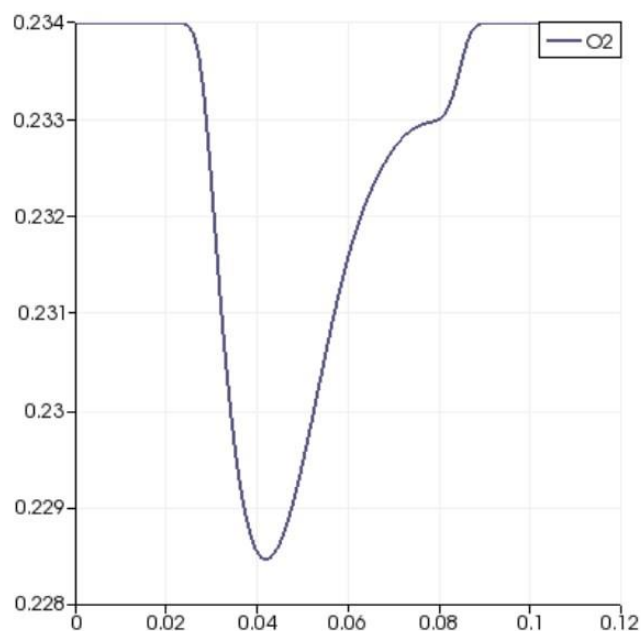


Figure.IV.10: O_2 volume graph within a cold flow in the combustion chamber.

The curve represents changes in oxygen levels as a function of distance, indicating a combustion process. Initially, the oxygen level remains constant at 0.23399 up to a distance of 0.0228631, suggesting no combustion reaction is occurring. Then, the oxygen level decreases to 0.228462 at a distance of 0.0415692. After this point, the oxygen level begins to rise again, reflecting either the end of the combustion process or the influx of oxygen from an external source, thus increasing its concentration.

f) For N2 Volume :

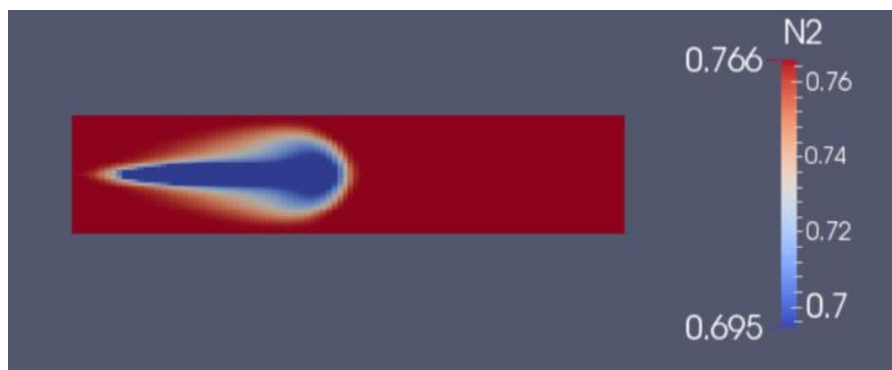


Figure.IV.11: Volume distribution of N2 at 1.4ms within the Cold Flow combustion.

IV.2.1 Hot Flow :

a) For temperature:

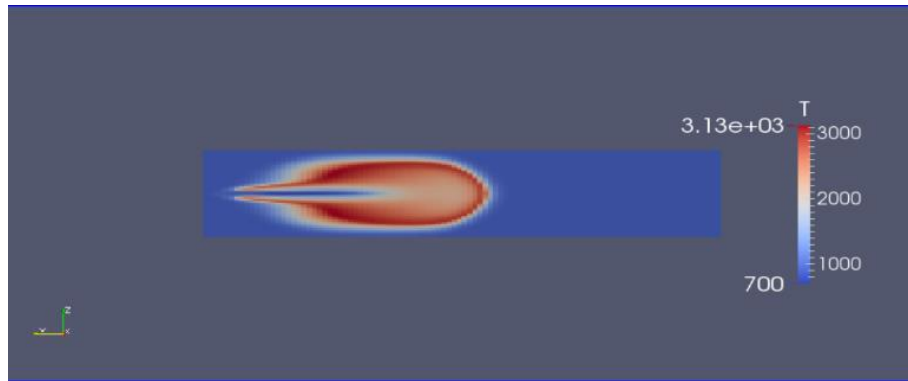


Figure.IV.12: temperature distribution at 1.4ms within the Hot Flow in the combustion chamber

ParaView visualization shows a well-defined, diffuse red zone characteristic of a high-temperature region or potential ignition zone. A distinct white plume trails behind, indicative of a gaseous wake likely composed of unburnt or partially burnt fuel and hot combustion products ejected by the spray.

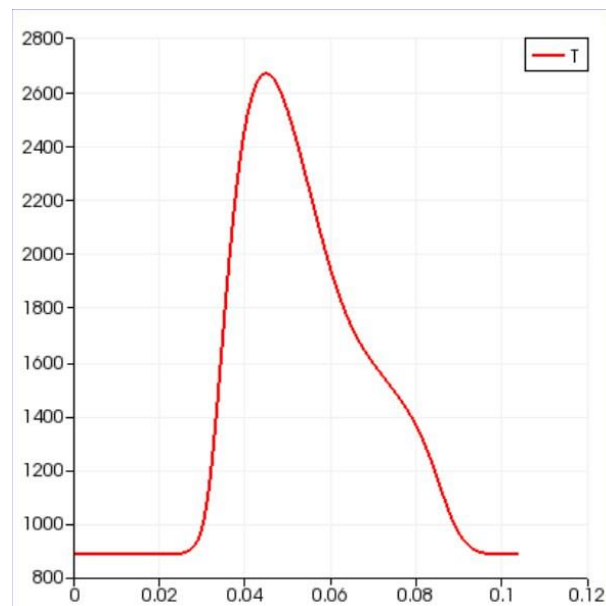


Figure.IV.13: temperature graph within a hot flow in the combustion chamber

The curve represents the change in temperature during the combustion process as a function of distance. Initially, the temperature remains constant at 888.845 K up to a distance of 0.0239 meters. Beyond this point, the temperature begins to increase sharply, reaching a peak value of 2661.05 K at a distance of 0.0426 meters. Following this peak, the temperature gradually decreases until it stabilizes

again at 893.393 K at a distance of 0.094 meters. This behavior reflects different stages of the combustion process: an initial stable temperature phase, followed by a significant increase due to the intense combustion reaction, and then a gradual decrease as the system cools down and returns to a stable state.

b) For velocity:

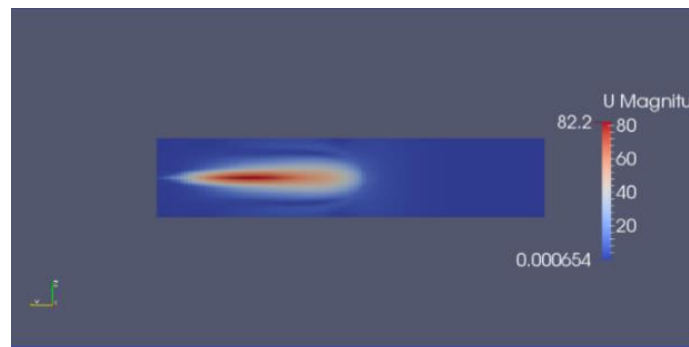


Figure.IV.14 : velocity distribution at 1.4ms within the Hot Flow combustion

in the *figure III.14*, captured at 1.4 milliseconds, shows the spray's speed. We see a thin, fast-moving red area (high velocity) within the spray. This high-speed zone might play a role in the quick ignition, which we know happens in less than 1.4 milliseconds.

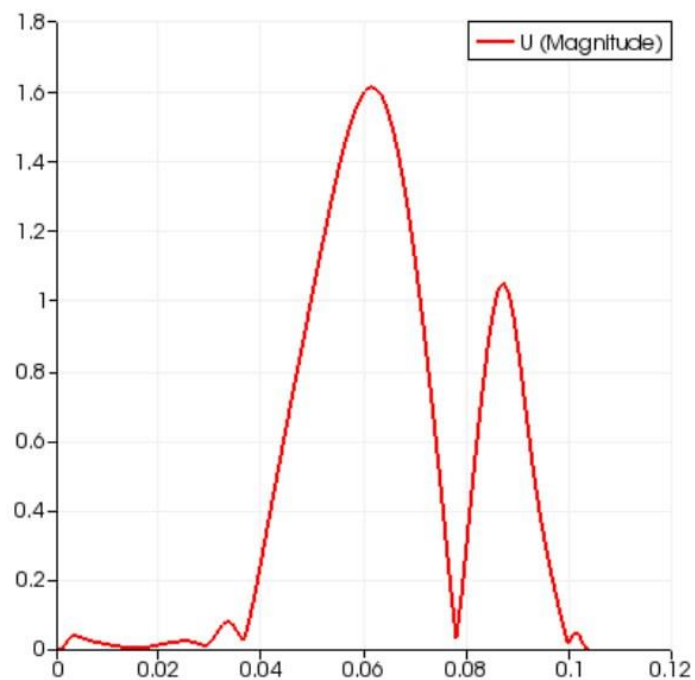


Figure.IV.15: velocity graph within a hot flow in the combustion chamber

The curve represents the change in velocity during the combustion process as a function of distance. Initially, there are oscillations in velocity until reaching the point (0.036 meters, 0.0268m/s). Following these oscillations, there is a significant increase in velocity, peaking at (0.060 meters, 1.60m/s). After this peak, the velocity decreases to (0.0779 meters, 0.033m/s), then rises again to (0.086 meters, 1.037m/s), and finally decreases until it reaches zero. This behavior indicates a dynamic combustion process with initial fluctuations in velocity, followed by periods of rapid acceleration and deceleration, reflecting the complex interactions and varying intensities within the combustion reactions before stabilizing.

c) For Density:

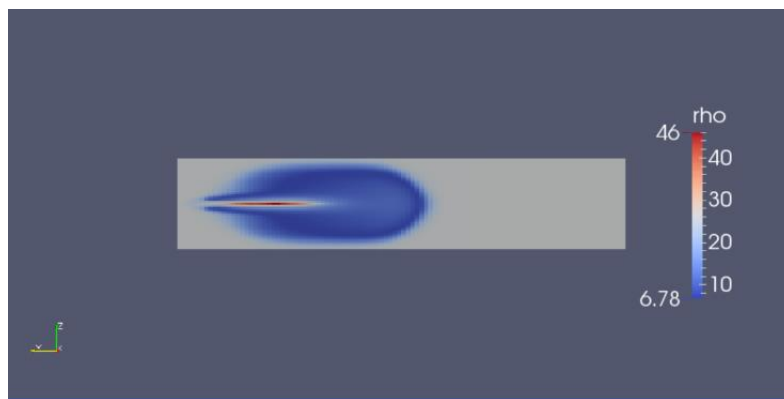


Figure.IV.16 : Density distribution at 1.4ms within the Hot Flow combustion

the figure (112212), captured at 1.4 milliseconds, shows the density distribution within the spray. A distinct, high-density region (red) appears within the core, potentially linked to the injector nozzle or a residual liquid core. The surrounding blue region represents the lower, almost constant density of the vaporized spray, since density remains relatively unchanged under these conditions.

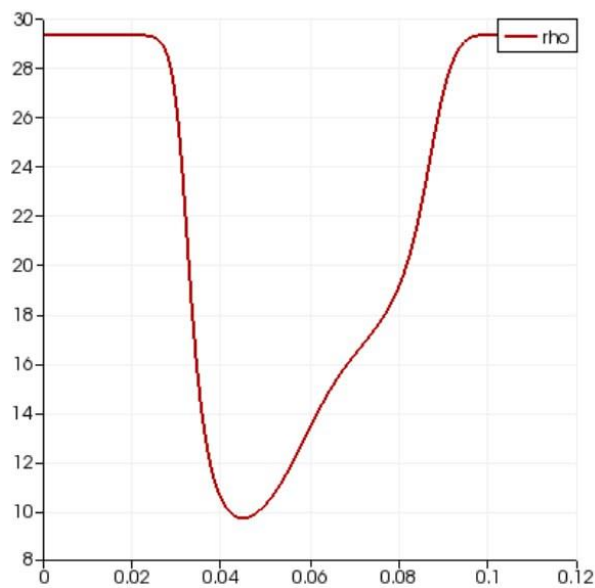


Figure.IV.17: Density graph within a hot flow in the combustion chamber

The curve represents the change in density during the combustion process as a function of distance. Initially, the density remains constant at 29.3685 until a distance of 0.02182 meters. Beyond this point, the density begins to decrease, reaching a low of 9.745 at a distance of 0.0436 meters. Following this decrease, the density gradually increases until it stabilizes again at 29.30 at a distance of 0.0966 meters. This behavior indicates different phases of the combustion process: an initial stable density phase, followed by a significant decrease due to the combustion reaction, and then a gradual recovery as the density returns to a stable state.

d) For C₇H₁₆ Volume :

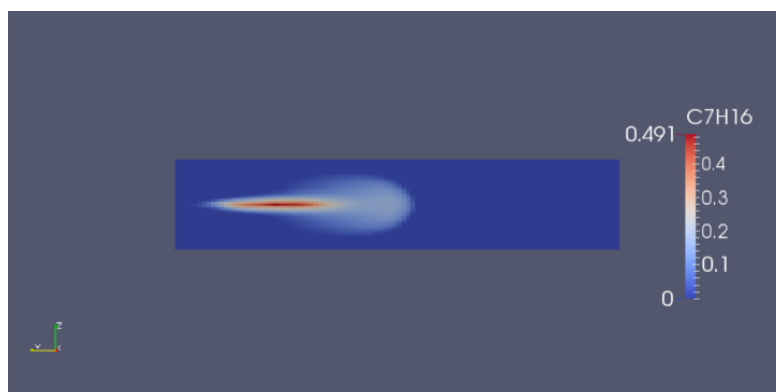


Figure.IV.18: Volume distribution of C₇H₁₆ at 1.4ms within the Hot Flow combustion .

1.4 milliseconds offers insights into the initial distribution of C7H16 (heptane) within the spray, a crucial factor influencing combustion behavior. The distinct red zone suggests a region with a higher concentration of C7H16, potentially corresponding to the injector nozzle or a denser core of the liquid fuel. This concentrated area could play a significant role in the initiation and development of the combustion process.

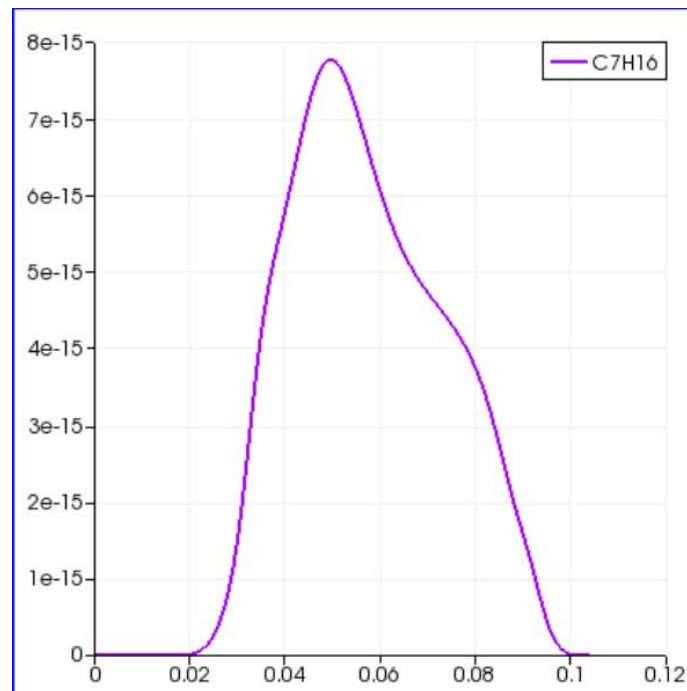


Figure.IV.19: C7H16 Volume graph within a hot flow in the combustion chamber

*The curve represents the change in C7H16 concentration during the combustion process as a function of distance. Initially, there is no C7H16 detected up to a distance of 0.019 meters. Beyond this point, the concentration of C7H16 begins to increase, reaching a peak value of (7.77×10^{-15}) at a distance of 0.0478 meters. After this peak, the concentration of C7H16 gradually decreases until it returns to zero at a distance of 0.097 meters. This behavior indicates that C7H16 is initially absent, then produced or released during the intermediate phase of combustion, and finally consumed or dissipated as the combustion process progresses to completion.

e) For Co2 Volume :

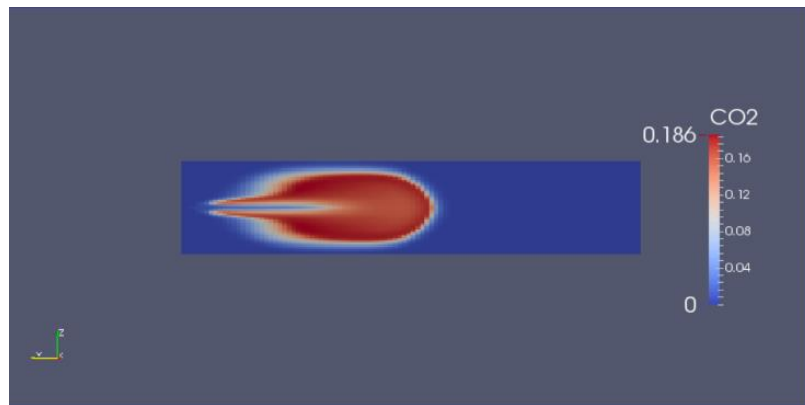


Figure.IV.20: Volume distribution of Co2 at 1.4ms within the Hot Flow combustion

at 1.4 milliseconds shows the distribution of CO₂ volume fraction within the spray. The text labels with numbers and scientific notation likely represent the CO₂ volume fraction values. The red region signifies a higher volume fraction of CO₂, potentially corresponding to the initial stages of combustion where CO₂ is being produced. The surrounding blue region represents a lower CO₂ volume fraction, which may be due to factors like incomplete mixing or CO₂ diffusion within the spray."

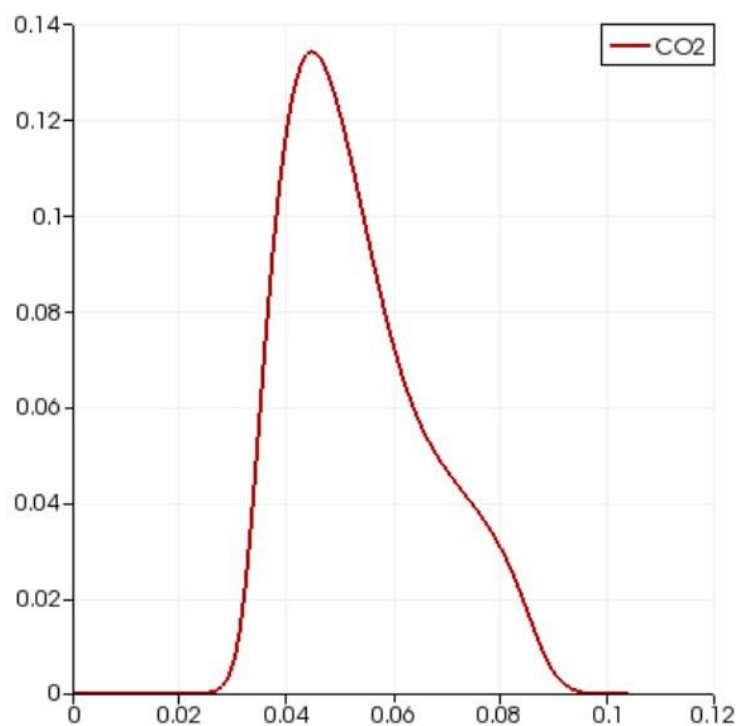


Figure.IV.21: Co2 Volume graph within a hot flow in the combustion chamber

The curve represents the change in CO₂ concentration during the combustion process as a function of distance. Initially, there is no CO₂ detected up to a distance of 0.0259 meters. Beyond this point, the CO₂ concentration begins to increase, reaching a peak of 0.1337 at a distance of 0.043 meters. After this peak, the CO₂ concentration gradually decreases until it returns to zero at a distance of 0.093 meters. This behavior suggests the stages of the combustion process: an initial phase with no CO₂ production, followed by an increase in CO₂ as combustion intensifies, and then a decrease as the combustion process completes and the CO₂ is either consumed or dissipates.

f) For H₂O Volume :

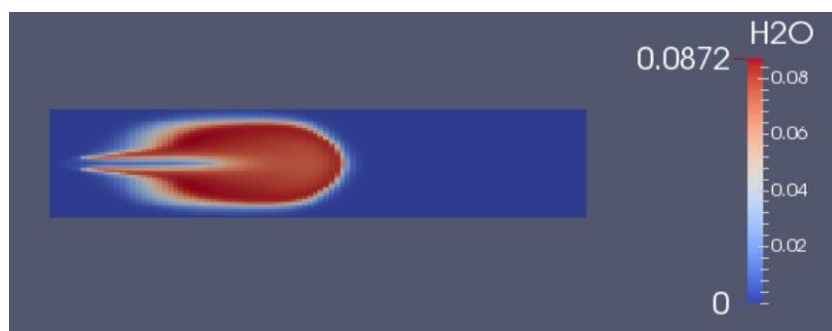


Figure.IV.22: Volume distribution of H₂O at 1.4ms within the Hot Flow combustion .

captured at 1.4 milliseconds, depicts the distribution of H₂O (water vapor) within the spray, a key product of the C₇H₁₆ (heptane) combustion reaction. The prominent red region signifies a higher volume fraction of H₂O, potentially indicating areas with a more intense combustion process. The surrounding blue region represents a lower H₂O volume fraction, which could be due to factors like incomplete mixing or the spatial distribution of the reacting fuel (C₇H₁₆). The text labels with numbers and scientific notation likely correspond to the specific H₂O volume fraction values in different parts of the spray."

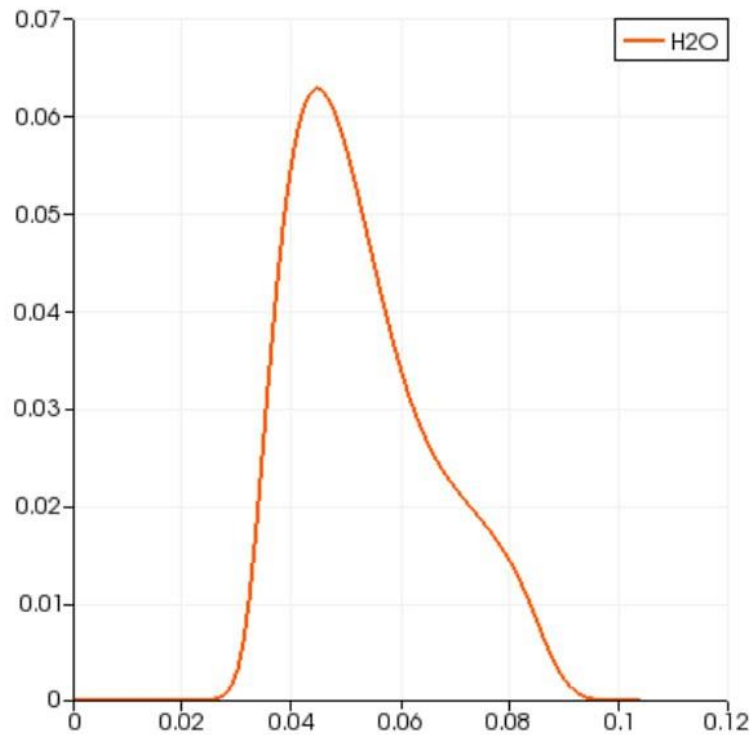


Figure.IV.23: H₂O Volume graph within a hot flow in the combustion chamber

The curve represents the change in H₂O concentration during the combustion process as a function of distance. Initially, there is no H₂O detected up to a distance of 0.0249 meters. Beyond this point, the H₂O concentration begins to increase, reaching a peak value of 0.0625 at a distance of 0.043 meters. After this peak, the concentration of H₂O gradually decreases until it returns to zero at a distance of 0.0935 meters. This behavior indicates that H₂O is initially absent, then produced during the intermediate phase of combustion, and finally consumed or dissipated as the combustion process progresses to completion.

g) For O₂ Volume :

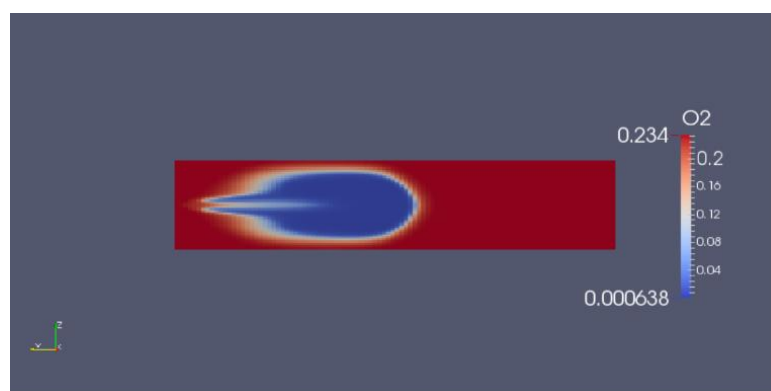


Figure.IV.24: Volume distribution of O₂ at 1.4ms within the Hot Flow combustion .

While the Para View visualization at 1.4 milliseconds does not show oxygen (O₂) directly, the observed transition from red to blue regions within the spray offers insights into the combustion process. The red region likely represents a zone with active combustion, potentially due to the presence of O₂ necessary for the reaction. The appearance of a distinct blue region surrounding the red area could be indicative of O₂ consumption as combustion progresses at this early stage (1.4 milliseconds)."

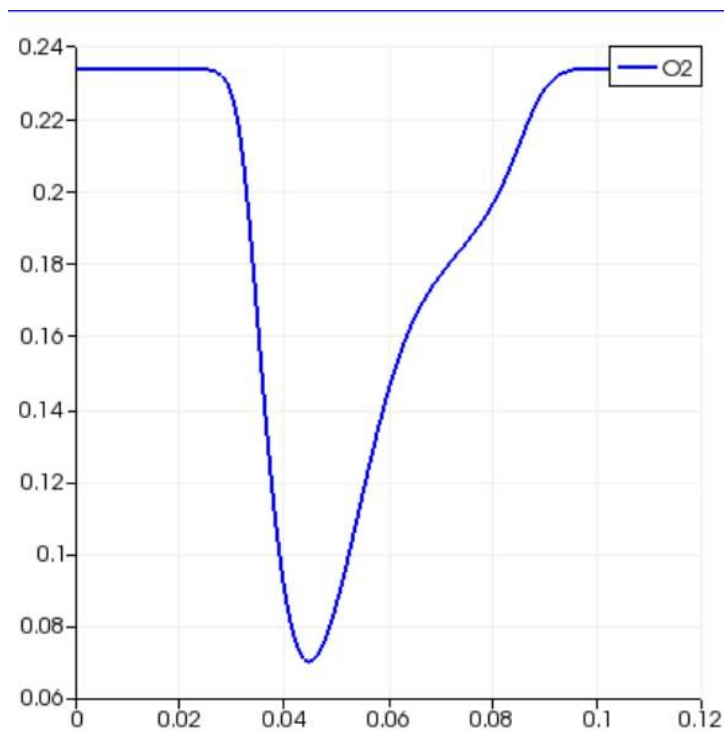


Figure.IV.25: O₂ Volume graph within a hot flow in the combustion chamber

The curve represents changes in oxygen levels as a function of distance, indicating a combustion process. Initially, the oxygen level remains constant at 0.23399 up to a distance of 0.0228631, suggesting no combustion reaction is occurring. Then, the oxygen level decreases to 0.228462 at a distance of 0.0415692, due to oxygen consumption in the combustion process. After this point, the oxygen level begins to rise again, reflecting either the end of the combustion process or the influx of oxygen from an external source, thus increasing its concentration.

g) For N₂ Volume :

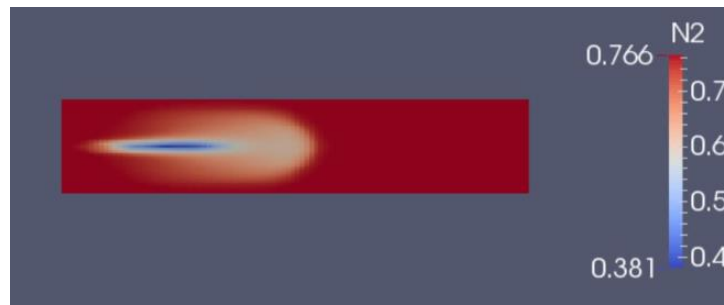


Figure.IV.26: Volume distribution of N2 at 1.4ms within the Hot Flow combustion

Even in hot flow conditions, nitrogen (N₂) remains relatively inert during combustion. This visualization might track a different aspect of the process, but due to its strong molecular bonds, N₂ wouldn't see a significant decrease in concentration despite the high temperatures.

IV.2.3 Soot Modeling :

The implementation of the soot model in the AachenBomb simulation involves a systematic approach to configure and execute the simulation. It begins with the placement of essential files such as `soot` and `G` (for incident radiation) in the `0/` folder of the case directory, followed by modifications to key configuration files. The `fvSolution` file is adjusted to include the necessary entry for `Gfinal`, crucial for the radiation model. Additionally, the `thermophysicalProperties` file in the `constant` folder undergoes editing to integrate inputs required for single-step reaction modeling. The `sprayCloudproperties` file is modified to ensure compatibility with the chosen breakup model. Detailed adjustments are made to the `radiationProperties` file within `constant`, focusing on incorporating inputs specific to the soot model, as outlined in the guidelines provided. The process continues with the execution of the `blockMesh` command to generate the mesh, establishing the necessary geometry and initial conditions for the simulation setup. Finally, the simulation is launched using `sprayFoam`, enabling the AachenBomb solver to run with the implemented soot model. This comprehensive workflow enables thorough investigation into combustion reactions and the accurate modeling of particulate matter formation within the simulated environment, yielding valuable insights into combustion dynamics and their environmental implications.

After executing this comprehensive setup, we expect to obtain the following results: a detailed analysis of combustion reactions, including the formation and distribution of particulate matter (soot, temperature, velocity, Density etc), within the simulated environment. This approach allows for a thorough exploration of combustion dynamics and their environmental impacts, providing valuable insights for optimizing combustion processes and reducing emissions[20].

a) For Temperature :

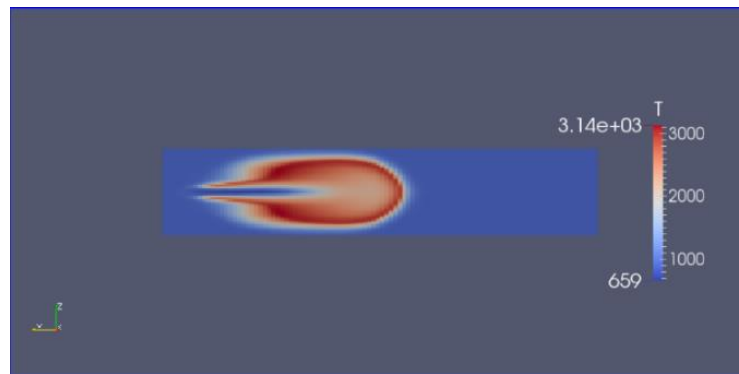


Figure.IV.27: Temperature distribution at 1.4ms within the 'SootModel' combustion.

This ParaView image depicts the temperature distribution within a spray. Warmer regions are represented by red colors, while blue areas signify cooler zones. The visualization reveals a unique spray shape with a more open center. This central area exhibits a distinct temperature profile compared to the surrounding region. The temperature difference between the center and the surrounding area is difficult to determine definitively without the specific color scheme used in the visualization, but it's evident that the open center plays a role in shaping the overall temperature distribution within the spray

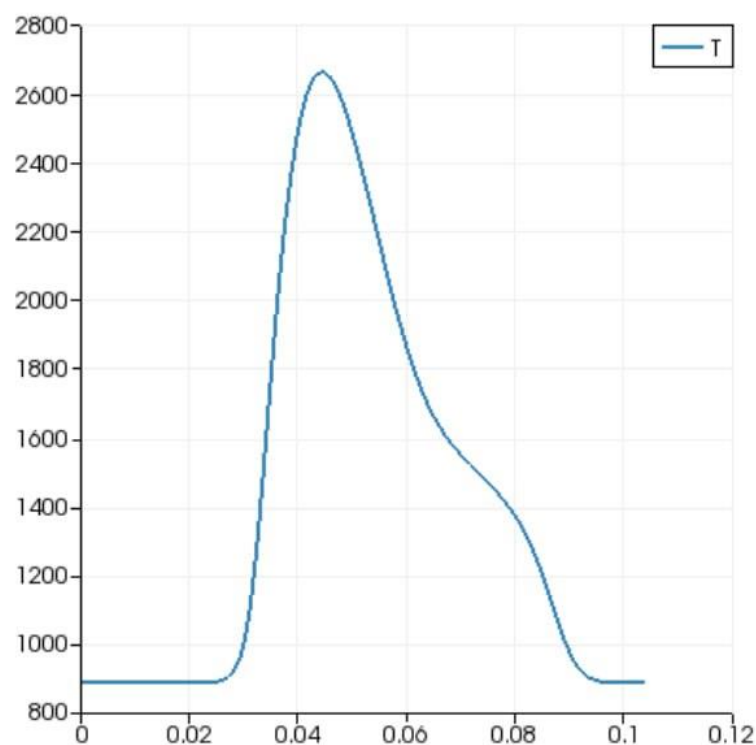


Figure.IV.28: Temperature graph within a 'SootModel' in the combustion chamber.

The curve represents the change in temperature during the combustion process as a function of distance. Initially, the temperature remains constant at 892.757 K until a distance of 0.0249415 meters. Beyond

this point, the temperature begins to increase sharply, reaching 2641.49 K at a distance of 0.0426085 meters. Following this peak, the temperature gradually decreases until it stabilizes at 896.43 K at a distance of 0.09457 meters. This behavior reflects different stages of combustion, starting with a stable burning phase, followed by an intense and rapid combustion phase, and finally entering a cooling and thermal stabilization phase.

b) For velocity :

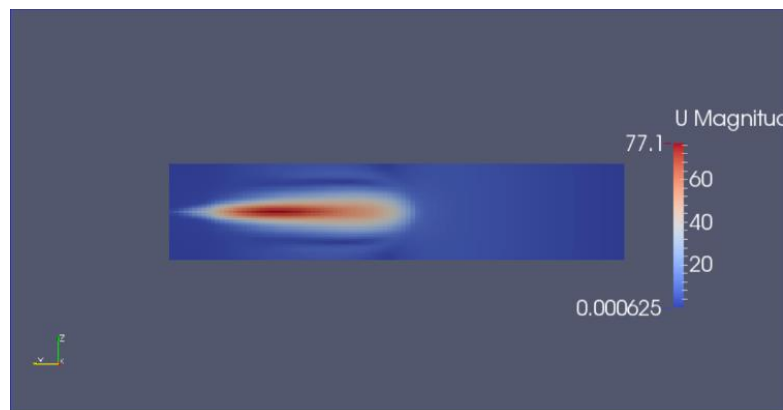


Figure.IV.29: velocity distribution at 1.4ms within the ‘SootModel’ combustion.

At first glance, this ParaView visualization from a soot model simulation captures the dynamics of a fuel injector spray 1.4 milliseconds after injection. The color variation immediately draws attention, with red hues likely representing areas of higher velocity and blue signifying slower ones. This suggests a well-defined structure, with a central zone of intense activity (red) surrounded by a region of progressively decreasing velocity (blue) that extends outwards.

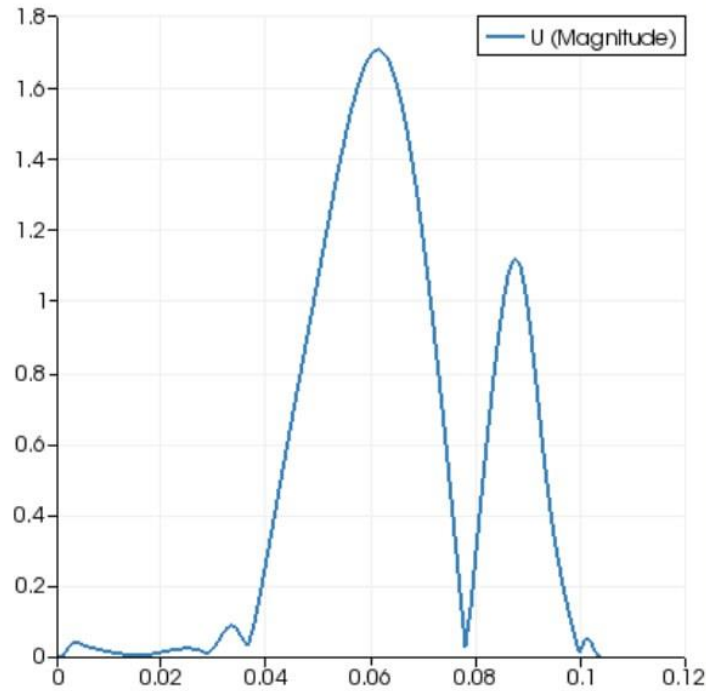


Figure.IV.30: Velocity graph within a ‘SootModel’ in the combustion chamber.

The combustion rate curve fluctuates as a function of distance, indicating varying combustion efficiency. Initially, it oscillates until reaching (0.0363731, 0.0320247), reflecting initial variability. The rate then rises sharply to (0.0602754, 1.69885), suggesting improved combustion conditions. It subsequently decreases to (0.0779423, 0.0315267), showing continued fluctuations. Finally, it rises again to (0.0872954, 1.11996) before ultimately declining to zero, marking the end of combustion. This analysis underscores the impact of environmental conditions on combustion performance.

c) For Density :

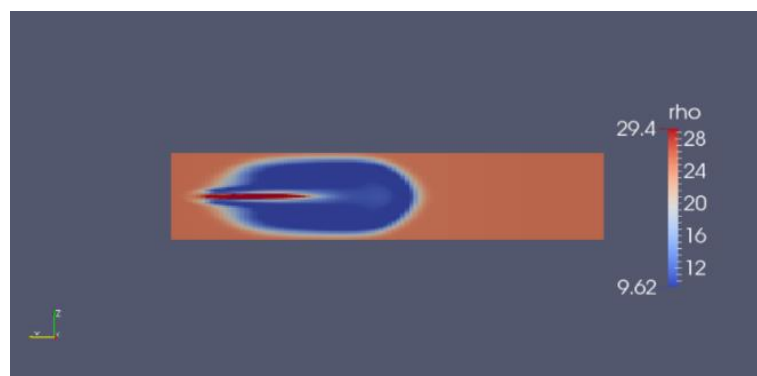


Figure.IV.31: Density distribution within a ‘SootModel’ in the combustion chamber.

This image, likely from a soot model simulation, shows the density (ρ) of a fuel injector spray at 1.4 milliseconds after injection. The color variation reveals a distinct pattern. Red areas, typically signifying higher density, appear concentrated in the center of the spray. This central zone likely holds a higher

concentration of fuel droplets compared to the surrounding areas. As we move outwards from the center, the color transitions to blue, indicating progressively lower density (less fuel).

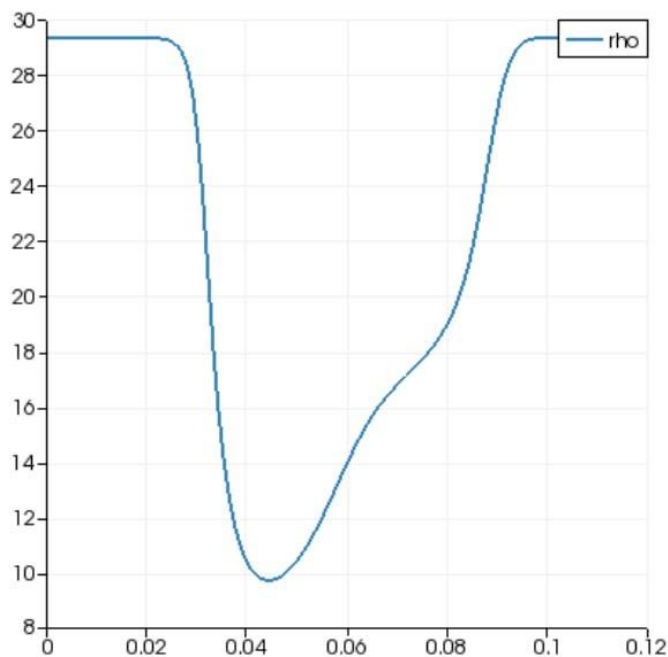


Figure.IV.32: Density graph within a ‘SootModel’ in the combustion chamber.

The curve represents the change in density during the combustion process as a function of distance. Initially, the density remains constant at 29.3351 until a distance of 0.0228631 meters. Beyond this point, the density begins to decrease, reaching a low of 9.74096 at a distance of 0.0436477 meters. After this, the density gradually increases until it stabilizes again at 29.3112 at a distance of 0.09484 meters. This behavior indicates different phases of the combustion process: an initial stable density phase, followed by a significant decrease in density likely due to the combustion reaction, and then a gradual increase as the system returns to a stable state.

d) For C7H16 Volume :

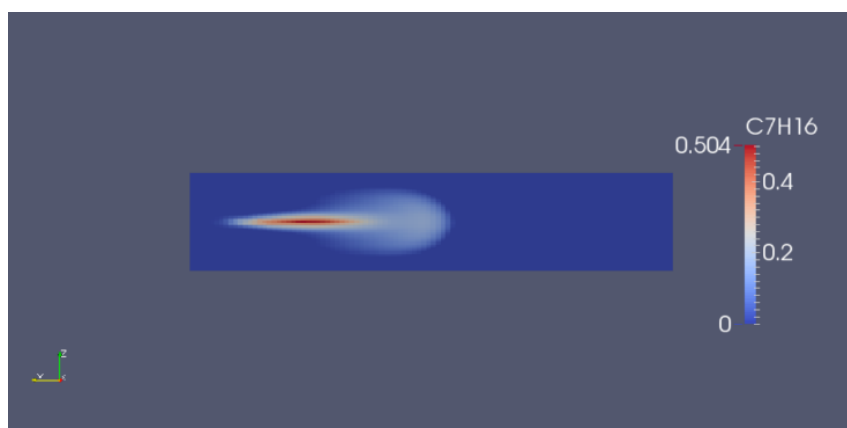


Figure.IV.33: Volume distribution of C7H16 within a ‘SootModel’ in the combustion chamber.

This image, likely from a C7H16 injection simulation, captures a snapshot at 1.4 milliseconds a distinct red color dominates the view, suggesting a clear presence of C7H16 within the visualization at that specific time frame.

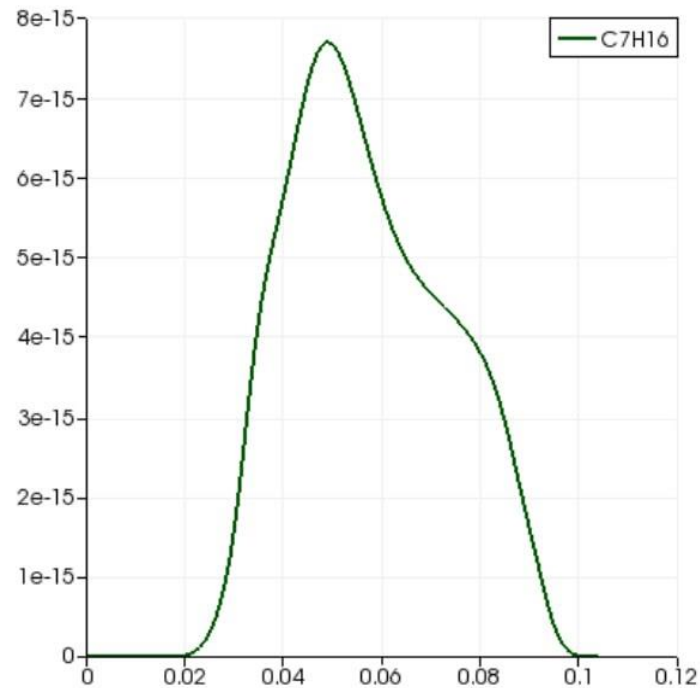


Figure.IV.34: C7H16 Volume graph within a ‘SootModel’ in the combustion chamber.

The curve depicting the changes in C7H16 (heptane) concentration over time consists of three main phases: initially, the concentration is zero up to a time of 0.02, indicating a period before the reaction or combustion begins. Then, the concentration gradually increases from 0.02 until it reaches a maximum value of $(0.0478046 - 7.66471 \times 10^{-15})$, reflecting the active reaction phase where heptane production intensifies. After reaching this peak, the concentration starts to gradually decrease until it returns to zero, indicating the complete consumption of heptane in the reaction or combustion process. This analysis helps in understanding the dynamics of the chemical reaction and the distribution of heptane concentration over time.

e) For CO₂ Volume :

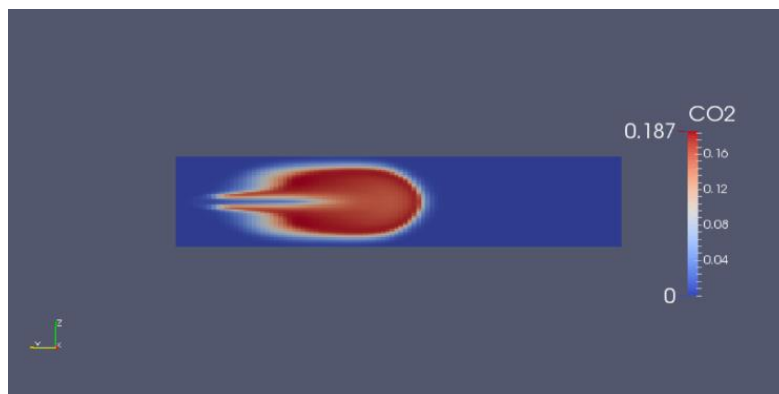


Figure.IV.35: Volume distribution of Co₂ within a 'SootModel' in the combustion chamber.

This ParaView image (likely soot model) shows CO₂ dominating the combustion chamber at 1.4 milliseconds (red color). The wide open space, particularly in the center, might be related to the soot model's ignition simulation. In such models, open areas could indicate less fuel or a different combustion stage compared to the denser regions.

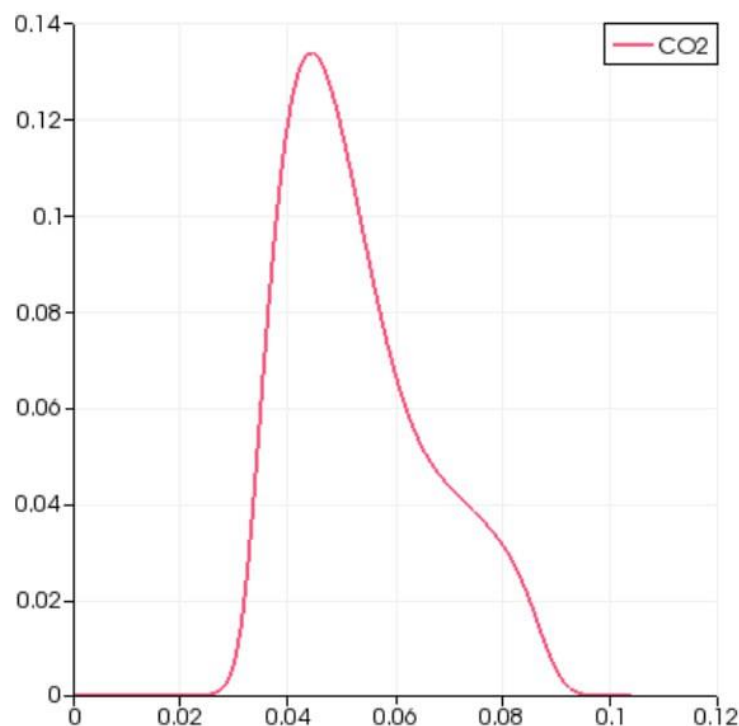


Figure.IV.36: Co₂Volume graph within a 'SootModel' in the combustion chamber

The CO₂ emissions curve during the combustion process initially shows a decrease or absence of CO₂ until a distance of 0.024, indicating incomplete combustion or significant close-range influences. The values then increase, peaking at (0.043647;0.133775), representing efficient and complete fuel combustion. Beyond this peak, the curve gradually declines, reflecting a reduction in combustion rates

or the impact of environmental conditions and available fuel. This analysis demonstrates how CO₂ levels vary with distance during combustion, influenced by chemical reactions and environmental factors.

f) For H₂O Volume:

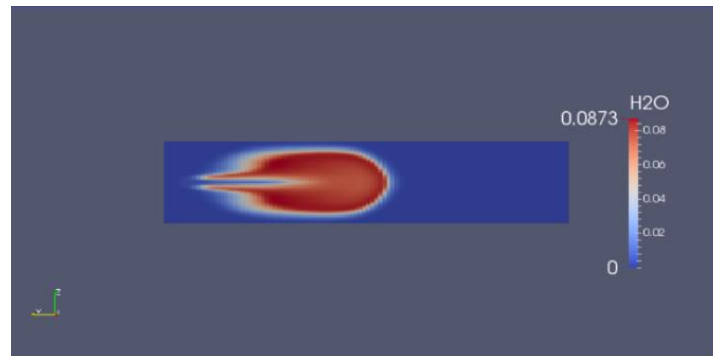


Figure.IV.37: Volume distribution of H₂O within a 'SootModel' in the combustion chamber.

As observed in this figure, the increase in water vapor (H₂O) from blue to red likely doesn't directly correspond to soot formation. Soot tends to form more readily in fuel-rich conditions (red) where there's excess fuel available. This suggests the model might be visualizing water vapor alongside another property that's more directly linked to soot formation.

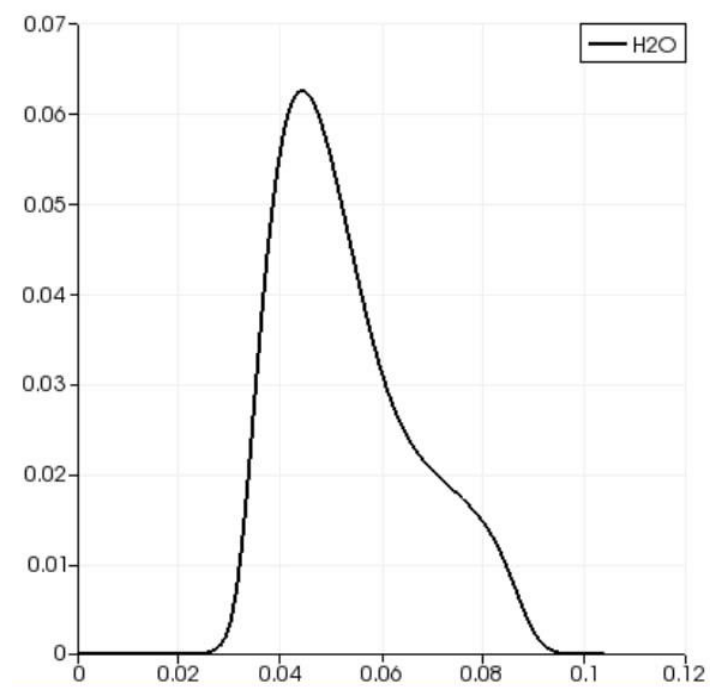


Figure.IV.38: H₂O Volume graph within a 'SootModel' in the combustion chamber.

The H₂O emissions curve during the combustion process initially shows a decrease or absence of H₂O

until a distance of 0.024, indicating incomplete combustion or significant close-range influences. The values then increase, peaking at (0.043647,0.06432), representing efficient and complete fuel combustion. Beyond this peak, the curve gradually declines, reflecting a reduction in combustion rates or the impact of environmental conditions and available fuel. This analysis demonstrates how H₂O levels vary with distance during combustion, influenced by chemical reactions and environmental factors.

g) For O₂ volume :

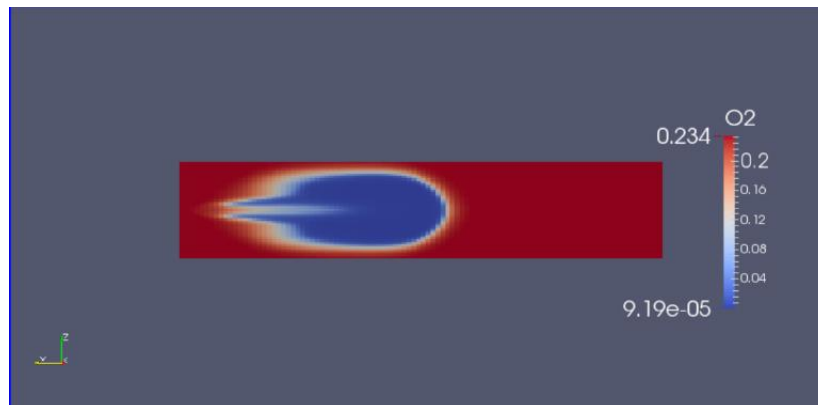


Figure.IV.39: Volume distribution of O₂ within a ‘SootModel’ in the combustion chamber.

This scientific visualization portrays a gradual increase in water vapor content (blue to red). While O₂ concentration isn't directly depicted, a real heptane combustion process would demonstrably exhibit a corresponding decrease in O₂ (oxygen depletion) as the fuel combusts. The blue region of the image likely aligns with this scenario, representing a leaner condition with a higher concentration of O₂ available for combustion.

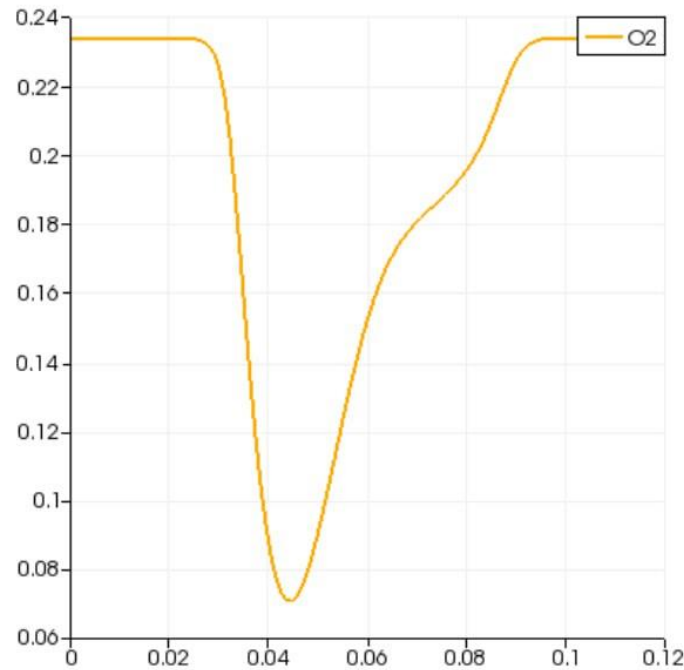


Figure.IV.40: O2 Volume graph within a ‘SootModel’ in the combustion chamber.

The oxygen (O₂) ratio curve relative to distance during combustion showcases distinct dynamics. Initially, the curve maintains stability until (0.0259808, 0.23336), indicating consistent oxygen levels early on. As distance progresses, there is a noticeable decline culminating at (0.0436477, 0.0709621), suggesting reduced oxygen ratios likely due to increased fuel consumption. Towards the end, an ascent is observed leading to (0.09457, 0.233443), possibly indicating adaptive combustion responses or environmental adjustments affecting oxygen availability. This illustrates the complex interplay between combustion processes, fuel efficiency, and environmental influences on oxygen utilization.

H) For N₂ volume:

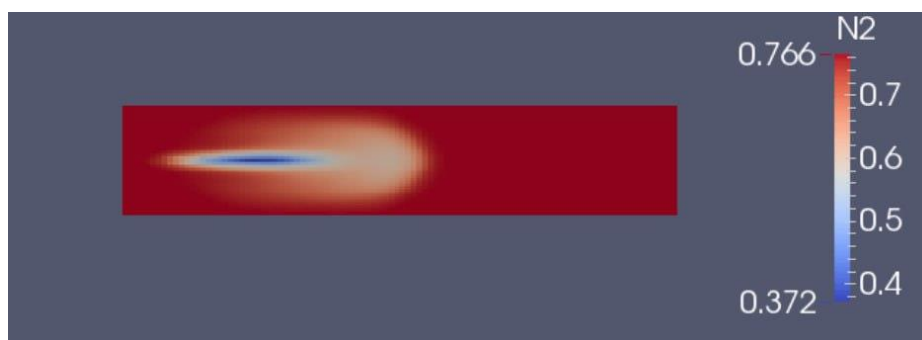


Figure.IV.41: Volume distribution of N₂ within a ‘SootModel’ in the combustion chamber.

Nitrogen (N₂) boasts exceptionally strong molecular bonds, making it highly resistant to breaking down during combustion, even in the presence of soot. As a result, a visualization like this likely wouldn't show a significant decrease in N₂ concentration. This suggests the visualization is likely tracking a different aspect of the combustion process, one that involves elements more susceptible to reactions or

breakdowns at high temperatures, potentially focusing on the behavior of the fuel or combustion products like soot itself.

i) For soot Volume:

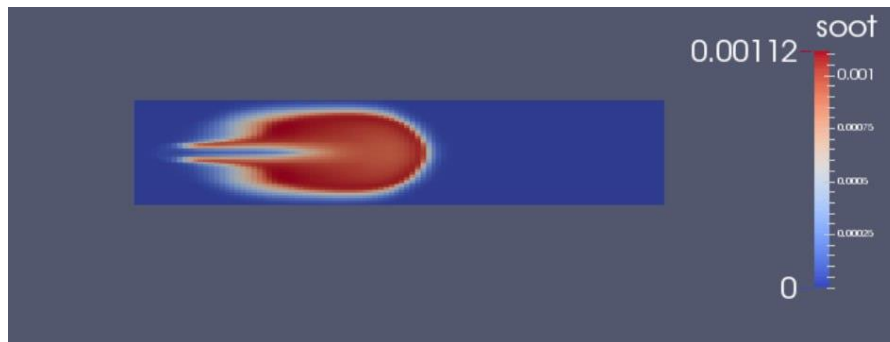


Figure.IV.42 Volume distribution of “Soot” within a ‘SootModel’ in the combustion chamber.

The ParaView image shows a cross-section of the combustion chamber after adding soot to the heptane spray. By tracking the soot, we can see a high concentration in the center of the spray, indicating intense combustion happening there. This concentration gradually decreases as we move away from the center, forming a cone-shaped distribution of soot. This distribution pattern is likely caused by the interaction between the heptane injection and the airflow within the chamber. Tracking soot in this way provides valuable information about the effectiveness of the combustion process, suggesting an improvement compared to without soot addition.

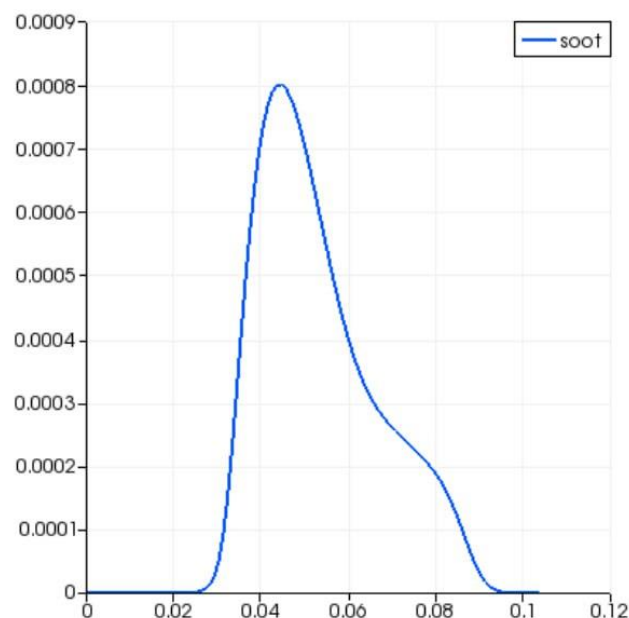


Figure.IV.43: Soot Volume graph within a ‘SootModel’ in the combustion chamber.

The graph reveals a trend in soot volume within the combustion chamber. A single data point indicates a soot volume of 0.000800602 cubic meters at a specific distance (0.0436477 meters). This suggests a potential relationship between distance and soot volume, but further data points would be needed to confirm the trend.

IV.3 Comparison of results:

The Aachenbomb c7h16 tutorial showcases a dramatic temperature difference between coldflow and hotflow simulations at 1.4ms, highlighting the significant heat release from hotflow combustion. Interestingly, the sootModel simulation displays a profile nearly identical to the hotflow case. This suggests that at this specific time (1.4ms), the soot particles might be making a **quiet difference**, possessing thermal properties similar to the hotflow combustion products.

Several factors could be contributing to this subtle influence:

a) **Soot Temperature:** The soot, likely due to its proximity to the hotflow flame, might reach very high temperatures. This elevated soot temperature could be causing it to behave thermally similar to other hotflow products.

b) **Soot Radiation:** The chosen soot model might consider the influence of soot radiation on temperature. If the soot particles are actively participating in radiative heat transfer, it could significantly heat them, explaining the alignment with the hotflow profile.

Unraveling the exact reasons behind this **quiet difference** requires further investigation into the specific soot model used and its assumptions regarding the radiative properties of soot at 1.4ms.

IV.3.1 Combustion Characteristics: Comparison of Soot and Hot Flow Cases

a) **Temperature comparison:**

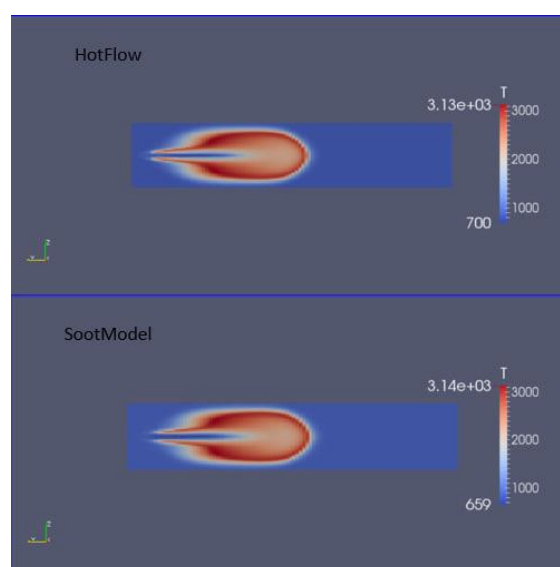


Figure.IV.44: Temperature distribution of Hotflow and 'SootModel' in the combustion chamber

Examining both figures reveals a clear link between temperature distribution and soot formation. Figure up (hot flow) displays a widespread zone of high temperatures, whereas Figure down (soot model) exhibits a much more concentrated, central region of soot formation. This aligns with the established principle that cooler, fuel-rich regions (like the center in Figure down) promote soot due to incomplete combustion, suggesting a potential correlation between broader hot zones (Figure down) and less favourable conditions for soot production.

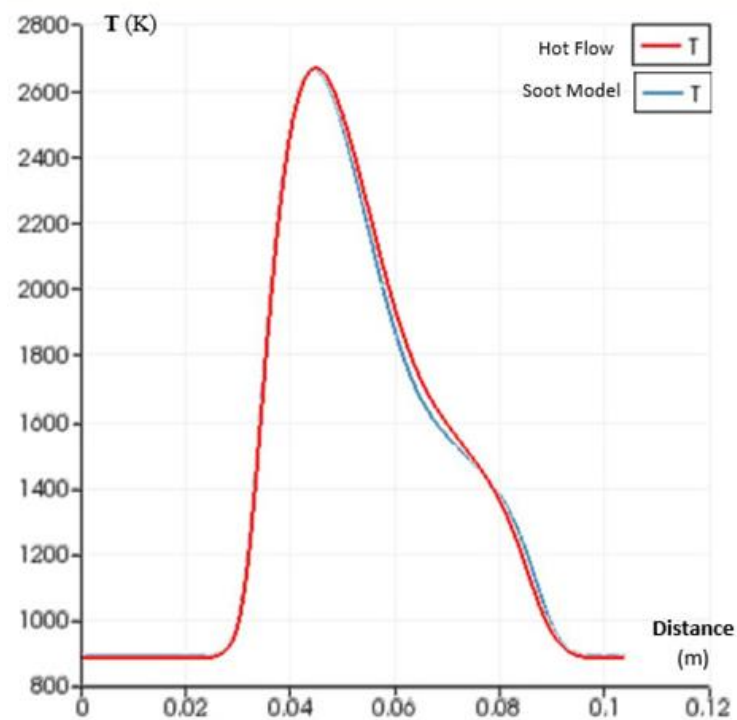


Figure.IV.45: Temperature graph within a Hold flow and SootModel in the combustion chamber.

This plot reveals a subtle difference in temperature profiles within a combustion chamber. The hot flow (red curve) exhibits a slightly steeper decline in temperature compared to the SootModel (blue curve) as distance from the injection point increases. This suggests a marginally faster cooling rate within the hot flow region.

b) For velocity :

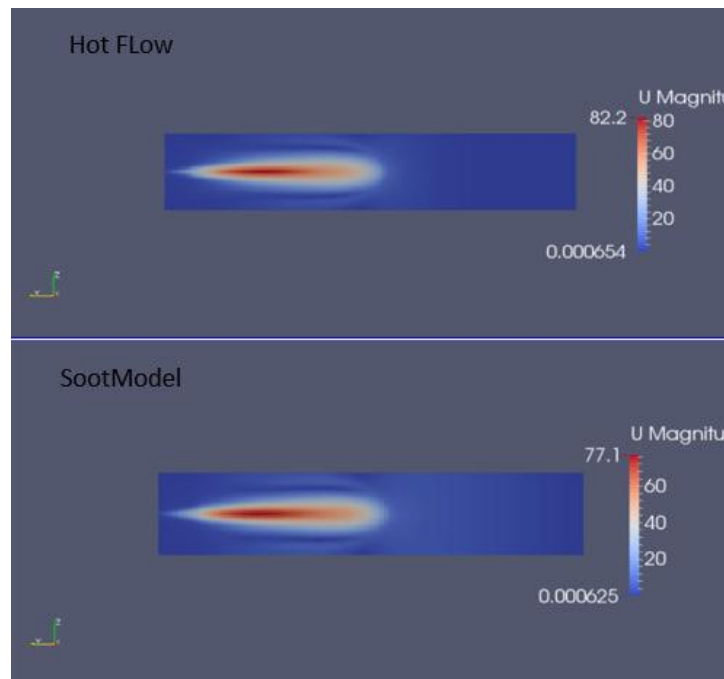


Figure.IV.46: Velocity distribution of Hotflow and 'SootModel' in the combustion chamber

Analyzing the velocity profiles at 1.4ms (Figures above: Hot Flow, below: Soot Model) reveals a stark contrast. Figure above, representing the hot flow case, exhibits a uniform distribution of arrows, indicating well-organized, likely high-velocity flow. This suggests a higher overall consumption rate within the combustion chamber. Conversely, Figure below, depicting the soot model, shows a more varied distribution of arrows, implying a less uniform and likely lower-velocity flow. This difference can be attributed to the presence of soot particles in the soot model, which can introduce drag, potentially altering the flow direction and reducing its overall speed compared to the hot flow case. In essence, the higher consumption rate in the hot flow scenario (Figure above) likely translates to a more organized and faster flow compared to the soot model (Figure below).

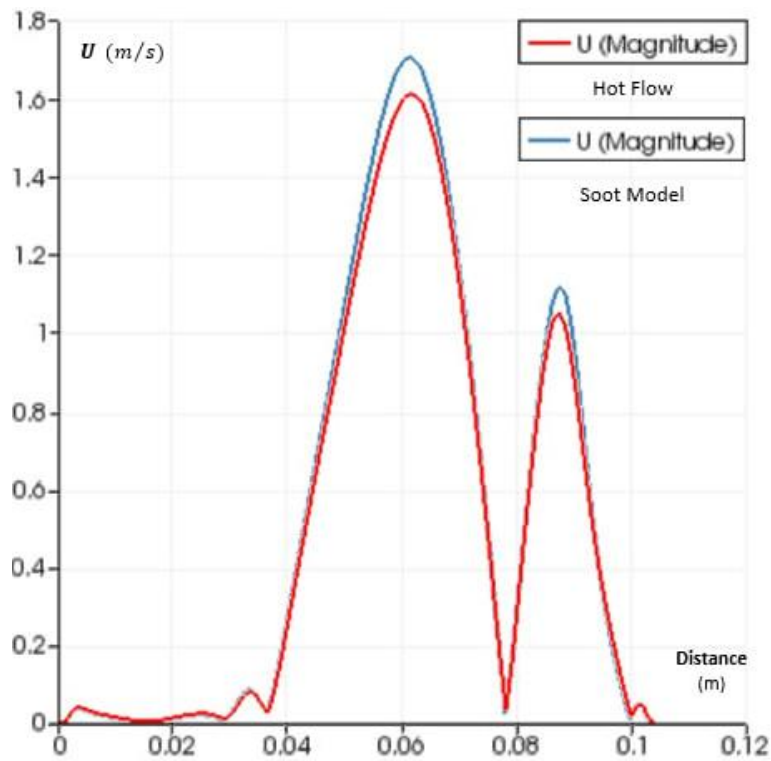


Figure.IV.47: Velocity graph within a Hold flow and SootModel in the combustion chamber

This plot reveals the contrasting velocity profiles within a combustion chamber. The hot flow (red) exhibits a steeper rise in velocity compared to the SootModel (blue) as distance from the injection point increases. This suggests a more significant acceleration within the hot flow region.

c) for Density :

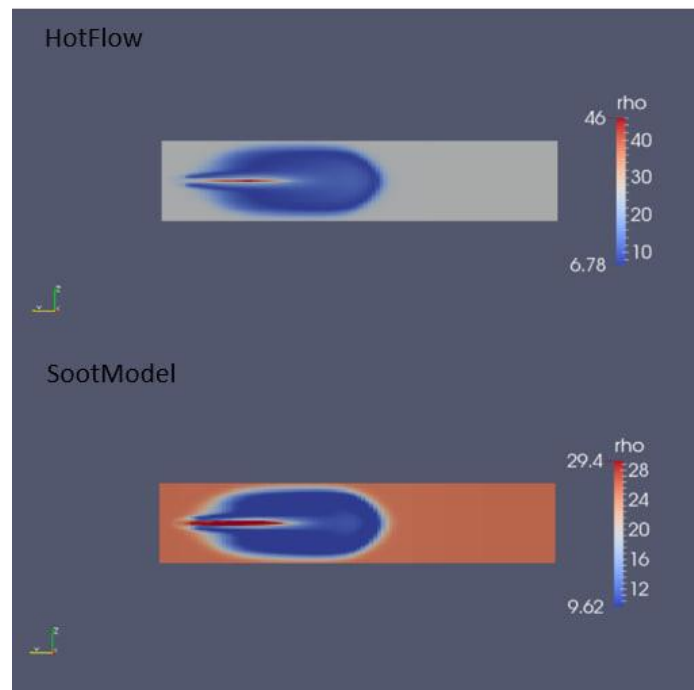


Figure.IV.48: Density distribution of Hotflow and ‘SootModel’ in the combustion chamber

Examining the density profiles (Figures up: Hot Flow, down: Soot Model) reveals a clear distinction. Figure up (Hot Flow) shows a centralized, denser core with a gradual decrease outwards, suggesting a potentially radially symmetric distribution. In contrast, Figure down (Soot Model) exhibits a more even density distribution across the chamber, potentially with slight variations on the bottom and left. This difference highlights the possible impact of temperature and injection patterns on the density distribution within the combustion chamber.

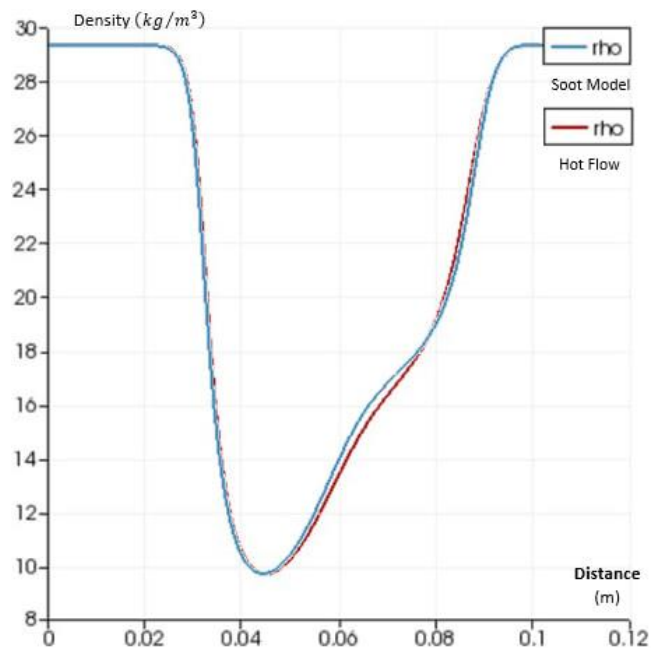


Figure.IV.49 Density distribution of Hotflow and 'SootModel' in the combustion chamber

The hot flow (red curve) exhibits a slightly steeper decline in density compared to the SootModel (blue curve) as distance from the injection point increases. This suggests a minor difference in density within the hot flow region. This subtle variation in density profiles might be a valuable point for further investigation and potential improvement in fuel combustion studies and innovations.

d) for species :

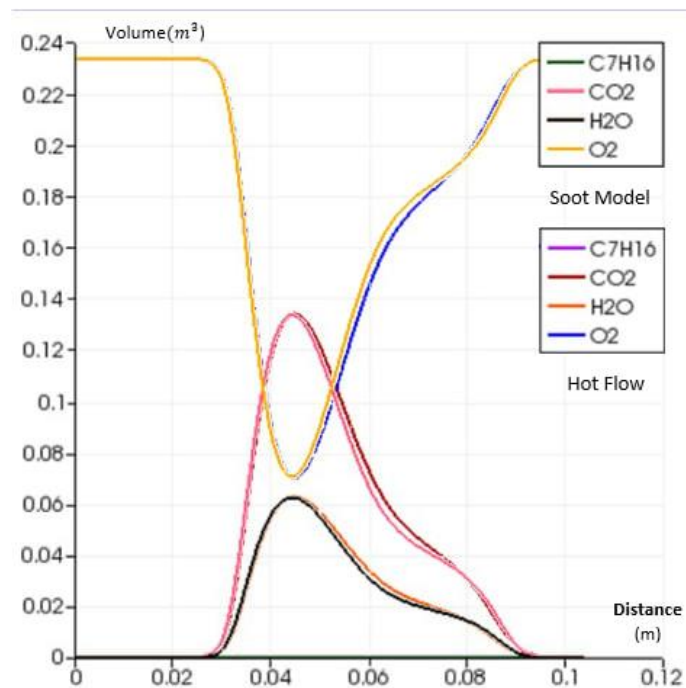


Figure.IV.50: Volume graph of the combustion species within a Hold flow and SootModel in the combustion chamber

The curves are nearly identical, but there is a clear difference between the species volume. This could lead that the soot model performs better than the hot flow case, which suggests that improving the injector spray could enhance its efficiency and effectiveness.

IV.4 Conclusion

Our analysis in Chapter 3 explored internal combustion engine simulations establishing a baseline case provided a reference point to evaluate cold and hot flow behaviors within the engine. Detailed results highlighted the critical importance of incorporating soot models into simulations. These models, compared to hot flow simulations alone, offered a deeper understanding of particulate matter formation and its interaction with combustion. This knowledge has significant implications for improving combustion efficiency and, more importantly, reducing soot emissions in future engines. The insights gained from this analysis are invaluable for guiding future simulations and applications in internal combustion engine technology. By integrating knowledge of soot behavior and fuel reactivity, future simulations can achieve more accurate predictions and optimizations, leading to enhanced engine performance and a reduced environmental footprint. This collaborative approach, utilizing open-source tools like OpenFOAM alongside ongoing research and advancements, paves the way for developing cleaner and more sustainable internal combustion engine technologies.

General conclusion:

This study utilized OpenFOAM, an open-source computational fluid dynamics (CFD) software, to simulate critical combustion processes within diesel engines. Focusing on injection, vaporization, mixing, ignition, and combustion, the research aimed to identify strategies for optimizing power generation, energy efficiency, and, crucially, emissions control.

A significant advancement emerged with the incorporation of soot models into the simulations. This led to a more comprehensive understanding of soot formation and behavior within the engine cylinder. While soot itself is detrimental to efficient combustion, this newfound knowledge enables researchers to predict and mitigate harmful soot emissions more effectively.

By optimizing injector design and operation to minimize soot formation, the path is paved for the development of cleaner engines with enhanced performance. Future advancements lie in integrating more sophisticated combustion models and real-time data analytics into the simulation framework. This holds promise for further refining engine efficiency and emissions control. Open-source tools like OpenFOAM play a vital role in this ongoing collaborative effort, propelling innovation towards the development of cleaner and more sustainable internal combustion engine technologies.

Bibliography :

- [1] Daghboudj Samir "LivreMaintenance des MoteursDiesel" May, 2006]
- [2] carburation, Université des Sciences et de la Technologie d'Oran - Mohammed Boudiaf, (année 2018).
- [3] Bensalem,Ch.. (2023). Master1 Courses in Thermal Engineering and Thermodynamics. University of Bouira (UAMOB), Bouira, Algeria.
- [4] Les moteur Diesel : évolutions des 30 dernières et des 10 prochaines années, Rapport rédigé par les élèves de la promotion 2005 d'IPSA, Brice Gonier, Kevin Dubot, Florent Geneste sous le conduit de : « M.RIVERE » professeur de moteur. Mai 2003.
- [5] Olivier Grondin, Modélisation du moteur à allumage par compression dans la perspective du contrôle et du diagnostic. Thèse de Doctorat à l'Université de Rouen, 2004 .
- [6] (de) Klaus Grewe, « Die Reliefdarstellung einer antiken Steinsägemaschine aus Hierapolis in Phrygien und ihre Bedeutung für die Technikgeschichte. Internationale Konferenz 13.–16. Juni 2007 in Istanbul », Bautechnik im antiken und vorantiken Kleinasien, Istanbul, Ege Yayınları/Zero Prod. Ltd., série Byzas, vol. 9, 2009, p. 429–454
- [7] <http://www.motorlegend.com>
- [8] Motors combustion description, Constructive, Bruxelles, 2012.
- [9] <http://www.techautoalgerie.wordpress.com>
- [10] H.M.Chollet, Cours pratique pour mécaniciens d'automobiles, Editions Spes Vevey, 1979]
- [11] Nova, I., & Tronconi, E. (Eds.). (Year). Selective Catalytic Reduction Technology. Springer.]
- [12] Numerical simulation of diesel combustion based on n-heptane and toluene Kesong Zhanga,b , Qiangzhi Xinb,n, Zhenqian Mub, Zhijian Niub, Zhiming Wang. School of Energy and Power Engineering, Shandong University, Jinan City, Shandong, China ; Zibo Diesel Engine Company, Zibo City, Shandong, China received 15 August 2018; accepted 7 January 2019 available online 14 February 2019
- [13] An experimental study of the effects of fuel properties on reactive spray evolution using primary Reference Fuels J.V. Pastor, J.M. García-Oliver , J.J. López, W. Vera-Tudela 1 CMT Motores Térmicos, Universitat Politècnica de València, Camino de Vera s/n, 46022 Valencia, Spain
- [14] Poinso, T., & Veynante, D. (2017). Turbulent Combustion Modelling and Experiments: Recent Trends and Developments. Springer.
- [15] Yakhot, V. (2010). Turbulent Combustion Modeling in CFD. Arab Academy for Science, Technology & Maritime Transport.

biibliography

- [16] <https://www.openfoam.com/documentation/user-guide>
- [17] "Modeling Soot Formation in Combustion Systems" by Heinz Pitsch
- [18] "Simulation of Soot Formation in Internal Combustion Engines" by Andrea Parente and Fulvio Masi
- [19] OpenFOAM v2.3.0: Physical Modelling: section: Combustion/Pyrolysis ; website: [http :
//www.openfoam.org/version2.3.0/physical – modelling.php](http://www.openfoam.org/version2.3.0/physical-modelling.php).
- [20] Muthuramalingam, V. P. (2015). Implementation of soot model for aachenBomb tutorial. Department of Thermo and Fluid Dynamics, Chalmers University of Technology.